Variable-Angle Electron Energy-Loss Spectroscopy of Polyatomic Molecular Systems

Thesis by

Kerry N. Walzl

In Partial Fulfillment of the Requirements
for the Degree of
Doctor of Philosophy

California Institute of Technology
Pasadena, California
1987

(Submitted June 2, 1986)

For my mother

ACKNOWLEDGMENTS

A veteran student realizes that everyone he knows is an invaluable teacher. The following people have acted as my teachers, in addition to their other roles as colleagues, friends, and relatives.

Aron Kuppermann was a source of chemical physics information and taught the importance of organization and completeness in scientific reasoning. Professors Zewail, Beauchamp, and Dervan were also providers of chemical insight and guided me along the proper path to graduation.

Both Charles Koerting and Isaac Xavier, Jr. aided me greatly in my experiments. Charles demonstrated the advantages of quickly initiating a project while Isaac demonstrated the advantages of a careful, detailed approach.

James Garvey lent his valuable scientific opinions and his chemical intuition and enthusiasm were inspiring. Diane Hood possessed an amazingly broad range of knowledge that sometimes forced me to think in uncommon directions. Steven Cuccaro likewise had a large, varied store of information which was coupled with an almost superhuman ability at proofreading. Garth Parker always seemed to know, or know where to find, the answers to thorny problems. Paul Hipes demonstrated an ability to make any explanation clear and precise. Jerry Winniczek, David Moll, and Dorothy Flanagan introduced me to the workings of the Kuppermann research group when I first joined. Timothy Mattson, Joseph Wong, and Jack Kaye have enlightened me regarding life after graduate school. Maria Arnazzi, Qiu Jin, Zhengwei Peng, Mark Wu, and Mary Rodgers have reminded me of the fun in starting new research.

Robert Scheid imparted his diplomatic wisdom along with his scientific knowledge. Edward Sleva, Lutfur Khundkar, and Norbert Scherer provided fresh perspectives on chemical physics research outside of my own group. Peter and

Patti Felker reminded me of the worth of patience and forthrightness. Wyman Williams demonstrated that the right work can be just like play. Lucas Kamp helped me practice planning and strategy.

Joyce Ferrante, Laurie Fletcher, Heidi Youngkin, and Adria McMillan convinced me of just how hard it is to play "guardian angel". Dan Zirin displayed a remarkable understanding of computers and computing and a willingness to help those less capable. Thomas Dunn, William Schuelke, Anton Stark, and the rest of the shop personnel displayed true artistry in their tasks.

Nancy, Kelly, Kristen, Christopher, James, Violet, and Karen offered constant encouragement and inspired me to perservere during difficulties.

ABSTRACT

The technique of variable-angle electron energy-loss spectroscopy has been used to study the electronic spectroscopy and structure of both open- and closed-shell molecules. The experiments were performed using incident electron beam energies between 25 eV and 100 eV and at scattering angles between 0° and 90°. Energy-loss regions from 0 eV to 16 eV were examined. Spin-forbidden, dipole symmetry-forbidden/quadrupole symmetry-allowed, and super-excited transitions were investigated by this method.

The three small carbonyl compounds formaldehyde (CH_2O), acetaldehyde (C_2H_4O), and acetone (C_3H_6O) were studied in the energy-loss region from 0 eV to 16 eV. Low-lying spin-forbidden $n \rightarrow \pi^*$ and $\pi \rightarrow \pi^*$ transitions were located on the basis of the angular behavior of their relative differential cross sections. High-lying (autoionizing in the case of formaldehyde) dipole symmetry-forbidden states were also assigned on the basis of differential cross section behavior. The effect of methyl substitution on the transition energies was also noted and discussed.

Five dicarbonyl compounds (biacetyl, acetylacetone, acetonylacetone, 1,2-cyclohexanedione, 1,4-cyclohexanedione) were investigated by this spectroscopic method in order to locate their low-lying spin-forbidden transitions. The energy difference between the lowest spin-allowed and spin-forbidden $n \rightarrow \pi^*$ excitations in the cyclic dicarbonyls was found to be much larger than in the acyclic dicarbonyls; this difference was discussed.

The spectrum of the methyl radical CH_3 was investigated by the same technique as the carbonyls except that the radical was generated by pyrolysis. Three source compounds were tried (tetramethyl tin, ethyl nitrite, di-*t*-butylperoxide) with temperatures ranging from ambient to 800°C. Using di-*t*-butylperoxide at a pyrolysis temperature of about 300°C, relative differential cross sections for the

lowest allowed $^2A_1' \leftarrow {}^2A_2''$ 3s Rydberg transition (5.73 eV) were determined at incident energies of 50 eV and 25 eV. The differential cross sections for this band do not indicate the presence of any underlying spin-forbidden transition.

Finally, preliminary investigations of the spectroscopy of pyridazine and cyclohexanone were undertaken. For pyridazine, a new low-lying spin-forbidden excitation was observed. The low-lying spin-forbidden transitions of cyclohexanone were also observed along with tentative relative differential cross sections at 30 eV and 50 eV. Rydberg bands in this molecule converging to the first ionization potential were seen and the positions tabulated.

TABLE OF CONTENTS

1. PRINCIPLES OF ELECTRON SPECTROSCOPY 1

1.1 Introduction 1

1.2 Theoretical Considerations 2

1.3 Experimental 4

References 7

2. ELECTRON-IMPACT SPECTROSCOPY OF FORMALDEHYDE, ACETALDEHYDE, AND ACETONE 9

References 25

Tables 28

Figures 34

3. ELECTRON-IMPACT SPECTROSCOPY OF VARIOUS DICARBONYL COMPOUNDS 51

References 64

Figures 67

4. AN ELECTRON-IMPACT SPECTROSCOPY INVESTIGATION OF CH_3 AND SOME OF ITS PYROLYTIC PRECURSORS 84

References 94

Figures 96

APPENDIX 1. PRELIMINARY ELECTRON-IMPACT INVESTIGATIONS 105

References 107

Table 108

Figures 109

APPENDIX 2. APPLICATION OF EIS TO THE ASSIGNMENT
OF POLYATOMIC AUTOIONIZING RYDBERG TRANSITIONS 114
References 118
Tables 119
APPENDIX 3. ELECTRON OPTICS DESCRIPTION
AND ANALYSES 121
References 125
Tables 126
Figures 127
APPENDIX 4. DESCRIPTION OF EIS III DATA
ANALYSIS PROGRAMS 128
References 134
APPENDIX 5. SMALL CARBONYL RYDBERG TRANSITIONS 135
References 141

CHAPTER 1. PRINCIPLES OF ELECTRON SPECTROSCOPY

1.1 Introduction

The investigation of the interaction of electrons with matter has important applications to many fields of research. The information obtained relates to certain upper-atmosphere processes,[1] electron beam transport,[2] gaseous discharges,[3–5] plasma physics,[6–8] electron beam-pumped lasers,[9,10] and astrophysics.[11] The emphasis of the following research is on the location and identification of electronic energy levels in molecules. This knowledge is especially useful in photochemistry and radiation physics.

In particular, the work reported here uses the technique called electron energy-loss spectroscopy (EELS) or electron-impact spectroscopy (EIS), both terms being used interchangeably. EIS involves focusing a monoenergetic beam of electrons of initial energy E_0 into a gaseous target and then measuring the energy of the scattered electrons at a scattering angle θ . Plotting scattered electron intensity versus energy lost by the incident electrons yields the energy-loss spectrum and is analogous to an optical spectrum. Details of the experimental technique are described in Section 1.3.

Several advantages exist in using EIS rather than more conventional optical spectroscopies. One advantage is that a single electron spectrometer is able to scan the range from the infrared (several meV energy-loss) to the x-ray (several hundred eV energy-loss), with constant resolution throughout. Several optical instruments would be required to accomplish this, with the resolution of the optical instruments worse in the far ultraviolet (and above). A second advantage in using EIS is that the experiment contains two variables that help determine the nature of the target excited states, namely, the incident electron energy E_0 and the scattering angle θ. The specifics of how these variables are exploited and further experimental

considerations are given in the following sections.

1.2 Theoretical Considerations

When an electron scatters from and electronically excites an atom or molecule, two mechanisms of excitation are possible. The first, termed Coulomb or direct excitation, involves energy absorption by the target from the electric field caused by the transit of the electron. The system energy is conserved; therefore, the amount of energy absorbed by the target is manifested in an equal energy-loss of the electron. Transitions excited primarily by such a mechanism exhibit a slow increase in intensity as E_0 increases from threshold to 50–100 eV above threshold, then show a slow decrease as E_0 is further increased.[12] Transitions excited in this direct way also exhibit an intensity peak at θ=0°, decreasing by one to two orders of magnitude as θ increases from 10° to 90°.[13,14] This "forward-peaked" scattering is due to the fact that the electrostatic force which drives the excitation is long-ranged and thus the electrons undergo little or no direction change after interacting with the target. In addition, at high E_0 and low θ, where the Born approximation applies,[15] this type of excitation obeys optical selection rules.[16,17]

The second mechanism of electronic excitation involves the physical exchange of the incident electron with a target electron. The incident electron may exchange with a target electron with either the same or opposite spin; the former may or may not leave the target in an excited state and the latter leaves the target in an excited spin-forbidden state. The overall spin of the system (incident electron + target) is conserved and the $\Delta S=0$ selection rule is not violated. Transitions excited primarily by this mechanism exhibit a rapid decrease in intensity as E_0 changes from values near threshold to higher values. These transitions also exhibit a nearly uniform angular distribution due to the loss of the directional information

carried by the incident electron when it spends time in the target vicinity.

The very different manner of these two types of excitations allows one to extract information regarding the nature of transitions by examining how spectral intensities change as a function of θ and E_0. More specifically, what is measured is the differential cross section $\frac{d\sigma}{d\Omega}$ (DCS); that is, the cross section per unit solid angle for scattering into a given direction defined by the spherical polar angles θ and ϕ. For experiments in the gas phase with randomly oriented molecules the DCS is independent of ϕ.[14] (In addition, another experimental value of interest is the integral cross-section Q which is the differential cross-section integrated over all scattering angles.)

How does the behavior of the DCS indicate the nature of the transition? A transition which exhibits an approximately isotropic DCS (constant to within a factor of 2 over the range θ=10°–90°) is due to a spin-forbidden excitation. A transition which displays a strongly forward peaked DCS which falls off by one to two orders of magnitude as θ increases from 10° to 90° is due to a fully allowed transition (or elastic scattering). A DCS of intermediate behavior is most likely due to a spin-allowed/symmetry-forbidden transition.

One can predict the aforementioned behavior from potential scattering theory.[14,18] The problem is mathematically described by a plane wave (the electron far from the target) incident upon a central field scattering potential. A partial wave analysis of the problem combined with the assumption that the potential has an "effective range" leads to the result[19]

$$\frac{d\sigma}{d\Omega} \approx \frac{1}{k^2} \left| \sum_{l=0}^{+\infty} (2l+1)\eta_l P_l(\cos\theta) \right|^2,$$

for small phase shifts η_l and relatively low impact energies. The magnitude of the electron wave-number vector is k and P_l is the l^{th} Legendre polynomial. By

examining the above equation one can see that for long-range potentials, such as the Coulomb interaction, more partial waves will contribute to the DCS than for short-range potentials such as those involved in the exchange mechanism. The more Legendre polynomials that are included the more forward peaked is the DCS; the direct mechanism produces a forward peaked DCS whereas the exchange mechanism produces a more isotropic DCS. A lower E_0 (a lower k) also implies inclusion of fewer partial waves and again a more isotropic DCS.

A few final comments can be made regarding the theory of electron spectroscopy. A relation between optical results and EIS results can be found in the first Born approximation; in fact, optical oscillator strengths can be obtained from electron scattering measurements.[17,20,21] Also, regarding certain types of symmetry-forbidden transitions, both Goddard[22] and Read and Whiterod[23] have used symmetry arguments to predict the behavior of the DCS.

1.3 Experimental

The results presented in this thesis were obtained using the electron spectrometer fully described in the Ph.D. thesis of C. F. Koerting.[18] For completeness, a very brief description of the spectrometer is given here, including any recent changes.

The vacuum system used in these experiments has been described previously by Rice[24] and Flicker.[25] The system consists primarily of a 70 l stainless steel chamber pumped by a mercury diffusion pump with a measured speed of 300–350 l/sec. In addition to the main chamber pumping, two other pumps are used. A 50 l/sec turbomolecular pump differentially pumps the electron optics which are enclosed in isolation housings. A gravity-fed liquid nitrogen cryotrap is located in the vicinity of the sample inlet source and acts as a beam dump and as an

aid to main chamber pumping. The main chamber base pressure is 2×10^{-7} to 1×10^{-6} torr. Two orders of magnitude in pressure can be maintained between the electron optics and the main chamber; during a scan the pressure in the optics region is kept at 1×10^{-6} to 4×10^{-6} torr.

The spectrometer and electronics are contained within an RF shielded enclosure providing 100 dB attenuation of electromagnetic frequencies in the range of 10^4 to 10^{11} Hz. Magnetic shielding consists of a single 0.050 inch μ-metal shield reducing the ambient magnetic field in the spectrometer to approximately 5 mG.

Two sets of electron optics exist which may be used with this instrument. The first set, designed by Flicker,[25] were used initially with no success (poor current at the scattering center and tuning difficulties). A second set was designed by Edmonson (as described by Rianda[26]) and, except for some recent minor design changes,[18] was used for the experiments reported here. A computer analysis and comparison of these two optics sets is included in Appendix 3. Briefly, electrons are emitted from a tungsten filament, focused onto the plane of a hemispherical-sector electron-energy analyzer (2.25 inch mean radius), energy selected, and focused onto the target gas. Typical beam currents at the scattering center range from 1–20 nAmp. Scattered electrons are then focused into a second hemispherical analyzer, energy analyzed again, and finally focused onto an electron multiplier and detected. The system resolution, measured as the full-width at half-maximum (FWHM) of the elastic peak, is typically 30–100 meV.

The monochromator is mounted on a rotatable gear wheel and may be turned from –15° to 110° about the rotation axis. The actual scattering angle varies from about -10° to 100° because the analyzer and monochromator lie in a plane 20° with respect to the horizontal (see Appendix 3).

Three gas target sources can be used with the present spectrometer. The first

is a static gas cell consisting of a copper tube, closed on one end, with a 0.060 inch wide slot cut 120° around its circumference at 20° with respect to the horizontal and also two 0.060 inch holes drilled opposite the slot at 0° and 55° . These holes allow the electron beam to exit into the analyzer and faraday cup, respectively. This tube slides onto another copper tube, by which the sample gas is admitted, passing through the center of the rotating table via a rotary seal. The second sample source is an effusive jet produced by a stainless steel hypodermic needle with a 0.050 inch ID and a length-to-diameter ratio equal to 6. The needle is fitted into a copper cap which slides onto the same inlet tube as the gas cell. The third inlet is a quartz pyrolysis tube. This inlet consists of a 0.25 inch OD quartz tube drawn to form a 0.060 inch ID capillary at one end where a stainless steel sheathed heater wire is wrapped. Temperatures in excess of 800° C, as measured by a thermocouple located on the heater assembly, have been attained with this source.

The detection of electrons is accomplished by a Galileo SEM 4219 Spiraltron electron multiplier. A MSC 8001 Z80-based computer acts as a programmable multichannel scaler and voltage sweep control. The spectrum that is collected is plotted and stored on a diskette for transfer to the chemistry department VAX 11/780 computer where the data is analyzed. The detection and scanning system is described in the thesis of Rianda.[26] Further discussion of the data analysis programs and their usage is given in Appendix 4.

REFERENCES

1. K. Takayanagi and Y. Itikawa, *Space Science Rev.* **11**, 380 (1970).
2. P. H. de Haan, R. N. Singh, H. J. Hopman, G. C. Janssen, E. H. Granneman, and P. S. Strelkov, *J. Phys. E* **14**, 373 (1981).
3. L. G. Huxley and R. W. Compton, *The Diffusion and Drift of Electrons in Gases* (John Wiley and Sons, New York 1974).
4. A. Gilardini, *Low Energy Electron Collisions in Gases; Swarm and Plasma Methods Applied to Their Study* (John Wiley and Sons, New York 1972).
5. E. W. McDaniel, *Collision Phenomena in Ionized Gases* (John Wiley and Sons, New York 1964).
6. T. Taniguchi, H. Tagashira, and Y. Sakai, *J. Phys. D* **10**, 2301 (1977).
7. P. D. Edgley and A. von Engel, *Proc. Roy. Soc.* **1370**, 375 (1980).
8. A. Kh. Mnatsakanyan, *High Temp.* **12**, 745 (1974).
9. C. S. Willett, *Introduction to Gas Lasers: Population Inversion Mechanisms* (Pergamon Press, New York 1974).
10. C. Brau in *Topics in Applied Physics*, vol. 30, *Excimer Lasers*, C. K. Rhodes, editor (Springer-Verlag, Berlin 1979), p. 87.
11. J. H. Black, *Astrophys. J.* **222**, 125 (1978).
12. H. S. Massey and E. H. Burhop, *Electronic and Ionic Impact Phenomena*, 2nd ed., vol. 3 (Oxford University Press, London 1969), pp. 437,880,968.
13. A. Kuppermann, J. K. Rice, and S. Trajmar, *J. Phys. Chem.* **72**, 3894 (1968).
14. S. Trajmar, J. K. Rice, and A. Kuppermann, *Adv. Chem. Phys.* **18**, 15 (1970).
15. N. F. Mott and H. S. Massey, *The Theory of Atomic Collisions*, 3rd ed. (Oxford University Press, London 1965), p. 87.

16. E. N. Lassettre and A. Skerbele in *Inelastic Electron Scattering, Methods of Experimental Physics*, vol. 3 (Academic Press, New York 1974), pp. 868–951.

17. E. N. Lassettre, A. Skerbele, and M. A. Dillon Jr., *J. Chem. Phys.* **50**, 1829 (1969).

18. C. F. Koerting, Ph.D. Thesis, California Institute of Technology, Pasadena CA (1985).

19. H. S. Massey and E. H. Burhop, *Electronic and Ionic Impact Phenomena*, vol. 1 (Oxford University Press, London 1969), pp. 379–84.

20. M. Inokuti, *Rev. Mod. Phys.* **43**, 297 (1971).

21. R. J. Celotta and R. H. Huebner in *Electron Spectroscopy: Theory, Techniques, and Applications*, vol. 3, edited by C. R. Brundle and A. D. Baker, (Academic Press, New York 1979), pp. 45–121.

22. W. A. Goddard III, D. L. Hustis, D. C. Cartwright, and S. Trajmar, *Chem. Phys. Lett.* **11**, 329 (1971).

23. F. H. Read, and G. L. Whiterod, *Proc. Phys. Soc.* **82**, 435 (1963).

24. J. K. Rice, Ph.D. Thesis, California Institute of Technology, Pasadena CA (1969).

25. W. M. Flicker, Ph.D. Thesis, California Institute of Technology, Pasadena CA (1976).

26. R. Rianda, Ph.D. Thesis, California Institute of Technology, Pasadena CA (1981).

CHAPTER 2

Paper 1: ELECTRON–IMPACT SPECTROSCOPY OF FORMALDEHYDE, ACETALDEHYDE, AND ACETONE

Electron–Impact Spectroscopy of Formaldehyde, Acetaldehyde, and Acetone[a]

K. N. Walzl[b], C. F. Koerting[c], and A. Kuppermann

Arthur Amos Noyes Laboratory of Chemical Physics,[d]

California Institute of Technology, Pasadena, CA 91125

(received)

Abstract

The three carbonyl-containing molecules formaldehyde, acetone, and acetaldehyde have been studied by the technique of low-energy, variable-angle electron energy-loss spectroscopy. With this method the low-lying, spin-forbidden transitions have been located by means of the behavior of the relative differential cross sections, providing the first identification by this technique of the low-lying spin-forbidden states in acetaldehyde. High-lying states (super-excited in the case of formaldehyde) were also investigated and some assignments were made on the basis of characteristic angular behavior, evident not only for the symmetric molecules formaldehyde and acetone but also for acetaldehyde. The trends in the allowed and forbidden transition energies were examined and found to be relatively linear with methyl substitution.

---

[a] This work was supported in part by the U. S. Department of Energy, Contract No. DE-AM03-76F00767, Project Agreement No. DE-AT03-76ER72004.

[b] Work performed in partial fulfillment of the requirements for the Ph.D. degree in Chemistry at the California Institute of Technology.

[c] Present address: E. I. Dupont de Nemours and Co., Inc., Wilmington, DE 19898.

[d] Contribution No.

1. INTRODUCTION

Small carbonyl compounds not only play an important role in terrestrial chemical and biological mechanisms, but the prototype molecule formaldehyde has even been detected in interstellar space. Acetone is equally interesting, containing the same symmetry elements as formaldehyde but with each hydrogen replaced by a methyl group. Acetaldehyde acts as a spectroscopically important intermediate case.

By means of optical experiments all three compounds are found to possess a weak absorption at approximately 4 eV[1-3] which is identified as belonging to the lowest $n \rightarrow \pi^*$ transition; the dipole symmetry-forbidden nature of this band explains its weakness. The spectra also possess a congested region above approximately 6.5 eV which is composed almost exclusively of transitions that are Rydberg in nature.[4-7] In particular, one sees first a band due to the 3s Rydberg series member (plus vibrational components), second a band due to the 3p Rydberg series member, next a band due to the 3d Rydberg series member, and then higher series members converging to the first ionization potential (IP).

Of the three molecules in this paper, formaldehyde has been the most extensively studied by electron spectroscopic techniques in the energy-loss region between 2.5 and 7.5 eV;[8-12] therefore, not a great deal is to be gained from a further detailed analysis of this region. An area of the formaldehyde spectrum that has not been greatly studied is that above the first IP, especially as a function of scattering angle, even though sharp structure has been observed.[13] Like formaldehyde, the interval of the acetone spectrum between 2.5 and 7.5 eV has been extensively examined,[10,12,14-18] but in this case doubt exists as to the identity of some of the transitions. The low energy-loss portion of the acetaldehyde spectrum has not been thoroughly investigated. Previous electron spectroscopy

work has been performed;[10,12,19] however, the low-lying spin-forbidden states have not been accurately identified through an examination of differential cross section (DCS) behavior.

A comparison of the spectra of small chromophore-bearing molecules enables one to ascertain the physical and chemical influences of various attached substituents on the chromophore. In addition, electron-impact spectroscopy is a powerful technique, both in its ability to elucidate the forbidden or allowed nature of a transition and in its ability to easily examine spectral features in the far ultraviolet. For this reason, a systematic study was undertaken of three simple molecules containing the CO chromophore: formaldehyde, acetaldehyde, and acetone.

2. EXPERIMENTAL

The electron-impact spectrometer and the methods of data accumulation and reduction have been described previously.[20] In brief, an electron beam is energy selected by a hemispherical electrostatic energy analyzer and scattered from the target vapor in a collision cell. Incident electron beam currents were between 0.5–10 nAmp and sample pressures in the cell were estimated to be between 1–10 mtorr. The electrons thus scattered at selected angles between –15° and 100° are energy analyzed with a second electrostatic energy analyzer and detected with an electron multiplier.

The typical resolution for these studies was between 50 meV and 90 meV as measured by the full-width at half-maximum (FWHM) of the elastically scattered peak. Some of the higher resolution spectra were measured with resolutions between 30 meV and 45 meV FWHM.

Acetone (Mallinckrodt 99.5%) and acetaldehyde (Baker 99+%) were degassed by several freeze-pump-thaw cycles and used without further purification.

Formaldehyde was generated by continuous heating of paraformaldehyde (Celanese 91–93%) at approximately 60° C. Air and water were removed from the sample by pumping on the paraformaldehyde during heating until the most intense features of the contaminant spectra were less than 1% of the mean intensity of the formaldehyde bands of interest.

The areas under the elastic peak and each of several inelastic features were obtained by numerical integration as described previously.[21] The relative DCS values for each molecule were also determined by a previously described method.[22] These cross sections are normalized by setting the elastic DCS at a given impact energy to 1.0 at the scattering angle $\theta = 40°$. The arbitrary units thus determined are different for each molecule and impact energy.

3. RESULTS AND DISCUSSION

Tables 1–4 summarize the excitation energies obtained and the assignments made for the transitions discussed in the following sections. (Additional transitions are tabulated in Appendix 5.) Peak locations determined from the electron-impact spectra have an estimated uncertainty of ±0.04 eV and the Franck-Condon limits for each transition are estimated to be within ±0.12 eV.

Energy-loss spectra at $E_0 = 25$ eV and $\theta = 10°$ for all three compounds (below the first IP) are shown in Figure 1. As mentioned previously, some general features are shared. The broad band at approximately 4 eV is due to the lowest spin-allowed n→ π^* transition; the sharp bands above 6 eV are due to various Rydberg transitions. Specifics for each molecule are discussed in the following separate sections.

3.1 Formaldehyde

Figure 2 shows the low energy-loss region of the formaldehyde spectrum for

several incident electron energies and scattering angles. At $E_0 = 50$ eV and $\theta = 10°$ (Figure 2a) the spectrum appears as it would if obtained by an optical technique.[4] The lowest energy band observed is that due to the n$\rightarrow \pi^*$ ($^1A_2$) transition with an onset at 3.35 eV and a maximum at 3.79 eV. Vibrational structure can be seen and is due to various numbers of quanta in both ν_1(C–H symmetric stretch) and ν_2(C–O stretch). The vibrational components of this band and the assignments are given in Table 1a. The agreement with the results of a comparable electron scattering experiment by Taylor *et al.*[11] and those of an optical study by Brand[1] is to within experimental error.

As the incident energy is lowered and the scattering angle is increased, several changes in the spectrum become apparent. The first is that the n$\rightarrow \pi^*$ band seems to shift to a lower energy-loss position, with the onset shifting from 3.35 eV to 3.00 eV and the maximum shifting from 3.79 eV to 3.50 eV. The explanation is that a spin-forbidden band partially overlaps the n$\rightarrow \pi^*$ ($^1A_2$) band, the spin-forbidden band being much lower in intensity at high E_0 and low θ but becoming of comparable intensity as E_0 is lowered and θ is increased. The identity of this underlying band is the n$\rightarrow \pi^*$ ($^3A_2$) transition and has been observed previously by Taylor *et al.* [11] and Robinson and Digiorgio.[23] Vibrational structure is observed and is due to various numbers of quanta in the modes ν_2 and ν_6 (out-of-plane bend) (Table 1b). The identification of these bands as being due to either spin-forbidden or spin-allowed transitions is made on the basis of the behavior of the differential cross section. It is known from previous work [24,25] that a band that exhibits a nearly constant DCS over the angular range $\theta = 10°$ to 90° and shows enhancement as the incident electron energy approaches threshold is due to a spin-forbidden transition while a band that falls off by 1 to 2 orders of magnitude over the same angular range is due to a fully-allowed transition. (A transition of intermediate behavior is most likely due to a spin-allowed/symmetry-forbidden

transition.) Figure 3 shows the differential cross sections for the n$\rightarrow \pi^*$ ($^1A_2$) and ($^3A_2$) bands and confirms the assignments.

The second spectral change that is observed is the appearance of a broad band with an onset at 4.93 eV and a maximum at 5.82 eV. The DCS for this band is shown in Figure 3; the relatively constant DCS between $\theta = 0°$ and 90° reveals that it is attributable to a spin-forbidden transition. Indeed, it corresponds to the $\pi \rightarrow \pi^*$ ($^3A_1$) transition. Vibrational structure is observed, due to excitation of ν_2; the transitions and assignments are listed in Table 1c. The corresponding $\pi \rightarrow \pi^*$ ($^1A_1$) band has not been observed even though many workers have calculated the excitation energy, with values spanning the range from 6 eV to 15 eV.[13,26–31] The consensus is that the $\pi \rightarrow \pi^*$ ($^1A_1$) transition most likely takes the form of a broad band underlying the somewhat congested Rydberg region between 7 eV and 12 eV.

A last observation that is made regarding the spectra shown in Figure 2 is the appearance of another set of spin-forbidden transitions at 6.74 eV, 6.83 eV, and 6.93 eV. The peak at 6.74 eV is assigned to the n$\rightarrow$3s ($^3B_2$) transition, the peaks at 6.83 eV and 6.93 eV being excitations of one and two quanta in ν_2. The spin-forbidden nature of these transitions is confirmed by the relatively constant DCS with scattering angle (Figure 4), particularly at $E_0 = 25$ eV.

Figure 1a includes the Rydberg region up to the first ionization potential (adiabatic IP = 10.88 eV[32]). A Rydberg transition is one in which the electron is excited far from the molecule into a hydrogen-like orbital surrounding an ionic core. Being hydrogen-like in nature, a simple Rydberg formula

$$E = IP - R/(n - \delta)^2,$$

can be used to fit the series.[33] E is the transition energy and R is the Rydberg

constant 13.605 eV. It is necessary to include a correction term δ called the quantum defect which is a measure of the penetration of the hydrogen-like orbital into the ionic core. For compounds of first row elements $\delta \sim 1.0$ for an s Rydberg series, $\delta \sim 0.6$ for a p Rydberg series, and $\delta \sim 0.1$ for a d Rydberg series.[34] Assignments for the transitions discussed in this research were made primarily on the basis of quantum defects. (Results are given in Table 1 in Appendix 5.) The $n_o \rightarrow ns\ (^1B_2)$ transitions were fit to a Rydberg series out to n = 9 with $\delta = 1.11$. Also, the n = 3 series member possesses vibrational structure by one and two quanta in ν_1. Three $n_o \rightarrow np$ series were observed. The $n_o \rightarrow np_y(b_2)$ transitions are dipole symmetry-allowed in formaldehyde and are fit with a quantum defect $\delta = 0.83$. The $n_o \rightarrow np_z(a_1)$ transitions are also symmetry-allowed and are fit with a quantum defect $\delta = 0.77$. A new $n_o \rightarrow np_z$ transition with one quantum of vibrational excitation in ν_2 has also been observed. The $n_o \rightarrow np_x(b_1)$ transitions are dipole symmetry-forbidden/quadrupole symmetry-allowed and indeed exhibit the angular behavior characteristic of such a transition, i.e., weak in intensity with respect to the dipole-allowed transitions at $E_0 = 100$ eV and $\theta = 0°$, but of comparable intensity at $E_0 = 100$ eV and $\theta = 10°$.[35] Transitions to the $3p_x$ Rydberg orbital with one and two vibrational quanta in ν_3 (in-plane bend) are observed; only the one quantum transition has been previously seen. The assignments of the transitions to either p_x –, p_y –, or p_z –type orbitals are also in accord with the magnitude of the quantum defects. The smallest quantum defect belongs to the transition to the p_x –type orbital ($\delta = 0.66$), the one with the smallest penetration into the ionic core (coordinate system, Figure 5). The p_y – and p_z –type transitions possess slightly higher quantum defects, penetrating the core to a greater extent. Two Rydberg series for $n_o \rightarrow nd$ transitions were found. The first, with a quantum defect of 0.40, is dipole symmetry-allowed and is assigned to transitions to d orbitals of either a_1 or b_2 symmetry. Peaks with

both one and two quanta in ν_2 are observed for transitions to the 3d orbital. The second series has a quantum defect of 0.12 and is attributed to a $n_o \rightarrow nd$ (b_1) series. A peak with one quantum also in ν_2 is seen for the transition to the 3d(b_1) orbital.

The far-uv spectrum of formaldehyde is very interesting in that it possesses sharp Rydberg structure beyond the lowest ionization potential and up to the fourth ionization potential. There is no difficulty in studying this region (corresponding to about 100 nm – 75 nm) by our technique; Figure 6 shows this region at $E_0 = 100$ eV and angles $\theta = 0°$ and $\theta = 10°$. The spectrum is very complicated due to the proximity of the three ionization potentials (IP2($1b_1$) = 14.39 eV (vertical), IP3($3a_1$) = 15.85 eV (adiabatic), IP4($1b_2$) = 17.0 eV (vertical)[32]) and again assignments are made primarily on the basis of quantum defects. Some aid is gotten by using symmetry arguments to predict that the Rydberg series of p_x(b_1)- and d(b_1)-type converging to the fourth IP are dipole symmetry-forbidden but quadrupole symmetry-allowed. Under the conditions of high incident energy such transitions should be enhanced relative to fully-allowed transitions upon an angular change from 0 to 10 degrees.[35] Peaks at 14.40, 14.86, 15.01, 15.17, 15.75, and 16.27 eV do indeed exhibit such an enhancement as can be seen in Figure 6 and summarized in Table 2. Weiss *et al.*[8] examined the spectrum of formaldehyde in this same region at $E_0 = 250$ eV, making assignments on the basis of quantum defects. They also noted that the broad band with a maximum at about 13.1 eV has a strong contribution due to autoionization (based on the work of Praet and Delwiche[36]). (Further tabulation of peak locations and assignments is given in Tables 2 and 3 in Appendix 5.)

3.2 Acetone

In Figure 7 is shown the low energy-loss region of the acetone spectrum at $E_0 = 50$ eV and $\theta = 10°$ and $E_0 = 25$ eV and $\theta = 40°$, $80°$ between 3.5 eV and

7.0 eV energy-loss. The $E_0 = 50$ eV and $\theta = 10°$ spectrum (Figure 7a) reproduces the result that one would obtain by an optical technique. The lowest band is due to the n$\rightarrow \pi^*$ singlet–singlet (S–S) transition, with an onset at 3.75 eV and a maximum at 4.38 eV. This low intensity band has been observed in previous electron scattering experiments[14,15] and the agreement is within experimental error. With an increase in scattering angle and a decrease in incident energy (Figures 7b, 7c), changes similar to those observed with formaldehyde are noticed. The n$\rightarrow \pi^*$ band appears to shift to lower energy, with the onset moving from 3.75 eV to 3.56 eV and the maximum moving from 4.38 eV to 4.18 eV. As with formaldehyde the reason for this apparent band shift is the increasing dominance of the underlying n$\rightarrow \pi^*$ singlet–triplet (S–T) transition as E_0 is lowered and θ is increased.

A second change that is noticed is the appearance of an additional band with an onset at 5.15 eV and a maximum at 5.88 eV. This is the $\pi \rightarrow \pi^*$ (S–T) band. The spin-allowed or spin-forbidden nature of all the aforementioned bands is confirmed through an examination of their respective DCS curves (Figure 8). In addition, none of these bands possess discernible vibrational structure. The information concerning these bands is summarized in Table 3a.

The last band visible in the spectra of Figure 7 is attributed to the n$\rightarrow$3s Rydberg transition; no peaks attributable to a spin-forbidden 3s Rydberg transition are found. Van Veen *et al.*[10] place the position of this spin-forbidden band at 6.26 eV. Figure 10 is an extension of the acetone spectrum up to the first IP (adiabatic IP = 9.71 eV) at an incident energy of 100 eV and scattering angles of 0, 3, and 10 degrees. The $n_o \rightarrow$ns series is fit up to n = 9 with a quantum defect of 1.03. Transitions with from 0 to 4 quanta in ν_4 (methyl group deformation) are observed for n = 3, transitions with 0 to 2 quanta in ν_4 are observed for n = 4,

and transitions with 0 and 1 quanta in ν_4 are observed for n = 5.

For Rydberg transitions of the type $n_o \rightarrow np$, a relatively weak series is fit with a quantum defect of 0.58. The 3p member shows structure, with transitions located at 7.42, 7.46, 7.54 and 7.59 eV. In addition, a change in the scattering angle from 0° to 10° causes the enhancement of features at 7.46, 7.95, and 9.11 eV; a shoulder at 7.59 eV also shows enhancement with increased angle. As previously discussed, this enhancement is indicative of a symmetry-forbidden/quadrupole-allowed band; Rydberg transitions to orbitals of b_1 symmetry are of this type. In this case the transition at 7.46 eV is assigned to the n=3 member of such a series and the transition at 7.59 eV is assigned as the forbidden transition to the $3p(b_1)$ orbital with one ν_4 vibrational quantum included. The peak at 7.42 eV is assigned to an allowed 3p Rydberg transition, the 7.54 eV transition being the same but with one quantum of ν_4 included.

Recently there has been some controversy regarding the assignment of the 3p Rydberg bands. Doering and McDiarmid[17] studied these 3p Rydberg transitions using an electron-impact energy-loss technique and concluded that the band origins that they found at 7.404 eV and 7.447 eV were due to a forbidden transition to the $3p(b_1)$ orbital and a false origin arising from the same transition enabled by the CO bending mode. In other words, the entire spectral region between 7.2 eV and 7.6 eV arises from a single forbidden transition, explaining the observed low intensity; the other two possible Rydberg transitions appeared to be inactive. They also found no evidence for forbidden transitions in the nonsymmetric molecule methyl ethyl ketone. Gedanken[18] performed a magnetic circular dichroism study of this same band in acetone and found evidence for two excited states, the assignment being to the two allowed 3p Rydbergs $^1A_1$ and $^1B_2$. The results of the present study suggest that a combination of the interpretations of Doering and McDiarmid and Gedanken is appropriate. The spectral intensity changes with E_0 = 100 eV

and θ varied between 0° and 10° do indeed demonstrate the presence of forbidden 3p Rydberg transitions but the fact that the 50 eV DCS curve for this band (Figure 9) decreases by over two orders of magnitude between 0 and 90 degrees reveals the contribution of a fully-allowed transition(s) (Table 4a). All three molecules in this study show similar behaviors and, as in the well-studied case of formaldehyde, the presence of both allowed and forbidden transitions is indicated.

Two $n_o \rightarrow nd$ Rydberg series are observed. The first is fit out to the n = 5 member with a quantum defect of $\delta = 0.37$. The second, which includes the bands at 7.95 eV and 9.11 eV, is fit with $\delta = 0.24$ and is assigned to a symmetry-forbidden series. The 4d′ member is not definitively observed; however, there is a slight intensity increase with angle in the shoulder at 8.75 eV which is suggestive of this transition. (Additional Rydberg peak positions and assignments are summarized in Table 4 in Appendix 5.)

The region of the acetone spectrum above the first IP also possesses structure, albeit slight. Broad features are observed at 10.32, 11.65, 12.32, 13.94, 14.51, and 15.27 eV. The bands at 13.94, 14.51, and 15.27 eV correlate fairly well with the ionization potentials at 14.06 (vertical), 14.4 (vertical), and 15.65 eV (vertical). The bands at 10.32, 11.65, and 12.32 eV roughly fit a Rydberg series converging to the second IP (12.78 eV, vertical) with $\delta = 0.59$. The values calculated with this quantum defect are 10.44, 11.61, and 12.08 eV. Based on the size of the defect this series could either be assigned to a p series or a strongly perturbed s series.

3.3 Acetaldehyde

Figure 11 shows the low energy-loss region of the acetaldehyde spectrum at $E_0 = 50$ eV, $\theta = 10°$ and $E_0 = 25$ eV, $\theta = 40°$, 70° between 3.0 eV and 7.0 eV. At $E_0 = 50$ eV and $\theta = 10°$ (Figure 11a) the optical result is reproduced with the lowest band (onset at 3.56 eV, maximum at 4.27 eV) again attributed to the $n \rightarrow \pi^*$ (S–S) transition. The low intensity of this band in acetaldehyde, which

possesses a symmetry (C_s) that does not make this transition forbidden, indicates that for this molecule the symmetry of the carbonyl local environment (C_{2v}) is more important in determining the selection rules. Like the other molecules studied in this series, with a decrease in E_0 and increase in θ this band is observed to shift to a lower energy (onset at 3.29 eV, maximum at 3.97 eV). The cause is the underlying n$\rightarrow \pi^*$ (S–T) band. With this same angular and energy change two other spectral features become prominent. The first, with an onset at 5.08 eV and a maximum at 5.99 eV, is due to the $\pi \rightarrow \pi^*$ (S–T) band. The second, relatively sharp, is located at 6.65 eV and is assigned as the n$\rightarrow$3s (S–T) Rydberg band. The assignments of these bands are supported by the DCS curves shown in Figures 12 and 13 and are tabulated in Table 3b.

Beginning with the last strong band in Figure 11 and continuing up to the first IP (10.21 eV, adiabatic[32]), the spectrum is dominated by Rydberg features (Figure 14). A $n_o \rightarrow$ns series is observed out to the n = 9 member and fit with δ = .94. Series members with one vibrational quantum in either ν_6 (OCH deformation) or ν_{10} (CCO deformation) are also observed. Two $n_o \rightarrow$np series are observed. One is fit with a quantum defect of 0.75, the other with a quantum defect of 0.61. The members of the second of these two series (at 7.80, 7.95, and 9.03 eV) exhibit the angular behavior characteristic of a dipole symmetry-forbidden/quadrupole symmetry-allowed transition as θ is changed from 0° to 10° in Figure 14 and are assigned as such. As previously mentioned, the carbonyl group local symmetry makes transitions to some p_π-type Rydberg orbitals dipole symmetry-forbidden. Vibrational quanta in either ν_6 or ν_{10} are observed for the n = 3 members of both series (Table 4b). Two $n_o \rightarrow$nd series are observed and fit with quantum defects of δ = 0.29 and δ = 0.01 out to the n = 5 series members. Peaks with a symmetry-forbidden nature are observed at 8.69 and 9.36 eV, just as a forbidden

p Rydberg series were also observed. (Additional results are summarized in Table 5 of Appendix 5.)

3.4 Discussion

The spectra of the three carbonyls are remarkably similar. All exhibit angular behavior that is characteristic of molecules possessing C_{2v} symmetry. This is contrasted with the results for methyl ethyl ketone in which Rydberg features do not behave in this manner, consistent with a compound of C_s symmetry.[17] Obviously a size threshold is passed in going from methyl to ethyl as a substituent; symmetry-forbidden Rydberg transitions in propionaldehyde most likely will not be found.

Only formaldehyde shows sharp structure above the first IP. This observation is mirrored in the photoelectron spectra for these three molecules. The lower bands (excluding the lowest) of formaldehyde are composed of sharp vibrational peaks while those of acetaldehyde and acetone are broad and relatively structureless.[32] This is due to the greater number of vibrational modes accessible in the larger compounds.

In Figure 15 are plotted the two lowest ionization potentials for the three molecules in this study along with the "term values" (term value = ionization potential of originating orbital – transition energy) for the three lowest valence transitions. The trends in ionization potentials demonstrate that the π molecular orbital is destabilized more per methyl group than the nonbonding molecular orbital (about 0.9 eV/methyl versus 0.6 eV/methyl). This has been explained as being caused by a delocalization effect, methylation increasing the delocalization of positive charge created by ionization thus stabilizing the ion,[37] and also an inductive effect, the methyl groups donating electron density and destabilizing the neutral.[38] The decrease in the term values for the three lowest valence transitions

demonstrate that the π^* orbital is also destabilized by increasing methylation by nearly the same degree as the π orbital (0.9 eV/methyl). Indeed, all the lower molecular orbitals studied are destabilized with methylation, including the Rydberg orbitals by about 0.2 eV/methyl for the s-type and about 0.02 eV/methyl for the d-type. The larger affect on the π and π^* orbitals suggests that a delocalization effect is probably dominant to the inductive effect. In fact, calculations by Harding and Goddard[39] find slightly more delocalization for triplet states than singlet states, which seems to be supported by the slightly larger influence on the $^3A_2$ and $^3A_1$ states (0.93 eV/methyl) versus the $^1A_2$ state and $^1A_1$ ground state (0.89 eV/methyl).

Since the energy changes are nearly linear with methylation the search for the spin-allowed $\pi \rightarrow \pi^*$ excitations in these compounds is simplified. If this transition is identified in one of the compounds its location can be accurately predicted for the other two compounds. In fact, it can be seen that since both the π and π^* orbitals are affected almost identically by methylation, the transition energy should be equal for all three molecules. Robin[40] argues for a location of about 9.0 eV but this value has not been definitively assigned.

4. SUMMARY

In summary, through the application of the technique of variable-angle electron energy-loss spectroscopy both low-lying singlet-triplet transitions and high-lying dipole symmetry-forbidden/quadrupole symmetry-allowed transitions have been observed for the three small carbonyl compounds formaldehyde, acetone, and acetaldehyde. The spin-forbidden bands have been accurately located and identified via the behavior of the relative differential cross sections. In the case of acetaldehyde this is the first location of these bands by this method. Symmetry-

forbidden autoionizing transitions in formaldehyde converging to the fourth IP have been characterized in a similar manner. In addition, apparent symmetry-forbidden Rydberg transitions in acetaldehyde have been detected even though the molecular symmetry is only C_s. It is observed that the energy levels of these compounds depend linearly on the number of methyls and is strongest for the π and π^* orbitals and weakest for the Rydberg orbitals. The effect seems to be primarily due to increased delocalization with increasing methyl substitution. An examination of the trends in the valence transition energies of these molecules indicates that the as yet unidentified spin-allowed $\pi \rightarrow \pi^*$ transition should be at the same spectral location for all three, most likely about 9 eV and obscured by strong Rydberg excitations.

References

1. I. C. Brand, *J. Chem. Soc.* , 858 (1956).
2. N. L. Allinger, T. W. Stuart, and J. C. Tai, *J. Amer. Chem. Soc.* **90**, 2809 (1968).
3. G. Herzberg, *Electronic Spectra of Polyatomic Molecules* (Van Nostrand Reinhold Co., New York (1966)), p. 543.
4. D. C. Moule and A. D. Walsh, *Chem. Rev.* **75**, 67 (1975).
5. A. B. Duncan, *J. Chem. Phys.* **3**, 131 (1935).
6. A. D. Walsh, *Proc. Roy. Soc. London* **A185**, 176 (1946).
7. K. Watanabe, *J. Chem. Phys.* **22**, 1564 (1954).
8. M. J. Weiss, C. E. Kuyatt, and S. Mielczarek, *J. Chem. Phys.* **54**, 4147 (1971).
9. A. Chutjian, *J. Chem. Phys.* **61**, 4279 (1974).
10. E. H. Van Veen, W. L. Van Dijk, and H. H. Brongersma, *Chem. Phys.* **16**, 337 (1976).
11. S. Taylor, D. Wilden, and J. Comer, *Chem. Phys.* **70**, 291 (1982).
12. R. H. Staley, L. B. Harding, W. A. Goddard, and J. L. Beauchamp, *Chem. Phys. Lett.* **36**, 589 (1975).
13. J. E. Mentall, E. P. Gentieu, M. Krauss, and D. Neumann, *J. Chem. Phys.* **55**, 5471 (1971).
14. R. Huebner, R. J. Celotta, S. R. Mielczarek, and C. E. Kuyatt, *J. Chem. Phys.* **59**, 5434 (1973).
15. W. M. St. John, R. C. Estler, and J. P. Doering, *J. Chem. Phys.* **61**, 763 (1974).
16. W. –C. Tam and C. E. Brion, *J. Electron Spectroscopy* **4**, 139 (1974).
17. J. P. Doering and R. McDiarmid, *J. Chem. Phys.* **76**, 1838 (1982).

18. A. Gedanken, *J. Phys. Chem.* **89**, 3781 (1985).

19. W. -C. Tam and C. E. Brion, *J. Electron Spectroscopy* **3**, 467 (1974).

20. (a) C. F. Koerting, K. N. Walzl, and A. Kuppermann, submitted to J. Chem. Phys.; (b) C. F. Koerting, Ph.D. Thesis, California Institute of Technology, Pasadena CA (1985).

21. O. A. Mosher, W. M. Flicker, and A. Kuppermann, *J. Chem. Phys.* **59**, 6502 (1973).

22. O. A. Mosher, M. S. Foster, W. M. Flicker, A. Kuppermann, and J. L. Beauchamp, *J. Chem. Phys.* **62**, 3424 (1975).

23. G. W. Robinson and V. E. Digiorgio, *Can. J. Chem. Soc.* , 31 (1958).

24. A. Kuppermann, J. K. Rice, and S. Trajmar, *J. Phys. Chem.* **72**, 3894 (1968).

25. S. Trajmar, J. K. Rice, and A. Kuppermann, *Adv. Chem. Phys.* **18**, 15 (1970).

26. J. L. Whitten and M. Hackmeyer, *J. Chem. Phys.* **51**, 5584 (1969).

27. R. J. Buenker and S. D. Peyerimhoff, *J. Chem. Phys.* **53**, 1368 (1970).

28. G. A. Segal, *J. Chem. Phys.* **53**, 360 (1970).

29. S. D. Peyerimhoff, R. J. Buenker, W. E. Kammer, and H. Hzu, *Chem. Phys. Lett.* **8**, 129 (1971).

30. D. L. Yeager and V. McKoy, *J. Chem. Phys.* **60**, 2714 (1974).

31. A. N. Singh and R. S. Prasad, *Chem. Phys.* **49**, 267 (1980).

32. D. J. Flanagan, Ph.D. Thesis, California Institute of Technology, Pasadena CA (1985) and references therein.

33. R. I. Hall and F. H. Read in *Electron-Molecule Collisions*, edited by I. Shimamura and K. Takayanagi, (Plenum Press, New York (1984)), p. 359.

34. M. B. Robin, *Higher Excited States of Polyatomic Molecules* vol. 1 (Academic

Press, New York (1974)), p. 51.

35. F. Read and G. Whiterod, *Proc. Phys. Soc.* **82**, 434 (1963).

36. M. Praet and J. Delwiche, *Intern. J. Mass Spect. Ion Phys.* **1**, 321 (1968).

37. D. W. Davis, U. C. Singh, and P. A. Kollman, *J. Molec. Struct. (THEOCHEM)* **105**, 99 (1983).

38. B. W. Levitt and L. S. Levitt, *Chem. Ind. (London)* , 725 (1972).

39. L. B. Harding and W. A. Goddard, *J. Amer. Chem. Soc.* **97**, 6293 (1975).

40. M. B. Robin, *Higher Excited States of Polyatomic Molecules* vol. 2 (Academic Press, New York (1974)), pp. 75–106.

Table 1. Formaldehyde valence transitions.[a]

(a) n→ π^*, $^1A_2$:

E	$\Delta\nu(\nu_1,\nu_2)$[b]	Taylor *et al.*[c]	Optical[d]
3.50	0.00 (0,0)	3.506	3.511
3.65	0.15 (0,1)	3.652	3.657
3.79	0.29 (0,2)	3.802	3.801
3.87	0.37 (1,0)	3.861	3.867
3.93	0.43 (0,3)	3.943	3.943
4.00	0.50 (1,1)	4.002	4.013
4.07	0.57 (0,4)	4.089	4.083
4.15	0.65 (1,2)	4.143	4.161
4.20	0.70 (0,5)	4.221	4.200

(b) n→ π^*, $^3A_2$:

E	$\Delta\nu(\nu_6,\nu_2)$[e]	Taylor *et al.*[c]	Optical[f]
3.13	0.00 (0,0)	3.128	3.124
3.19	0.06 (0,1)	3.191	3.191
3.27	0.14 (1,0)	3.279	3.283
3.35	0.22 (1,1)	3.347	3.346
3.56	0.43 (3,0)	3.575	
3.71	0.58 (4,0)	3.711	
4.28	1.15 (8,0)	4.283	
4.44	1.31 (9,0)	4.411	

(c) $\pi \rightarrow \pi^*$, $^3A_1$:

E	ν^g	Taylor *et al.*[h]
5.03	3	5.03
5.15	4	5.15
5.27	5	5.26
5.38	6	5.38
5.50	7	5.49
5.60	8	5.61
5.71	9	5.71
5.82	10	5.82
5.93	11	5.92
6.02	12	6.02
6.13	13	6.12
6.22	14	6.22
6.31	15	6.31
6.41	16	6.41
6.53	17	6.51
6.61	18	6.59
6.69	19	6.69

a) All energies are in eV.
b) $\Delta\nu\ (\nu_1, \nu_2) = E(\nu_1, \nu_2) - E(0,0)$. ν_1=0.37 eV, ν_2=0.14 eV; all have 1 quantum in ν_6 =0.08 eV.
c) Reference 11.
d) Reference 1.
e) $\Delta\nu\ (\nu_6, \nu_2) = E(\nu_6, \nu_2) - E(0,0)$. ν_2=0.15 eV, ν_6 =0.07 eV.
f) Reference 23.
g) ν_2=0.11 eV.
h) Values are taken from Reference 11, corrected by –0.04 eV.

Table 2. Formaldehyde Rydberg transitions, IP=17.0 eV.

(a) $\pi(1b_2) \rightarrow ns$:

E	n[a]	δ[a]	Calc[b]
13.34	3	1.07	13.35
13.50	3 $(+1\nu)$[c]	1.03	
13.66	3 $(+2\nu)$		
13.83	3 $(+3\nu)$		
13.99	3 $(+4\nu)$		
15.41	4	1.07	15.42
16.13	5	1.05	16.12

(b) $\pi(1b_2) \rightarrow np$:

E	n	δ	Calc[d]
14.14	$3(a_1)$	0.82	14.14
14.40	$3(b_1)$	0.71	14.43
15.66	$4(a_1)$	0.81	15.65
15.75	$4(b_1)$	0.70	15.75
16.21	$5(a_1)$	0.85	16.22
16.27	$5(b_1)$	0.68	16.26

(c) $\pi(1b_2) \rightarrow nd$:

E	n	δ	Calc[e]
14.83	$3(a_1)$	0.50	14.82
14.86	$3(b_1)$	0.48	
14.98	$3(a_1)$ $(+1\nu)^f$	0.40	
15.01	$3(b_1)$ $(+1\nu)$	0.39	
15.11	$3(a_1)$ $(+2\nu)$	0.32	
15.17	$3(b_1)$ $(+2\nu)$	0.27	
15.25	$3(a_2$ or $a_1)$	0.21	15.25
15.89	$4(a_1 + b_1)$	0.50	15.89
15.96		0.38	
16.08	$4(a_2$ or $a_1)$	0.15	16.05
16.36	$5(a_1 + b_1)$	0.39	16.33
16.41	$5(a_2$ or $a_1)$	0.20	16.41
16.57	$6(a_1 + b_1)$	0.38	16.55

a) Using formula $E = IP - R/(n - \delta)^2$.
b) Calculated with δ =1.07.
c) ν_2=0.16 eV.
d) Calculated with δ =0.82 and δ =0.70.
e) Calculated with δ =0.50 and δ =0.21.
f) ν_2=0.15 eV.

Table 3. Valence transitions.

(a) Acetone:

Transition	Onset	Maximum Expt	Maximum Lit	End
n→ π^*(S–T)	3.56	4.18	4.16[a]	4.96
n→ π^*(S–S)	3.75	4.38	4.37[a],4.39[b] 4.42[c]	5.28
$\pi \rightarrow \pi^*$(S–T)	5.15	5.88	5.88[a]	6.18

(b) Acetaldehyde:

Transition	Onset	Maximum Expt	Maximum Lit	End
n→ π^*(S–T)	3.29	3.97	3.91[d],3.75[e]	4.89
n→ π^*(S–S)	3.56	4.27	4.29[f]	5.16
$\pi \rightarrow \pi^*$(S–T)	5.08	5.99	6.31[d],6.25[e]	

a) Reference 15.
b) Reference 2.
c) Reference 14.
d) Reference 10.
e) Reference 12.
f) Reference 3.

Table 4. $n_o \rightarrow np$ Rydberg transitions[a]

(a) Acetone, IP=9.71 eV:

E	n	δ	Calc[b]	Lit[c,d]
7.42	3p	0.56	7.39	7.42,7.39
7.46	3p′	0.54		7.44
7.54	3p $(+1\nu)$[e]			7.55,7.52
7.59	3p′ $(+1\nu)$			7.56
8.44	4	0.73	8.55	8.41,8.42
9.01	5	0.59	9.01	8.82,8.98

(b) Acetaldehyde, IP=10.21 eV:

E	n	δ	Calc[f]	Lit[g]
7.44	3p	0.78	7.52	7.47
7.58	3p $(+1\nu)$[h]			7.59
7.74	3p $(+2\nu)$			7.78
7.80	3p′	0.62	7.83	
7.91	3p $(+3\nu)$			7.90
7.95	3p′ $(+1\nu)$			
8.95	4p	0.71	8.92	8.96
9.03	4p′	0.60	9.03	9.06
9.50	5p		9.46	9.51
9.74	6p		9.72	

a) n_o is oxygen nonbonding orbital.
b) Calculated with $\delta = 0.58$.
c) Reference 16.
d) Reference 14.
e) $\nu_4 = 0.12$ eV.
f) Calculated with $\delta = 0.75$ or $\delta = 0.61$.
g) Reference 19.
h) $\nu_6 = 0.16$ eV.

Figure Captions

1. Energy-loss spectra at 25 eV and 10° for: a) formaldehyde, b) acetaldehyde, and c) acetone. Incident electron current = 5 nAmp, sample pressure = 10 mtorr. Lower portion of spectra are multiplied by the indicated expansion factor before plotting.

2. Formaldehyde energy-loss spectra at: a) 50 eV and 10° , b) 25 eV and 40° , and c) 25 eV and 80° . Conditions same as Figure 1.

3. Formaldehyde valence band DCS curves (integrated over the range of the band): a) 25 eV, b) 50 eV. □ = elastic peak (EP) × 0.1, ○ = n→ π^* (3.0 to 4.9 eV), △ = $\pi \rightarrow \pi^*$ (S–T) (5.0 to 6.4 eV). The arbitrary units are the same for all curves.

4. Formaldehyde Rydberg band DCS curves: a) 25 eV, b) 50 eV. □ = 3s (S–S) (7.0 to 7.7 eV), ○ = 3s (S–T) (6.5 to 6.9 eV), + = 3p (S–S) (7.9 to 8.8 eV), △= 3p (S–T) (7.7 to 7.9 eV), × = 3d (8.8 to 9.5 eV).

5. Coordinate system for the carbonyl molecules, R = H or CH_3. The three bond axes represented by the heavy lines are in the yz-plane.

6. Formaldehyde energy-loss spectra between 11 eV and 16 eV at E_0 = 100 eV and θ = 0° , 10° . The arbitrary units for each of the two spectra differ by a factor of 50 and have different baselines, as indicated.

7. Acetone energy-loss spectra at: a) 50 eV and 10° , b) 25 eV and 40° , and c) 25 eV and 80° . Conditions same as Figure 1.

8. Acetone valence band DCS curves: a) 25 eV, b) 50 eV. □ = EP × 0.1, ○ = n→ π^* (3.5 to 5.1 eV), △ = $\pi \rightarrow \pi^*$ (S–T) (5.2 to 6.2 eV).

9. Acetone Rydberg band DCS curves: a) 25 eV, b) 50 eV. □ = 3s (6.2 to 6.9 eV), △ = 3p (S–S) (7.2 to 7.7 eV), ○ = 3p (S–T) (6.9 to 7.2 eV).

10. Acetone energy-loss spectra between 7 eV and 10 eV at E_0 = 100 eV and θ = 0° , 3° , and 10° . The arbitrary units for the 3° spectrum differ by a factor of 2.5 and for the 10° spectrum differ by a factor of 25 from the 0° spectrum. The corresponding baselines are indicated.

11. Acetaldehyde energy-loss spectra at: a) 50 eV and 10° , b) 25 eV and 40° , and c) 25 eV and 80° . Conditions same as Figure 1.

12. Acetaldehyde valence band DCS curves: a) 25 eV, b) 50 eV. □ = EP × 0.1, ○ = n→ π^* (3.3 to 5.2 eV), △ = $\pi \rightarrow \pi^*$ (S–T) (5.1 to 6.6 eV).

13. Acetaldehyde Rydberg band DCS curves: a) 25 eV, b) 50 eV. ○ = 3s (6.7 to 7.3 eV), △ = 3p (7.3 to 8.0 eV), □ = 3d (8.2 to 8.7 eV).

14. Acetaldehyde energy-loss spectra between 7 eV and 11 eV at E_0 = 100 eV and θ = 0° , 10° .

15. Transition energies plotted versus the number of methyls for the carbonyl compounds studied, 0 = formaldehyde, 1 = acetaldehyde, 2 = acetone. n $\rightarrow \infty$ and $\pi \rightarrow \infty$ represent the two lowest ionization energies, (n→ π^*)^{1,3} and ($\pi \rightarrow \pi^*$)^3 represent the "term value" for that transition ("term value" = IP of the originating orbital – transition energy).

FIGURE 1.

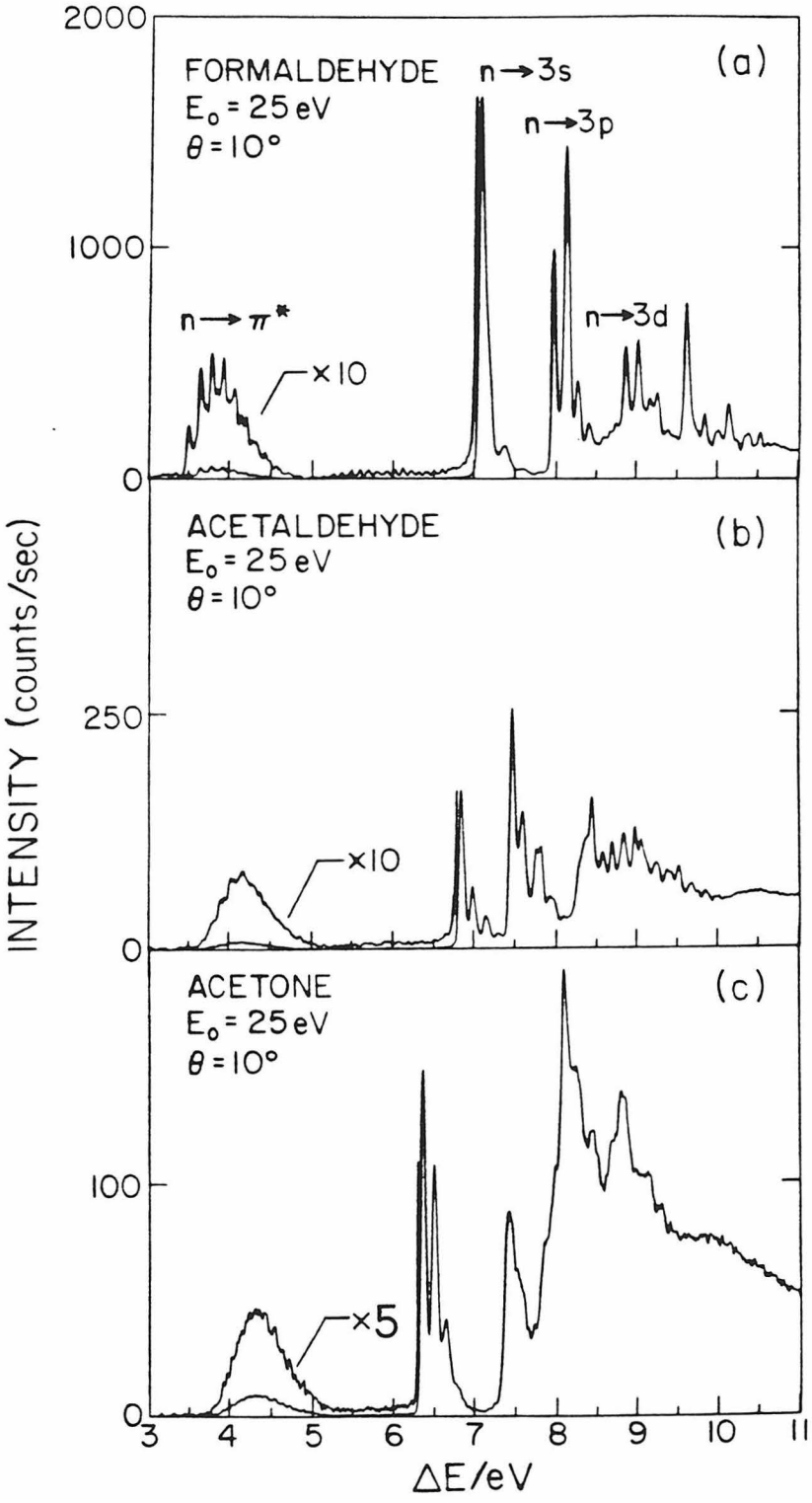
2000
1000
0
FORMALDEHYDE
E_o = 25 eV
θ = 10°
(a)
n→3s
n→3p
n→3d
n→π*
×10
ACETALDEHYDE
E_o = 25 eV
θ = 10°
(b)
250
0
×10
ACETONE
E_o = 25 eV
θ = 10°
(c)
100
0
×5
INTENSITY (counts/sec)
3
4
5
6
7
8
9
10
11
ΔE/eV

FIGURE 2.

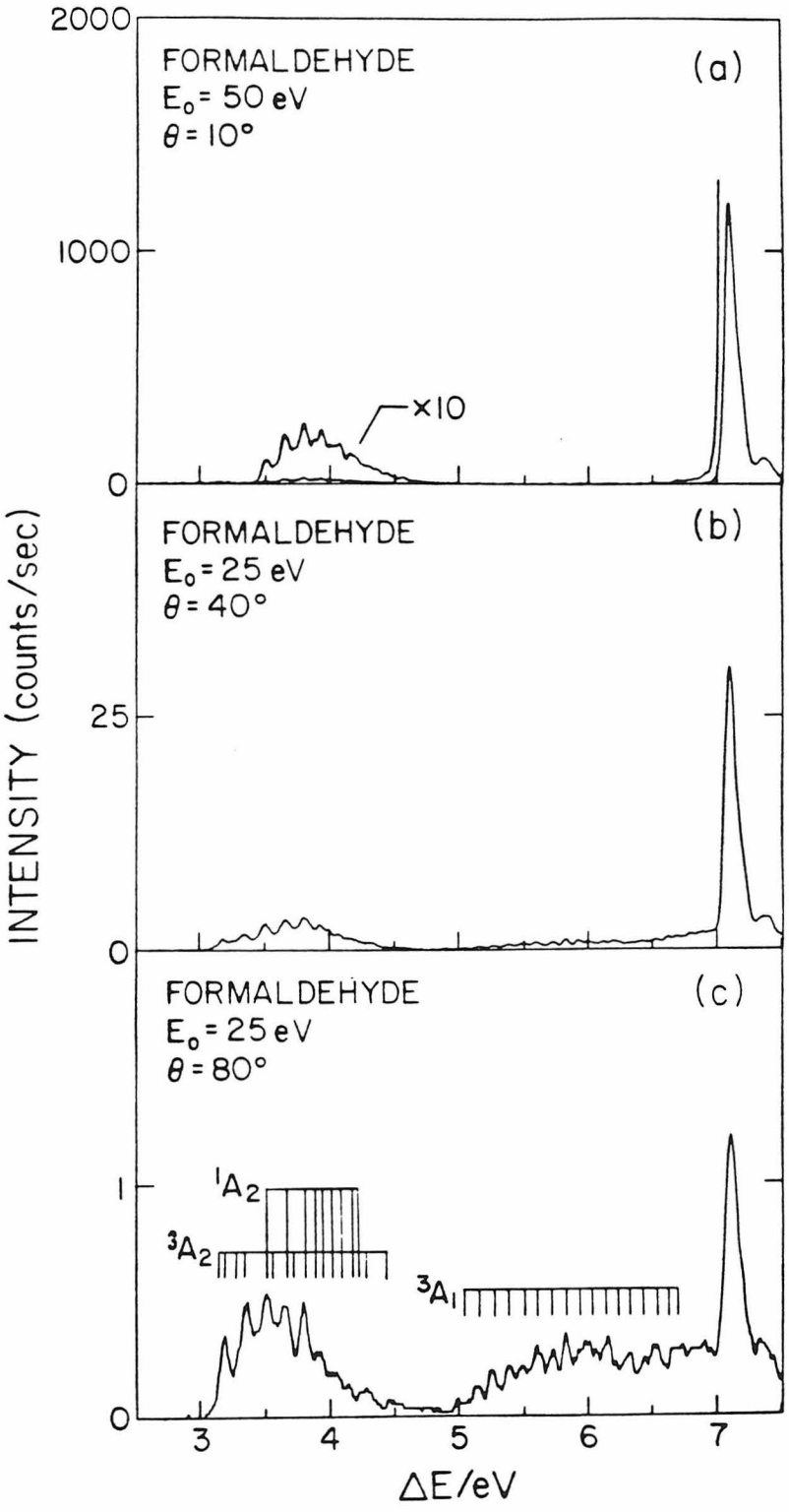
2000
1000
0
FORMALDEHYDE
E_0 = 50 eV
θ = 10°
(a)
×10
FORMALDEHYDE
E_0 = 25 eV
θ = 40°
(b)
25
0
FORMALDEHYDE
E_0 = 25 eV
θ = 80°
(c)
1
0
$^1A_2$
$^3A_2$
$^3A_1$
INTENSITY (counts/sec)
3
4
5
6
7
ΔE/eV

FIGURE 3.

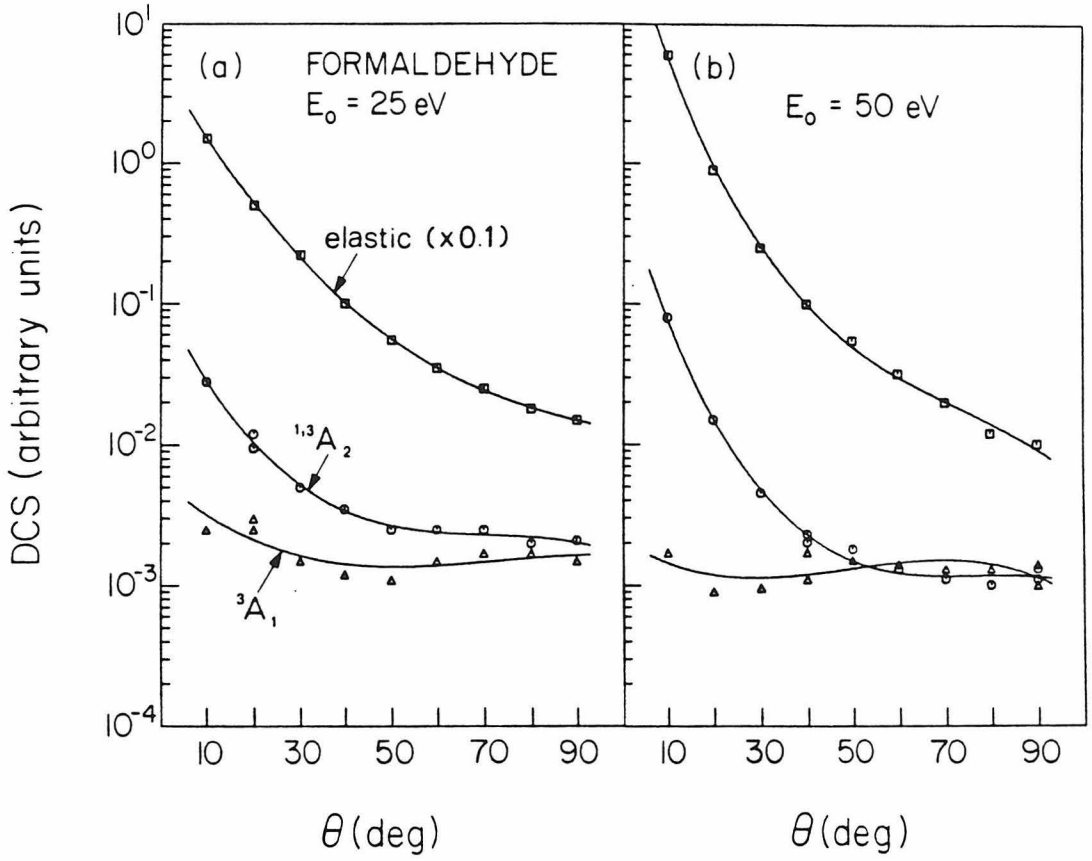
(a)
FORMALDEHYDE
E_o = 25 eV
elastic (x0.1)
$^{1,3}A_2$
$^3A_1$
(b)
E_o = 50 eV
DCS (arbitrary units)
10^1
10^0
10^{-1}
10^{-2}
10^{-3}
10^{-4}
10
30
50
70
90
θ (deg)
θ (deg)

FIGURE 4.

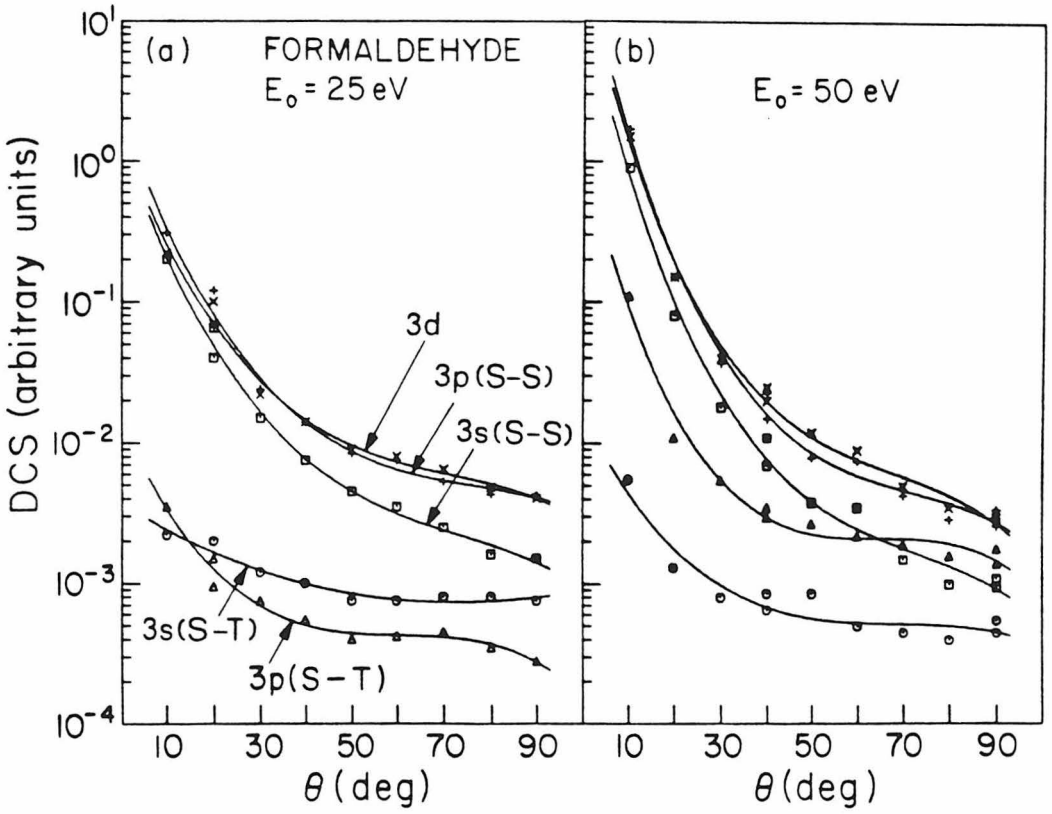
(a)
FORMALDEHYDE
E_0 = 25 eV
(b)
E_0 = 50 eV
DCS (arbitrary units)
10^1
10^0
10^{-1}
10^{-2}
10^{-3}
10^{-4}
3d
3p(S-S)
3s(S-S)
3s(S-T)
3p(S-T)
10
30
50
70
90
θ (deg)

FIGURE 5.

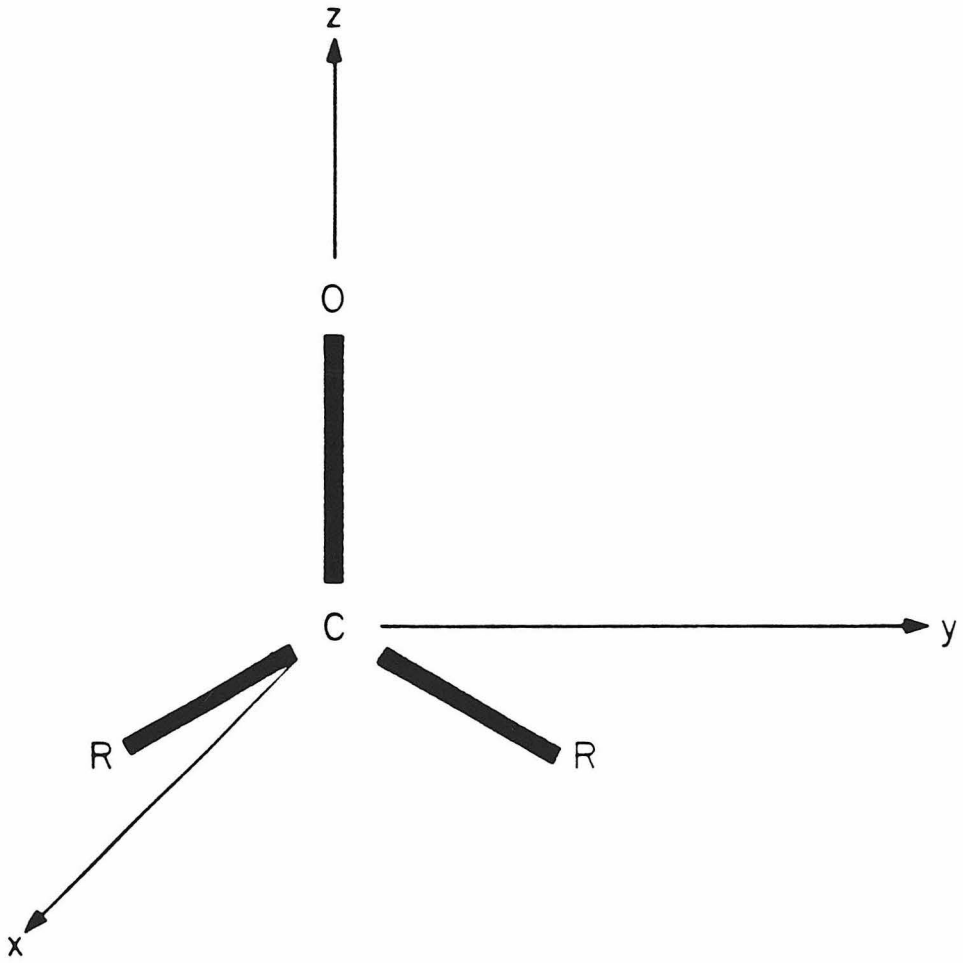

FIGURE 6.

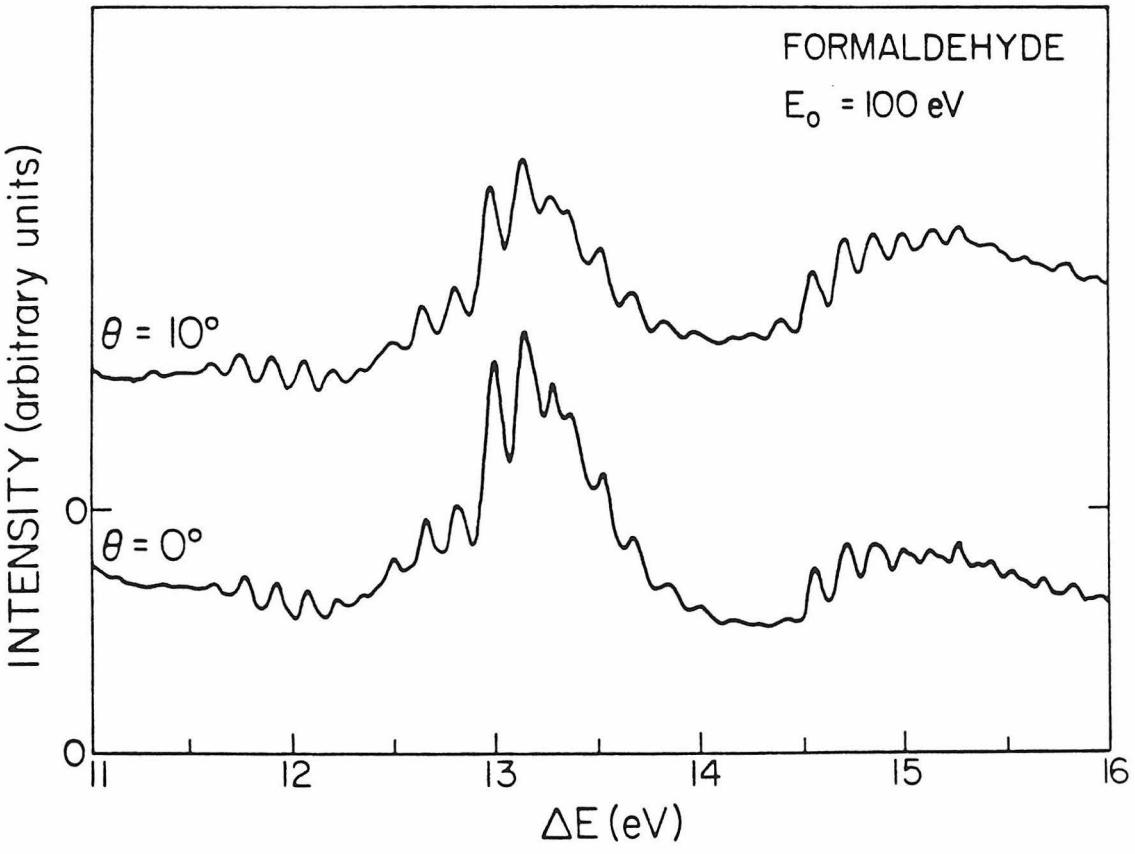
FORMALDEHYDE
E_0 = 100 eV
θ = 10°
θ = 0°
INTENSITY (arbitrary units)
0
0
11
12
13
14
15
16
ΔE (eV)

FIGURE 7.

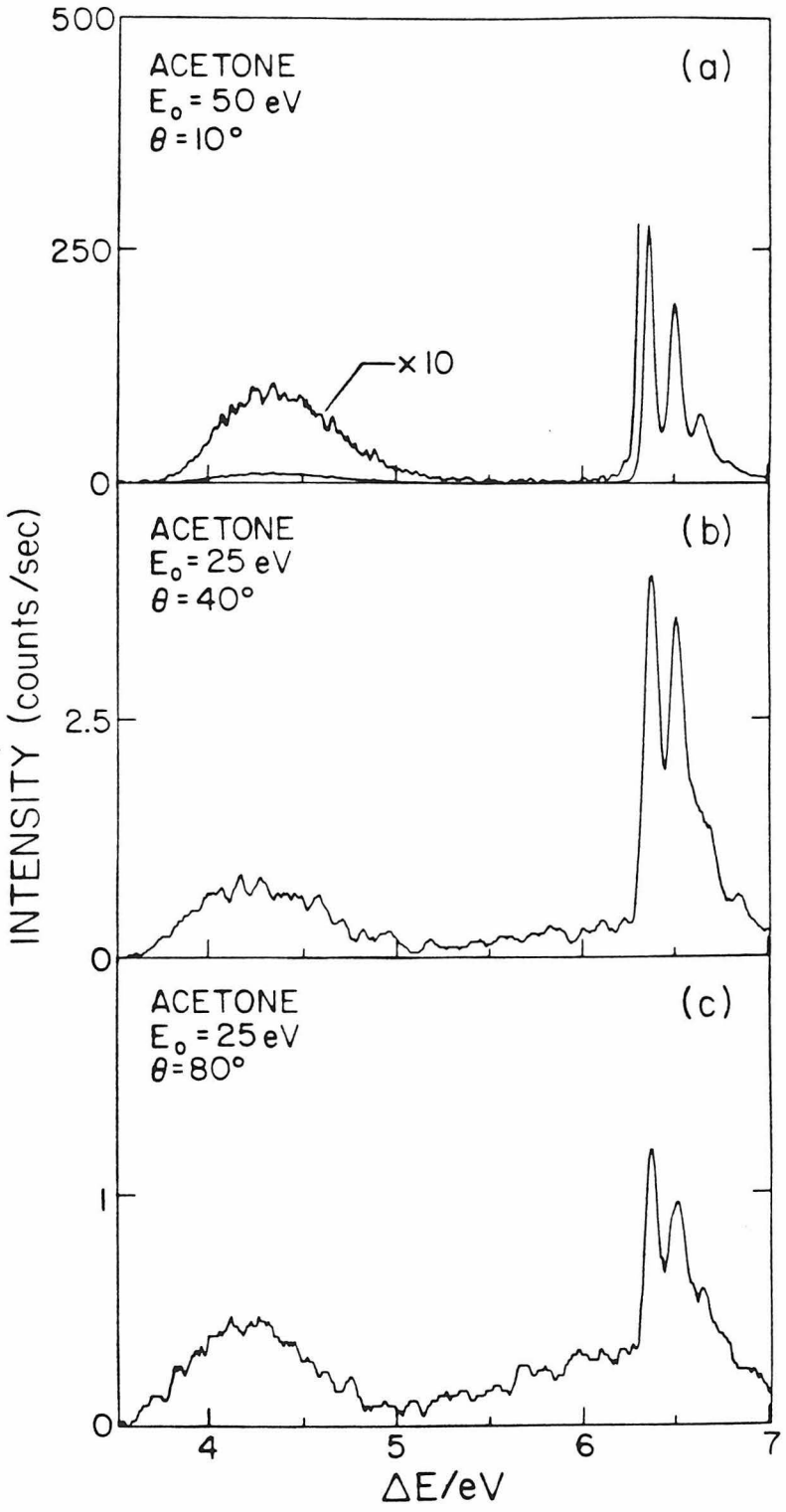
500
250
0
ACETONE
E_0 = 50 eV
θ = 10°
(a)
×10
ACETONE
E_0 = 25 eV
θ = 40°
(b)
2.5
0
ACETONE
E_0 = 25 eV
θ = 80°
(c)
1
0
INTENSITY (counts/sec)
4
5
6
7
ΔE/eV

FIGURE 8.

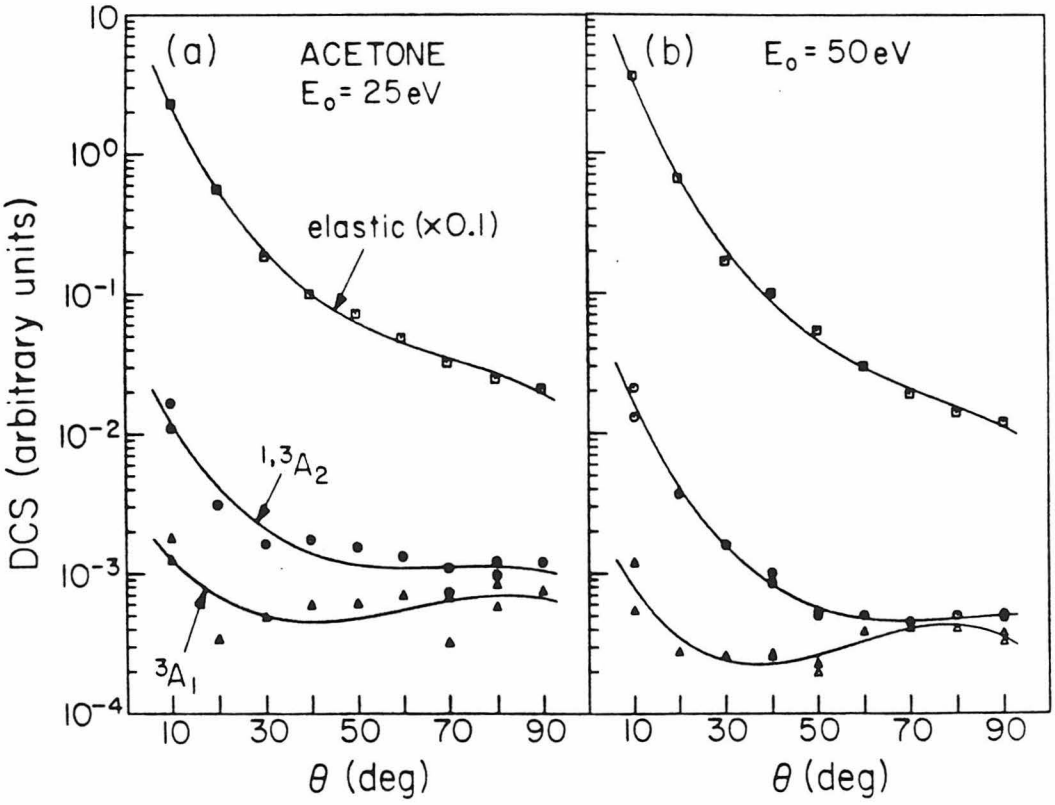
(a)
ACETONE
E_o = 25 eV
elastic (×0.1)
$^{1,3}A_2$
$^3A_1$
(b)
E_o = 50 eV
DCS (arbitrary units)
θ (deg)
θ (deg)
10
10^0
10^{-1}
10^{-2}
10^{-3}
10^{-4}
10
30
50
70
90

FIGURE 9.

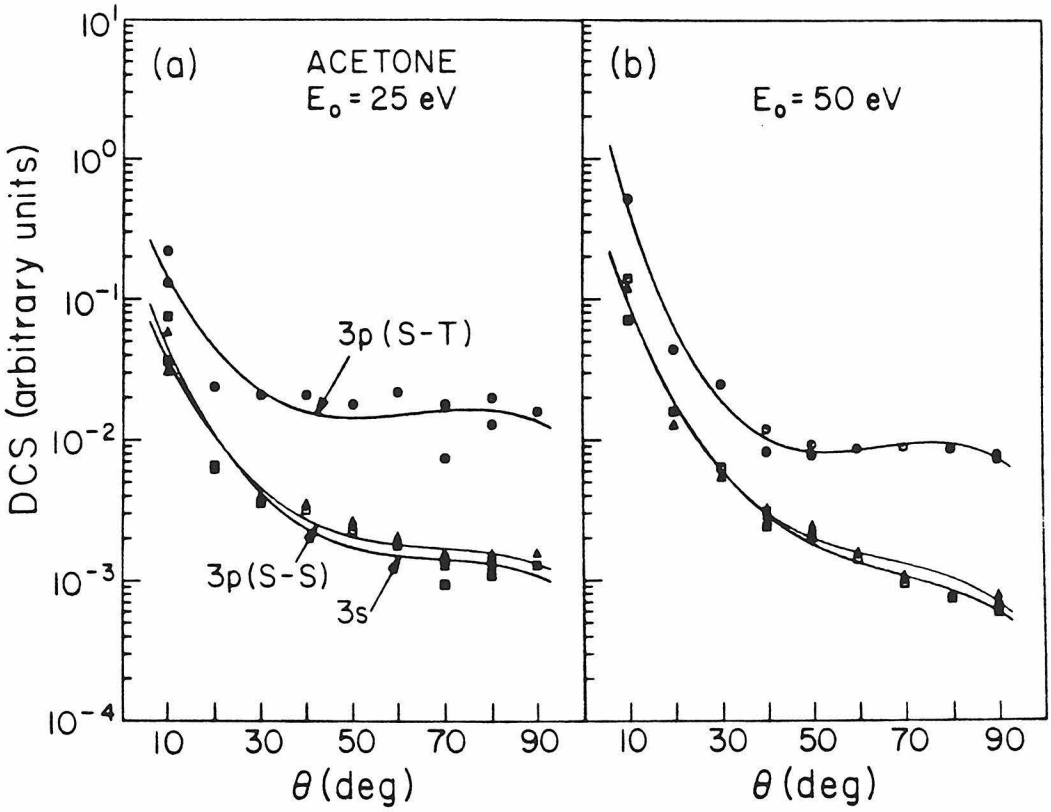
(a)
ACETONE
E_o = 25 eV
(b)
E_o = 50 eV
DCS (arbitrary units)
10^1
10^0
10^{-1}
10^{-2}
10^{-3}
10^{-4}
3p (S-T)
3p(S-S)
3s
10
30
50
70
90
θ (deg)

FIGURE 10.

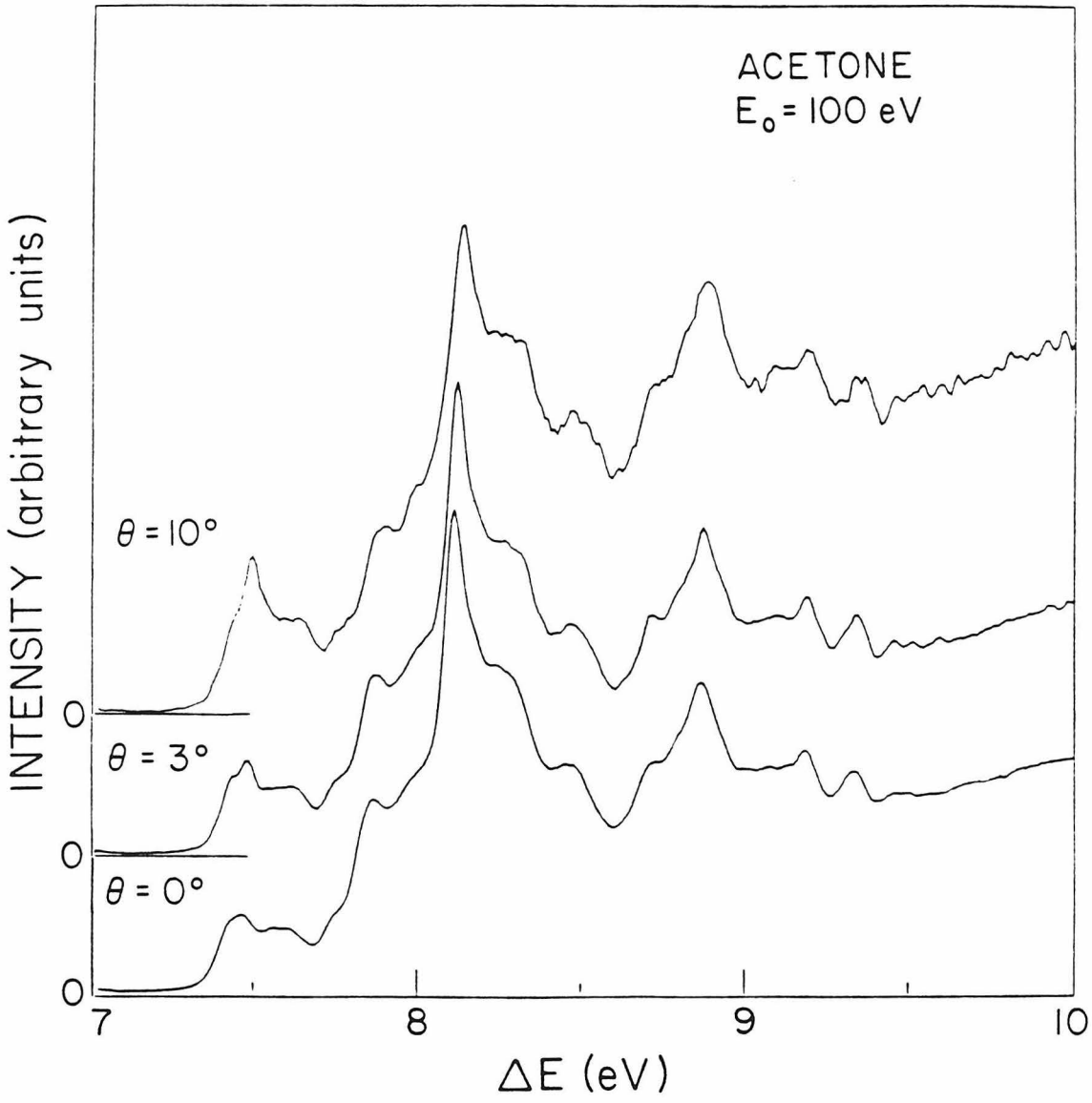
ACETONE
E_o = 100 eV
θ = 10°
θ = 3°
θ = 0°
0
0
0
INTENSITY (arbitrary units)
7
8
9
10
ΔE (eV)

FIGURE 11.

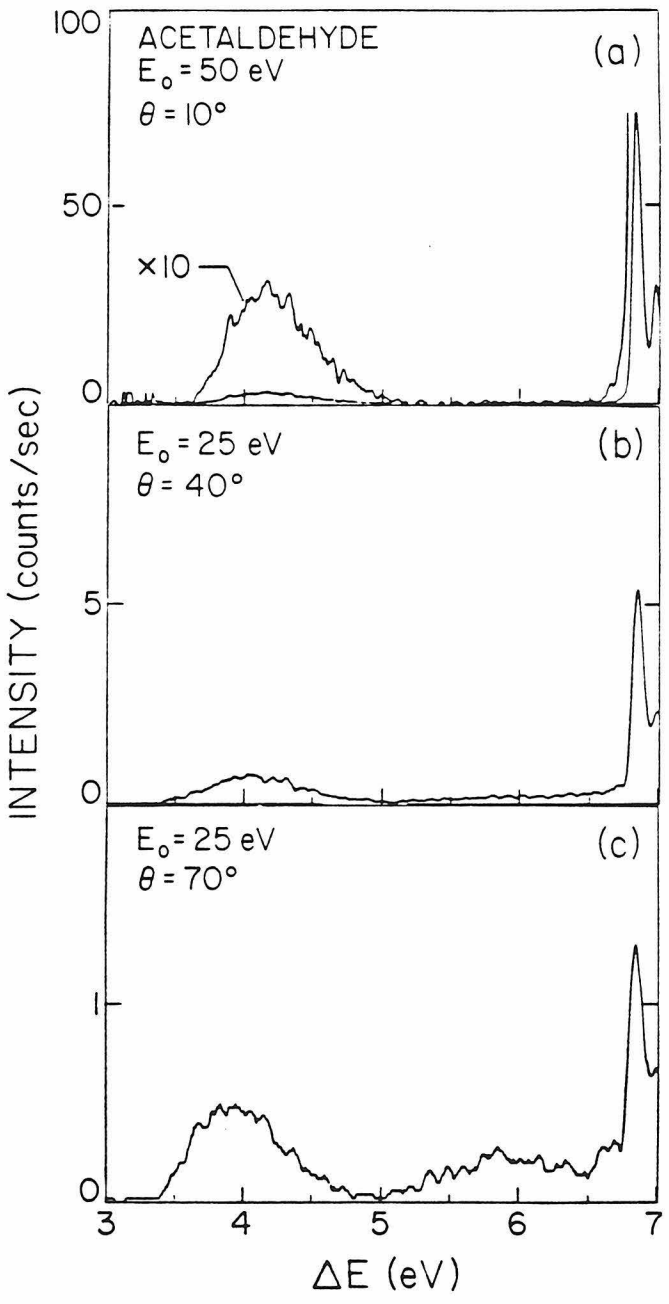
ACETALDEHYDE
E_0 = 50 eV
θ = 10°
(a)
100
50
0
×10
E_0 = 25 eV
θ = 40°
(b)
5
0
E_0 = 25 eV
θ = 70°
(c)
1
0
INTENSITY (counts/sec)
3
4
5
6
7
ΔE (eV)

FIGURE 12.

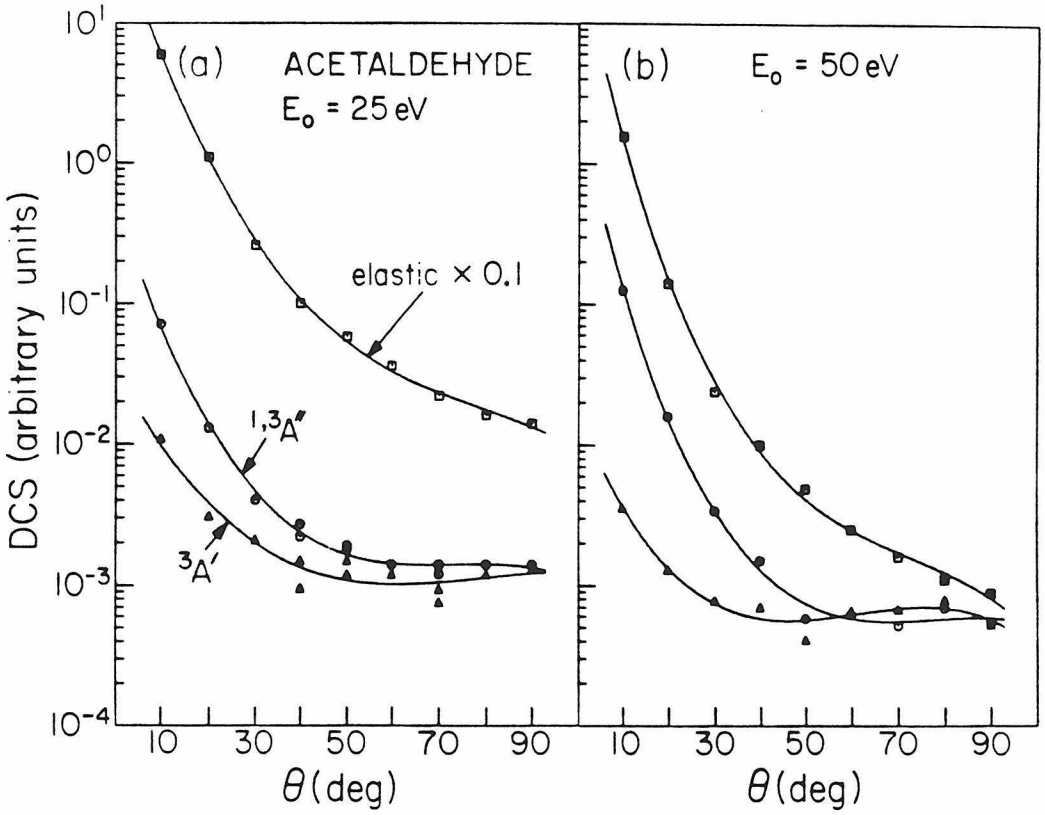
(a)
ACETALDEHYDE
E_o = 25 eV
elastic × 0.1
$^{1,3}A''$
$^{3}A'$
(b)
E_o = 50 eV
DCS (arbitrary units)
10^{1}
10^{0}
10^{-1}
10^{-2}
10^{-3}
10^{-4}
10
30
50
70
90
θ(deg)

FIGURE 13.

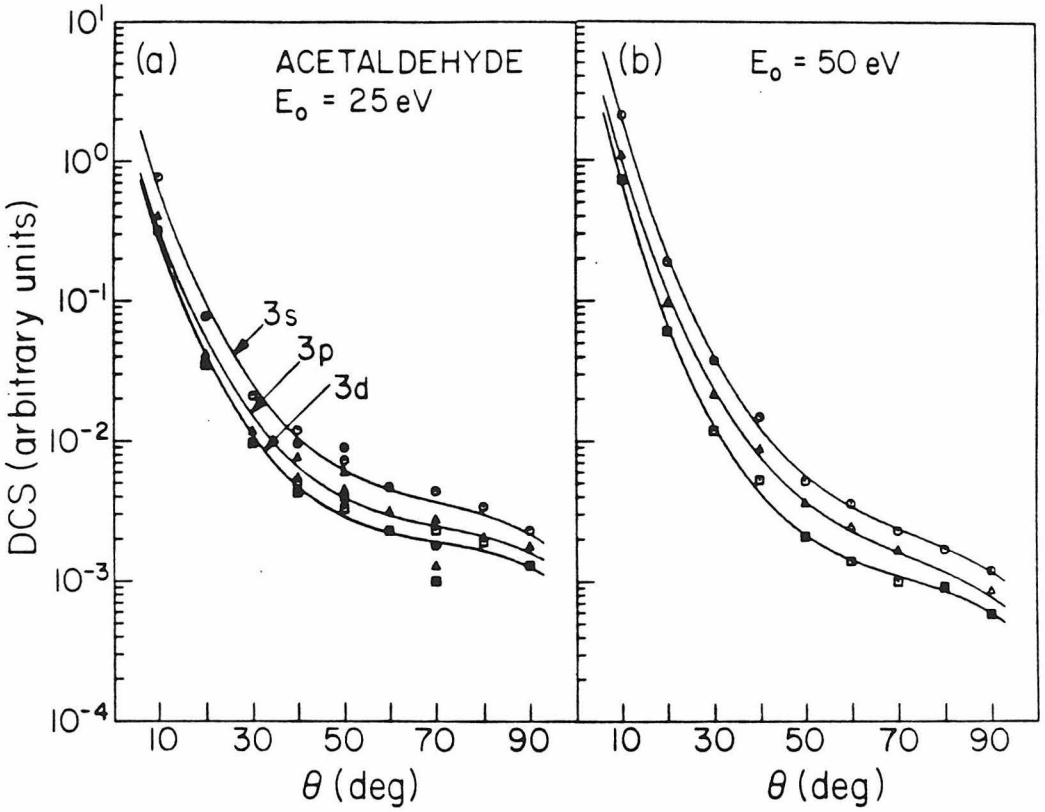
(a)
ACETALDEHYDE
E_o = 25 eV
(b)
E_o = 50 eV
3s
3p
3d
DCS (arbitrary units)
10^1
10^0
10^{-1}
10^{-2}
10^{-3}
10^{-4}
10
30
50
70
90
θ (deg)

FIGURE 14.

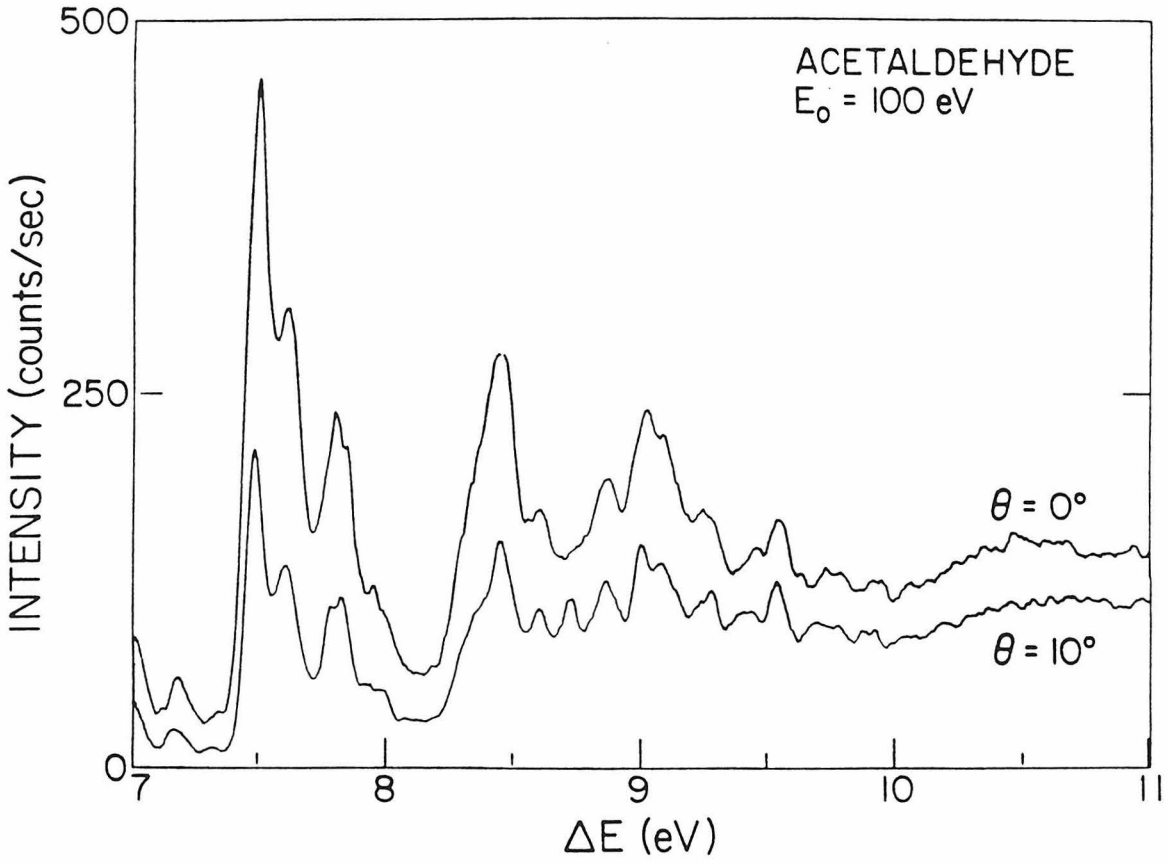
ACETALDEHYDE
E_o = 100 eV
θ = 0°
θ = 10°
INTENSITY (counts/sec)
500
250
0
7
8
9
10
11
ΔE (eV)

FIGURE 15.

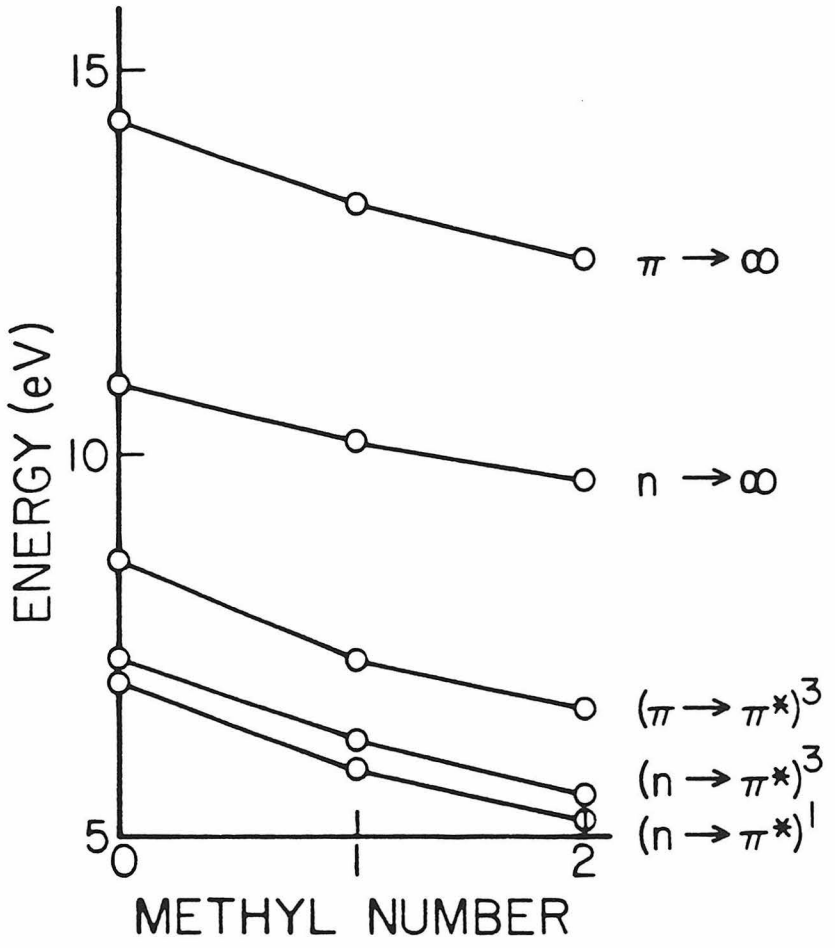

CHAPTER 3

Paper 2: ELECTRON–IMPACT SPECTROSCOPY OF VARIOUS DICARBONYL COMPOUNDS

Electron–Impact Spectroscopy of Various Dicarbonyl Compounds[a]

K. N. Walzl[b], I. M. Xavier Jr.[c], and A. Kuppermann

Arthur Amos Noyes Laboratory of Chemical Physics,[d]

California Institute of Technology, Pasadena, CA 91125

(received)

Abstract

The dicarbonyl compounds biacetyl, acetylacetone, acetonylacetone, 1,2-cyclohexanedione, and 1,4-cyclohexanedione have been studied by the technique of low-energy variable-angle electron energy-loss spectroscopy. With this method low-lying, spin-forbidden transitions have been located and their relative differential cross sections determined. The energy difference between the lowest spin-allowed and spin-forbidden n→ π^* excitations in the acyclic dicarbonyls is found to be nearly the same as that of comparable acyclic monocarbonyl compounds; in 1,2-cyclohexanedione however, this energy difference is almost twice as large. This difference in the magnitude of the n→ π^* singlet-triplet splittings is attributed to a larger overlap of the initial and final orbitals in 1,2-cyclohexanedione compared to the other dicarbonyls.

---

[a] This work was supported in part by the U. S. Department of Energy, Contract No. DE-AM03-76F00767, Project Agreement No. DE-AT03-76ER72004.

[b] Work performed in partial fulfillment of the requirements for the Ph.D. degree in Chemistry at the California Institute of Technology.

[c] On leave from Departamento de Quimica Fundamental; Universidade Federal de Pernambuco; 50000, Recife, Pernambuco; Brazil.

[d] Contribution No.

1. INTRODUCTION

Due to their importance in photochemistry and photophysics, dicarbonyls have been studied extensively by both spectroscopic[1-5] and theoretical[6-9] methods. Dicarbonyl compounds provide useful structures for the study of intramolecular energy transfer, found to be a relevant process in both singlet and triplet excited states[10] and interactions involving remote carbonyl groups.[11] Much work has been performed, primarily photoelectron spectroscopy,[12] in order to identify the mechanism by which carbonyl groups interact with each other. Even though the "through-space" interaction is expected to be small between two carbonyl groups in the same molecule,[8,13] the "through-bond" interaction leads to molecular orbitals with clearly split energies.[14]

In order to more fully understand the nature of the interaction between the carbonyl groups in dicarbonyl compounds it is helpful to have a complete picture of the low-lying electronic states, both allowed and forbidden. With the exception of biacetyl, the low-lying triplet states have not been definitively detected in most larger dicarbonyls. In biacetyl the two lowest singlet-triplet transitions have been observed in fluorescence[2] and by opto-acoustic spectroscopy.[1] Electron-impact spectroscopy is a useful technique for observing and identifying forbidden, especially spin-forbidden, transitions in spectra. Also, spectral features in the far ultraviolet are easily examined. The compounds biacetyl, acetylacetone, acetonylacetone, 1,2-cyclohexanedione, and 1,4-cyclohexanedione were chosen for study as representative samples of such compounds.

2. EXPERIMENTAL

The electron spectrometer and the methods of data accumulation and analysis have been described previously.[15] Briefly, an electron beam is energy selected by

a hemispherical electrostatic energy analyzer (and the associated focusing lenses) and scattered from target vapor in a collision cell. In this work the incident beam current was between 0.5–10 nAmp and was typically 3 nAmp. Sample pressures were estimated to be between 1–10 mtorr. Energy-loss spectra were collected at angles between 0° – 90° by means of a second electrostatic energy analyzer and detector.

The spectrometer resolution (as measured by the full-width at half-maximum of the elastically scattered feature) varied between 50 meV and 125 meV for all reported spectra and was typically 85 meV. Peak locations determined from the spectra have an estimated uncertainty of ±.07 eV and Franck-Condon limits are estimated to be within ±.15 eV.

The relative differential cross sections (DCS's) for the elastic peak and each of several inelastic features were obtained by a previously described method.[16,17] In the case of severely overlapping bands, dividing points for calculating DCS's were chosen at an arbitrary midpoint between the maxima. These cross sections (for a particular compound at a given collision energy) are normalized by setting the value for the elastic peak equal to 1 at the scattering angle 40° . The arbitrary units thus determined are necessarily the same only for a given molecule and impact energy.

Liquid samples of biacetyl (Matheson, Coleman and Bell 97+%), acetylacetone (J. T. Baker 99.7%), acetonylacetone (Aldrich 97%) and 1,2-cyclohexanedione (Aldrich 98%) were subjected to three freeze-pump-thaw cycles and used without further purification. 1,4-Cyclohexanedione (Aldrich 98%), a room temperature solid, was warmed to approximately 50° C during scanning to increase the vapor pressure.

3. RESULTS

2,3-BUTANEDIONE (BIACETYL)

The biacetyl molecule is of C_{2h} symmetry with the two highest occupied molecular orbitals being largely nonbonding and localized on the oxygen atoms. The degeneracy is lifted by the interaction of the two oxygen nonbonding orbitals, n_1 and n_2. The levels arising from the symmetry-adapted linear combinations of these orbitals are designated n_+ and n_-, where $n_\pm = 1/\sqrt{2}\ (n_1 \pm n_2)$. The energy difference is 1.9 eV, with IP1 (n_+, a_g) = 9.55 eV and IP2 (n_-, b_u) = 11.45 eV.[18] For two carbonyl groups bonded directly together the difference in energy between the n_+ and n_- orbitals is found to be relatively independent of torsional angle,[18] implying that the through-bond interaction dominates the through-space interaction even for biacetyl. The next two lower occupied π orbitals have ionization potentials IP(b_g) = 13.20 eV and IP(a_u) = 14.73 eV.[19] The two lowest unoccupied molecular orbitals are analogous to these, being π^* in nature with $\pi^*(b_g)$ higher than $\pi^*(a_u)$.

Figure 1 shows the low energy-loss region of the biacetyl spectrum between 2.0 eV and 7.0 eV at $E_0 = 25$ eV and $\theta = 10°$, $30°$, and $90°$. In the $10°$ spectrum (Figure 1a) one observes two low energy-loss features and a shoulder on the edge of a very intense band at about 7.0 eV. The lowest is the $\tilde{A}\ ^1A_u \leftarrow \tilde{X}\ ^1A_g$ transition with an onset at 2.67 eV, maximum at 2.91 eV, and extending to 3.45 eV.[20] Lying between 3.82 eV and 5.28 eV with a maximum at 4.49 eV is a transition that recent results indicate should be designated $\tilde{B}\ ^1B_g \leftarrow \tilde{X}\ ^1A_g$.[6] The broadness of this band may be due to the presence of an enolic $\pi \rightarrow \pi^*$ excitation.[21] The sharp peak at 6.24 eV is the first 3s member of an s Rydberg series converging to the lowest ionization potential, IP = 9.53 eV. As the scattering angle is increased three spin-forbidden features become apparent (Figure 1b, 1c). The lowest,

overlapping greatly with the $\tilde{A}\ ^1A_u \leftarrow \tilde{X}\ ^1A_g$ band, has an onset at 2.28 eV and a maximum at 2.54 eV. It is attributed to a combination of the $\tilde{a}\ ^3B_u \leftarrow \tilde{X}\ ^1A_g$ spin-forbidden excitation,[1] previously seen in fluorescence experiments,[2] and a $^3A_u \leftarrow ^1A_g$ excitation,[20] the latter being the dominant contributor. A second spin-forbidden band is seen in the region between 5 eV to 6 eV with a maximum at 5.47 eV. Calculations place several $\pi \rightarrow \pi^*$ spin-forbidden transitions in this region,[6,22] particularly a $^3B_u \leftarrow ^1A_g$ excitation predicted to be at 5.56 eV.[22] A last relatively sharp feature is observed at 5.80 eV and seems to be identifiable as the spin-forbidden counterpart of the 3s Rydberg excitation. The DCS curves for the valence bands are given in Figure 2. Due to the great deal of band overlap, all the 25 eV curves show spin-forbidden behavior while the 50 eV curves exhibit the expected spin-allowed/spin-forbidden distinction.

The spectral region extending from 5 eV to 10 eV (just beyond the lowest IP) is shown in Figure 3 under the optical conditions $E_0 = 100$ eV and $\theta = 3°$. All the transitions observed appear to be Rydberg in nature and indeed members of three series can be distinguished. Peaks at 6.24, 8.05, and 8.70 eV can be fit as the first three members of an s Rydberg series with a quantum defect $\delta = 0.97$. The s members are now much weaker than in the 25 eV spectra due to the fact that the $n_g \rightarrow$3s transition is parity forbidden by dipole selection rules. The first two members of a p series at 7.21 eV and 8.42 eV are fit with $\delta = 0.58$ and a feature at 7.72 eV is assigned to a 3d excitation. Transitions at 6.28 eV and 7.20 eV have been observed previously by Ells.[3]

2,4-PENTANEDIONE (ACETYLACETONE)

As a room temperature vapor, acetylacetone consists of two structural isomers. One is the expected diketo molecular structure; however, acetylacetone exists predominantly as an enol.[23,24] In the diketo form the two highest occupied

molecular orbitals have mostly oxygen nonbonding character and are labeled n_- (IP = 9.60 eV) and n_+ (IP = 10.15 eV).[23] The highest occupied molecular orbitals in the enol compound are of π type (IP = 9.00 eV) and nonbonding type (IP = 9.60 eV).[25]

In Figure 4 are shown spectra of acetylacetone between 3.0 eV and 6.0 eV energy loss at E_0 = 25 eV and θ = 10° , 30° , and 90° . At 10° (Figure 4a) one sees a very strong band between 4.10 eV and 5.73 eV with a maximum at 4.70 eV. It is identified with the lowest spin-allowed $\pi \rightarrow \pi^*$ transition in the enol molecule.[24] One also observes a weak band with an onset at 3.83 eV and maximum at 4.04 eV due to the first spin-allowed $n \rightarrow \pi^*$ band in the acetylacetone diketo form.[7,24,26] An increase in scattering angle (Figure 4b, 4c) reveals the presence of a spin-forbidden transition beginning at 3.15 eV with a maximum at 3.57 eV and overlapping with the diketo $n \rightarrow \pi^*$ (S–S) band. This feature can either be attributed to a $\pi \rightarrow \pi^*$ (S–T) excitation in the acetylacetone enol or possibly a $n \rightarrow \pi^*$ (S–T) excitation in the acetylacetone keto form. The DCS curves at E_0 = 25 eV and 50 eV for these three valence transitions are given in Figure 5. An additonal spin-forbidden excitation is evident at 5.52 eV and is assigned as a singlet-triplet 3s Rydberg excitation in the enol.

The 3.5 eV to 8.5 eV energy-loss region of the spectrum measured at E_0 = 100 eV and θ = 10° is shown in Figure 6. All the structure above 5.5 eV is due to Rydberg transitions converging to the first IP of the enol. Indeed, peaks at 5.84 eV and 7.50 eV are the first two members of an s series with δ = 0.93, peaks at 6.52 eV and 7.75 eV are the first members of a p series with δ = 0.66, and peaks at 7.32 eV and 8.10 eV are the first members of a d series with δ = 0.15. This disagrees with the assignment of Nakanishi *et al.*[27] who observed transitions at 7.4 eV and 8.08 eV and assigned the former as a valence $\pi \rightarrow \pi^*$ excitation and the latter as a valence $\sigma \rightarrow \sigma^*$ excitation.

2,5-HEXANEDIONE (ACETONYLACETONE)

The similarity between the ultraviolet absorption of 1,4-diketones and their corresponding monoketones is striking, suggesting that the two carbonyl groups in the dicarbonyls can be considered isolated in the ground and first excited states.[10] In fact, Schippers and Dekkers,[13] using a simple electrostatic model,[28] calculated that the splitting of the n$\rightarrow \pi^*$ levels should only be 50 cm^{-1} . This calculation results in an underestimate of the splitting, however, because it neglects any through-bond interaction. Indeed, Dougherty *et al.*[12] using photoelectron spectroscopy found that for the (limited) group of 1,4-dicarbonyls they investigated the mean splitting of the nonbonding orbitals was 0.3 eV. This splitting is still relatively small, explaining why Schippers and Dekkers[11] found that the spectra of certain rigid, cyclic 1,4-diketones were equivalent to that of the complementary monoketones except that the diketone spectra were approximately twice as intense.

The region of the acetonylacetone spectrum between 2.5 eV and 6.5 eV is displayed in Figure 7. At E_0 = 25 eV and θ = 10° (Figure 7a) one observes two broad bands and the onset of a third. The lowest, between 3.97 eV and 5.15 eV with a maximum at 4.40 eV, can be assigned with confidence as the spin-allowed n$\rightarrow \pi^*$ excitation. The second band onsets at 5.34 eV and possesses a maximum at 5.85 eV. Since the splitting between n,π^* states is expected to be very small, an assignment for this band is the lowest $\pi \rightarrow \pi^*$ (S–S) excitation. This transition is not observed in the smaller monoketones but expected to be at a relatively high energy-loss (~9.0 eV) superimposed by Rydberg bands.[29] The large peak beginning about 6.2 eV is the n$\rightarrow$3s Rydberg excitation (*vide infra*). Increasing the scattering angle to 30° and 90° (Figure 7b, 7c) produces two changes. The first is an apparent change in the onset and maximum of the spin-allowed n$\rightarrow \pi^*$ transition to 3.55 eV and 4.16 eV respectively. As discussed

previously this is due to the superposition of a relatively enhanced spin-forbidden n$\rightarrow \pi^*$ transition. The second spectral change is the relative increase in intensity in the region between 5.15 eV to 5.34 eV and is caused by a singlet-triplet contribution. A definitive band maximum is not obtained from the spectra. The behaviors of the DCS curves for these valence excitations (Figure 8) support the conclusion of underlying spin-forbidden bands in this region of the spectrum.

The Rydberg portion of the acetonylacetone spectrum is included in Figure 9, which was measured under the optical conditions $E_0 = 100$ eV and $\theta = 10°$ and spans the energy-losses between 3.5 eV and 8.5 eV. Peaks are observed at 6.62, 7.49, and 8.17 eV. Assuming the transition at 6.62 eV corresponds to the n$\rightarrow$3s excitation, the transition at 7.49 eV to the n$\rightarrow$3p excitation, and the transition at 8.17 eV to the n$\rightarrow$3d excitation, the best fit to previously measured ketone (and diketone) quantum defects[29] is found using an ionization potential IP = 9.95 eV. Specifically, for an IP = 9.95 eV one calculates δ (n$\rightarrow$3s) = 0.98, δ (n$\rightarrow$3p) = 0.65, and δ (n$\rightarrow$3d) = 0.24. An additional peak was observed at 8.84 eV and is possibly due to an overlapping combination of n$\rightarrow$4s, 4p, and 4d transitions.

1,2-CYCLOHEXANEDIONE

Even though 1,2-cyclohexanedione is exclusively in the ketonic form in the solid state,[30] it exists to a large extent in the enolic form in solution.[31] Calculations indicate that it may be primarily enolic in the gas phase as well.[32] Figure 10 shows spectra in the energy-loss region between 2.5 eV and 6.0 eV at $E_0 = 50$ eV, $\theta = 10°$, 30° and $E_0 = 25$ eV, $\theta = 50°$. The similarity between the spectrum of acetylacetone and 1,2-cyclohexanedione in this energy-loss region is striking. At $E_0 = 50$ eV and $\theta = 10°$ (Figure 10a) one sees an intense band between 4.34 eV and 5.70 eV with a maximum at 4.84 eV. As with acetylacetone, this band is

assigned to the lowest spin-allowed $\pi \rightarrow \pi^*$ enol transition. The weak band with an onset at 3.69 eV and maximum at 4.02 eV is due to the lowest spin-allowed $n \rightarrow \pi^*$ transition of the ketonic form. Even though the orientation of the carbonyl groups is different than in biacetyl , one expects nearly the same energy difference (1.9 eV) between the n_+ and n_- orbitals because of the dominance of the through-bond interaction.[18] Thus the second lowest spin-allowed $n \rightarrow \pi^*$ transition should be at approximately 5.9 eV and obscured by enol Rydberg bands. An increase in scattering angle and decrease in incident electron energy (Figure 10b, 10c) reveals the presence of a spin-forbidden band beginning at 2.70 eV with a maximum at 3.18 eV assigned as the lowest $n \rightarrow \pi^*$ (S–T) excitation of the ketonic form. The DCS curves for these valence transitions (Figure 11) confirm their spin-allowed or spin-forbidden nature.

The higher energy-loss region, between 4 eV to 10 eV, at $E_0 = 100$ eV and $\theta = 10°$ is shown in Figure 12. Only three distinct Rydberg bands are evident, located at 6.10, 6.92, and 7.48 eV. An ionizaton potential IP = 9.40 eV is determined if one assumes the three bands are due to transitions to the 3s, 3p, and 3d orbitals and also assumes quantum defects $\delta = 0.97$, 0.66, and 0.34 respectively.

1,4-CYCLOHEXANEDIONE

1,4-Cyclohexanedione has D_2 symmetry (a "twist" configuration[33]) with coaxial carbonyl groups. Through-space interactions provide a minimum contribution, thus the splitting of the two highest occupied nonbonding orbitals is relatively small (0.2 eV) when compared to that in other 1,4-diketones,[12,18] with the measured ionization potentials being $IP(n_-) = 9.65$ eV and $IP(n_+) = 9.85$ eV.[12]

Figure 13 shows the 3.0 eV to 6.5 eV energy-loss region of the 1,4-cyclohexanedione spectrum at $E_0 = 50$ eV, $\theta = 5°$ and $E_0 = 25$ eV, $\theta = 35°$. The low intensity of the spectra arises from the relatively low sample pressure

achieved for this compound ($\sim$ 2 mtorr). Under optical conditions (Figure 13a) one observes a band with an onset at 3.73 eV and a maximum at 4.68 eV. This is due to the n$\rightarrow \pi^*$,^{1}A$\leftarrow ^1$A dipole symmetry-forbidden transition and has been seen previously in solution (maximum = 4.34 eV)[34] and low-temperature single crystals (onset = 3.89 eV, maximum = 4.40 eV).[35] The onset of a broad band, which appears to be superimposed by a 3s Rydberg transition, is observed at 5.66 eV and may be due to the $\pi \rightarrow \pi^*$,^{1}B$_1$ $\leftarrow ^1$A excitation. When the incident energy is lowered and the scattering angle increased (Figure 13b) the n$\rightarrow \pi^*$,^{3}A$\leftarrow ^1$A transition becomes evident, onsetting at 3.20 eV and maximizing at 4.13 eV. The presence of another spin-forbidden band with maximum at 5.78 eV is indicated. Contributions to the intensity may come from either the $\pi \rightarrow \pi^*$,^{3}B$_1$ $\leftarrow ^1$A excitation or the n$\rightarrow$3s (S–T) Rydberg excitation.

The 1,4-cyclohexanedione spectrum under optical conditions (Figure 13a) is extended to 10 eV energy-loss in Figure 14. Main peaks are observed at 6.58, 7.36, and 7.95 eV. (The peak at 6.67 eV is due to an Hg impurity in the vacuum system.) Using an IP = 9.75 eV, the mean of IP(n$_-$) and IP(n$_+$),[12] assignments and quantum defects of n$\rightarrow$3s (δ = 0.93) at 6.58 eV, n$\rightarrow$3p (δ = 0.61) at 7.36 eV, and n$\rightarrow$3d (δ = 0.25) at 7.95 eV are determined.

4. DISCUSSION AND CONCLUSIONS

As one might expect from previous results,[10] the energies of the lowest n$\rightarrow \pi^*$ excitations for the acyclic dicarbonyls, as the distance between carbonyl groups increases, approach those of acetone. The lowest spin-allowed and spin-forbidden n$\rightarrow \pi^*$ excitations are 2.91 eV and 2.54 eV for biacetyl , 4.04 eV and 3.57 eV for acetylacetone , 4.40 eV and 4.16 eV for acetonylacetone , and 4.38 eV and 4.18 eV for acetone.[29,36] The values for these transitions in 1,4-

cyclohexanedione are also comparable, the lowest singlet-singlet and singlet-triplet $n \rightarrow \pi^*$ excitations being 4.68 eV and 4.13 eV respectively. This behavior appears to hold also for the lowest spin-forbidden $\pi \rightarrow \pi^*$ excitation, at least as regards the band onsets; the onset is 5.15 eV for both acetonylacetone and acetone. The band maximum could not be determined for acetonylacetone .

The mean value for the singlet-triplet splitting of the n,π^* state in the acyclic dicarbonyls examined in this paper is 0.35 eV, a splitting comparable to the mean value of 0.30 eV for small monocarbonyls such as formaldehyde, acetaldehyde, and acetone.[29] A remarkable contrast is provided by 1,2-cyclohexanedione, in which the singlet-triplet splitting for the n,π^* state is 0.84 eV. The singlet-triplet energy difference for a given electron orbital configuration results from the stronger correlation of electron motions in the triplet state than in the singlet state; i.e., the Pauli principle acts as a force minimizing electron-electron repulsion in the triplet state.[37] A simple qualitative analysis[38] reveals that the magnitude of the singlet-triplet energy splitting is proportional to the overlap (integral) of the initial and final orbitals. For a single carbonyl group the highest occupied nonbonding orbital is analogous to an oxygen p_y orbital (Figure 15a) and is oriented such that there is minimum overlap with the π and π^* orbitals. This small n,π^* overlap also applies to the case of biacetyl . The highest occupied n orbital and lowest unoccupied π^* orbital are linear combinations of the corresponding isolated orbitals; however, since the carbonyl groups are oriented in a trans arrangement (Figure 15b), the overlap is still small. In 1,2-cyclohexanedione a different orientation exists, due to the constraint imposed by the ring (Figure 15c). The overlap of the highest occupied n orbital with the lowest unoccupied π^* orbital is now larger, thus the n,π^* singlet-triplet splitting is larger.

In summary, the low-energy variable-angle electron energy-loss spectroscopy of five dicarbonyl compounds with varying carbonyl separations and orientations

has been investigated. The increase in the number of bands compared to the monocarbonyls is in accord with the splitting caused by the through-bond interaction of like orbitals. Low-lying, spin-forbidden excitations have been observed and, in the case of 1,2-cyclohexanedione, a very large singlet-triplet splitting arises from increased overlap of initial and final orbitals.

References

1. K. Kaya, W. R. Harshbarger, and M. Robin, *J. Chem. Phys.* **60**, 4231 (1974).
2. G. M. Almy, H. Q. Fuller, and G. D. Kinzer, *J. Chem. Phys.* **8**, 37 (1940).
3. V. R. Ells, *J. Amer. Chem. Soc.* **60**, 1864 (1938).
4. J. W. Sidman and D. S. McClure, *J. Amer. Chem. Soc.* **77**, 6461 (1955).
5. G. Porter and M. W. Windsor, *Proc. Roy. Soc.* **A245**, 238 (1958).
6. T. -K. Ha, *Chem. Phys. Lett.* **57**, 64 (1978).
7. G. S. Hammond, W. G. Borduin, and G. A. Guter, *J. Amer. Chem. Soc.* **81**, 4682 (1959).
8. D. J. Pasto, D. M. Chipman, and J. J. Worman, *J. Phys. Chem.* **86**, 3981 (1982).
9. R. Hoffmann *Acc. Chem. Res.* **4**, 1 (1971).
10. E. A. Lissi, M. V. Encinas, F. Castañeda, and F. A. Olea, *J. Phys. Chem.* **84**, 251 (1980).
11. P. H. Schippers and H. P. Dekkers, *J. Amer. Chem. Soc.* **105**, 145 (1983).
12. D. Dougherty, P. Brint, and S. P. McGlynn, *J. Amer. Chem. Soc.* **100**, 5597 (1978).
13. P. H. Schippers and H. P. Dekkers, *J. Chem. Soc. P2* **1982**, 1429 (1982).
14. R. Hoffmann, E. Heilbronner, and R. Gleiter, *J. Amer. Chem. Soc.* **92**, 706 (191970).
15. C. F. Koerting, Ph. D. Thesis, California Institute of Technology, Pasadena CA (1985) and references therein.
16. O. A. Mosher, W. M. Flicker, and A. Kuppermann, *J. Chem. Phys.* **59**, 6502 (1973).
17. O. A. Mosher, M. S. Foster, W. M. Flicker, A. Kuppermann, and

J. L. Beauchamp, *J. Chem. Phys.* **62**, 3424 (1975).

18. D. O. Cowan, R. Gleiter, J. Hashmall, E. Heilbronner, and V. Hornung, *Angew. Chem. Internat. Ed.* **10**, 401 (1971).
19. S. P. McGlynn and J. L. Meeks, *J. Electron Spectroscopy* **6**, 269 (1975).
20. G. Herzberg, *Electronic Spectra of Polyatomic Molecules* (Van Nostrand Reinhold Co., New York (1966)), p. 667.
21. D. Ben-Amotz and I. Y. Chan, *J. Phys. Chem.* **86**, 2428 (1982).
22. J. M. LeClercq, C. Mijoule, and P. Yvan, *J. Chem. Phys.* **64**, 1464 (1976).
23. J. Powling and H. J. Bernstein, *J. Amer. Chem. Soc.* **73**, 4553 (1951).
24. H. Nakanishi, H. Morita, and S. Nagakura, *Bull. Chem. Soc. Jap.* **50**, 2255 (1977).
25. A. Schweig, H. Vermeer, and U. Weidner, *Chem. Phys. Lett.* **26**, 229 (1974).
26. R. S. Rasmussen, D. D. Tunnidiff, and R. R. Brattain, *J. Amer. Chem. Soc.* **71**, 1068 (1949).
27. H. Nakanishi, H. Morita, and S. Nagakura, *Bull. Chem. Soc. Jap.* **51**, 1723 (1978).
28. F. London, *J. Phys. Chem.* **46**, 305 (1942).
29. K. N. Walzl, C. F. Koerting, and A. Kuppermann, to be submitted.
30. C. Duval and J. Lecomte, *Compt. Rend.* **254**, 36 (1962).
31. G. Schwarzenbach and C. Wittwer, *Helv. Chim. Acta* **30**, 663 (1947).
32. W. E. Noack, *Theo. Chem. Acta* **53**, 101 (1979).
33. P. Dowd, T. Dyke, and W. Klemperer, *J. Amer. Chem. Soc.* **92**, 6327 (1970).
34. K. Ozeki, M. Inagaki, and J. Tanaka, *Bull. Chem. Soc. Jap.* **42**, 3076 (1969).

35. K. Ozeki and J. Tanaka, *Bull. Chem. Soc. Jap.* **42**, 3390 (1969).

36. W. M. St. John, R. C. Estler, and J. P. Doering, *J. Chem. Phys.* **61**, 763 (1974).

37. N. J. Turro, *Modern Molecular Photochemistry* (The Benjamin/Cummings Publishing Co., Menlo Park (1978)), pp. 28–32.

38. S. P. McGlynn, F. J. Smith, and G. Cilento, *Photochem. Photobio.* **3**, 269 (1964).

Figure Captions

1. 2,3-Butanedione energy-loss spectra at an incident electron energy E_0 = 25 eV and scattering angles: a) $\theta = 10°$, b) $\theta = 30°$, and c) $\theta = 90°$. Incident electron current = 2 nAmp. Spectra are multiplied by any indicated expansion factors before plotting.

2. 2,3-Butanedione valence band DCS curves (integrated over the range given): a) E_0 = 25 eV, b) E_0 = 50 eV. $\square$ = elastic peak (EP) $\times 0.1$, $\diamond = {}^3B_u \leftarrow {}^1A_g \times 10$ (5.29 eV to 5.90 eV), $+ = {}^3A_u \leftarrow {}^1A_g$ and ${}^3B_u \leftarrow {}^1A_g \times 10$ (2.28 eV to 2.67 eV), $\triangle = \tilde{B}\ {}^1B_g \leftarrow \tilde{X}\ {}^1A_g$ (3.82 eV to 5.28 eV), and $\bigcirc = \tilde{A}\ {}^1A_u \leftarrow \tilde{X}\ {}^1A_g$ (2.67 eV to 3.46 eV). Curves are multiplied by any indicated expansion factors before plotting.

3. 2,3-Butanedione energy-loss spectrum between 5.0 eV and 10.0 eV at E_0 = 100 eV and $\theta = 3°$. The peak at 6.67 eV is due to an Hg contamination in the vacuum system.

4. 2,4-Pentanedione energy-loss spectra at an incident energy E_0 = 25 eV and scattering angles: a) $\theta = 10°$, b) $\theta = 30°$, c) $\theta = 90°$. Incident electron current = 2 nAmp.

5. 2,4-Pentanedione valence band DCS curves: a) E_0 = 25 eV, b) E_0 = 50 eV. $\square$ = EP $\times 0.1$, $+$ = enol $\pi \rightarrow \pi^*$ (S–S) (4.10 eV to 5.73 eV), $\triangle$ = diketone $n \rightarrow \pi^*$ (S–S) $\times 10$ (3.83 eV to 4.10 eV), $\bigcirc$ = diketone $n \rightarrow \pi^*$ (S–T) $\times 10$ (3.15 eV to 3.83 eV).

6. 2,4-Pentanedione energy-loss spectrum between 3.5 eV and 8.5 eV at E_0 = 100 eV and $\theta = 10°$.

7. 2,5-Hexanedione energy-loss spectra at an incident energy E_0 = 25 eV and scattering angles: a) $\theta = 10°$, b) $\theta = 30°$, and c) $\theta = 90°$. Incident electron current = 4 nAmp.

8. 2,5-Hexanedione valence band DCS curves: a) $E_0 = 25$ eV, b) $E_0 = 50$ eV. $\square$ = EP $\times 0.1$, $\triangle$ = n$\rightarrow \pi^*$ (S–S) $\times 10$ (4.16 eV to 5.15 eV), $\bigcirc$ = n$\rightarrow \pi^*$ (S–T) $\times 10$ (3.55 eV to 4.16 eV), $\blacksquare$ = $\pi \rightarrow \pi^*$ (S–S) (5.34 eV to 6.2 eV), $+$ = $\pi \rightarrow \pi^*$ (S–T) (5.15 eV to 5.34 eV).

9. 2,5-Hexanedione energy-loss spectrum between 3.5 eV and 8.5 eV at $E_0 =$ 100 eV and $\theta = 10°$.

10. 1,2-Cyclohexanedione energy-loss spectra at: a) $E_0 = 50$ eV and $\theta = 10°$, b) $E_0 = 50$ eV and $\theta = 30°$, and c) $E_0 = 25$ eV and $\theta = 50°$. Incident electron current = 0.5 nAmp.

11. 1,2-Cyclohexanedione valence band DCS curves: a) $E_0 = 25$ eV, b) $E_0 =$ $50°$. $\square$ = EP $\times 0.1$, $+$ = enol $\pi \rightarrow \pi^*$ (S–S) (4.34 eV to 5.7 eV), $\triangle$ = diketone n$\rightarrow \pi^*$ (S–S) (3.69 eV to 4.34 eV), $\bigcirc$ = diketone n$\rightarrow \pi^*$ (S–T) (2.70 eV to 3.68 eV).

12. 1,2-Cyclohexanedione energy-loss spectrum between 4.0 eV and 10.0 eV at $E_0 = 100$ eV and $\theta = 10°$.

13. 1,4-Cyclohexanedione energy-loss spectra at: a) $E_0 = 50$ eV, $\theta = 5°$ and b) $E_0 = 25$ eV, $\theta = 35°$. Incident electron current = 5 nAmp.

14. 1,4-Cyclohexanedione energy-loss spectrum between 3.0 eV and 10.0 eV at $E_0 = 50$ eV and $\theta = 5°$.

15. a) Orientation of the n and π^* orbitals for an isolated carbonyl group; the xz-plane is the plane of the page. b) Orientation of the two interacting nonbonding orbitals (n_1 and n_2) in biacetyl; The π^* orbitals are oriented with respect to the axes as in a). c) Approximate orientation of the π^* and n′ orbitals in 1,2-cyclohexanedione .

FIGURE 1.

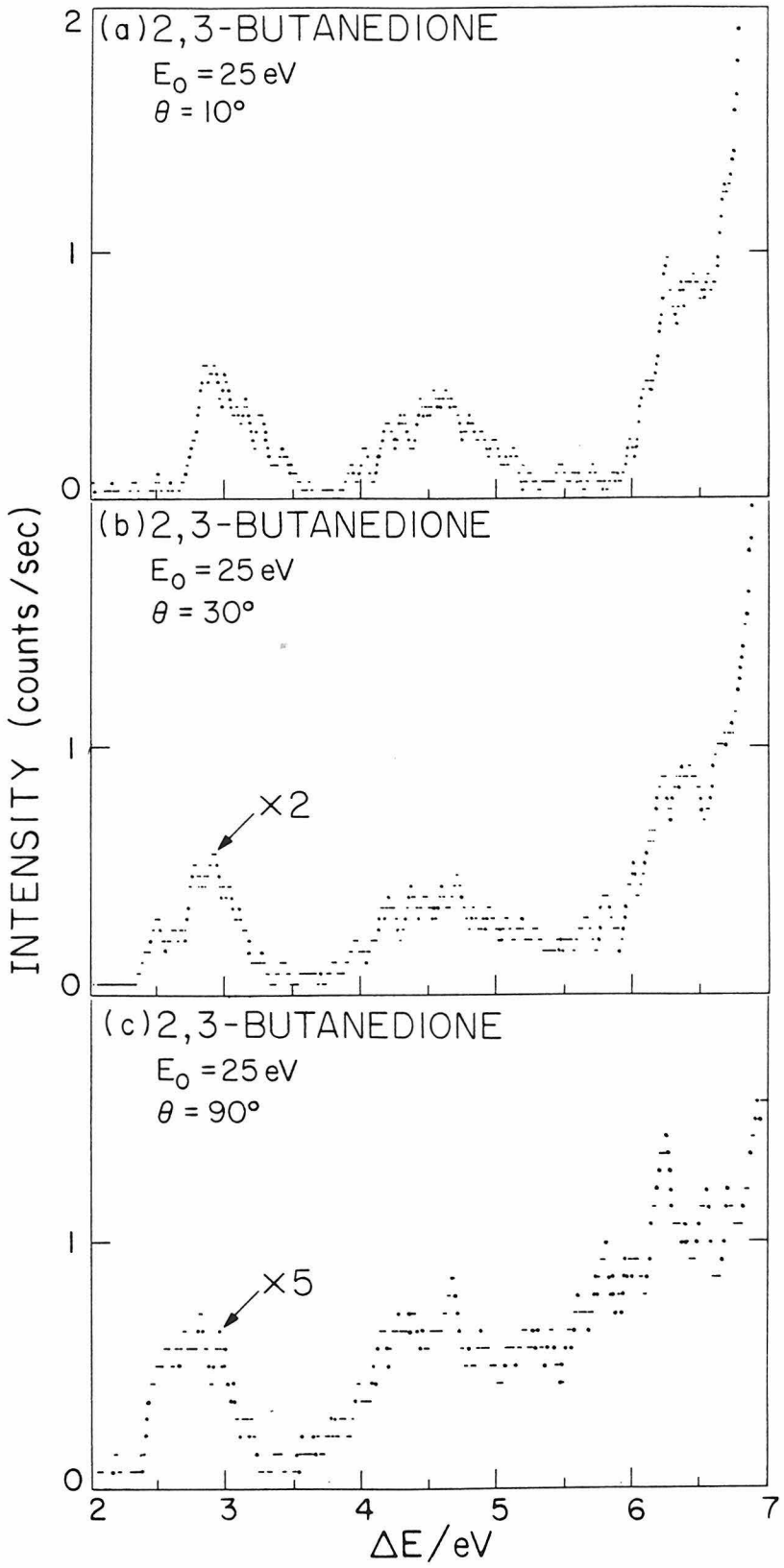
(a)2,3-BUTANEDIONE
E_0 = 25 eV
θ = 10°
(b)2,3-BUTANEDIONE
E_0 = 25 eV
θ = 30°
×2
(c)2,3-BUTANEDIONE
E_0 = 25 eV
θ = 90°
×5
INTENSITY (counts/sec)
ΔE/eV
0
1
2
3
4
5
6
7

FIGURE 2.

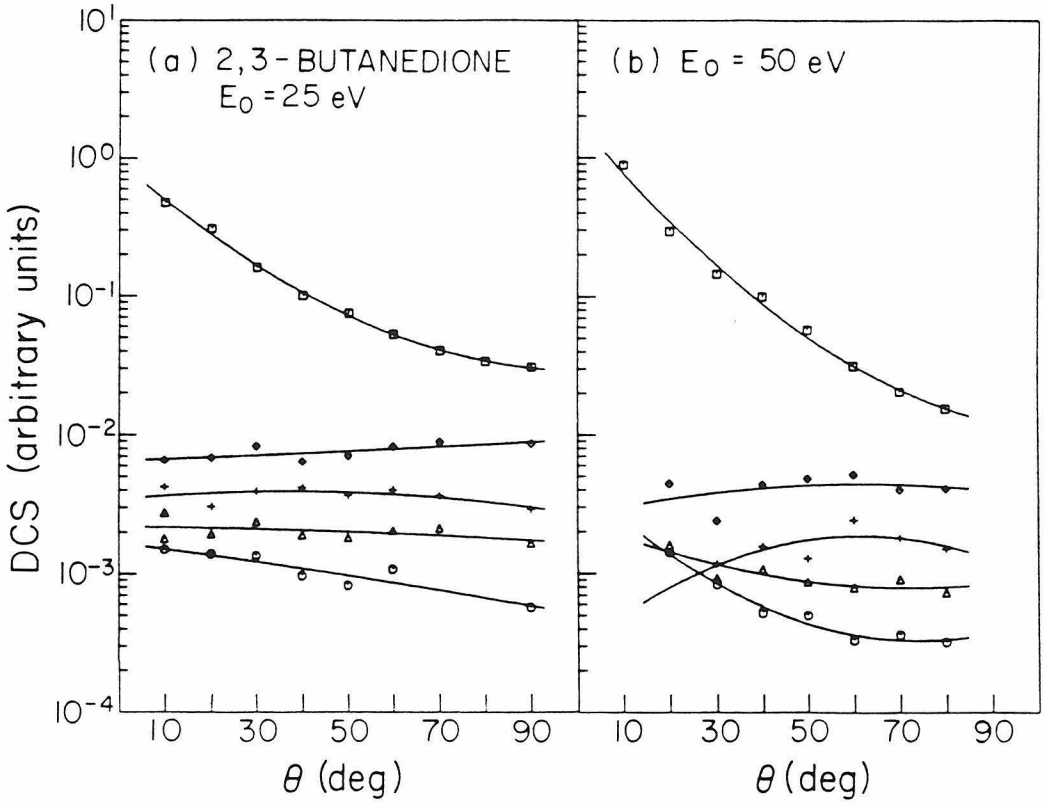
(a) 2,3-BUTANEDIONE
E0 = 25 eV
(b) E0 = 50 eV
DCS (arbitrary units)
θ (deg)
θ (deg)
10^1
10^0
10^-1
10^-2
10^-3
10^-4
10
30
50
70
90

FIGURE 3.

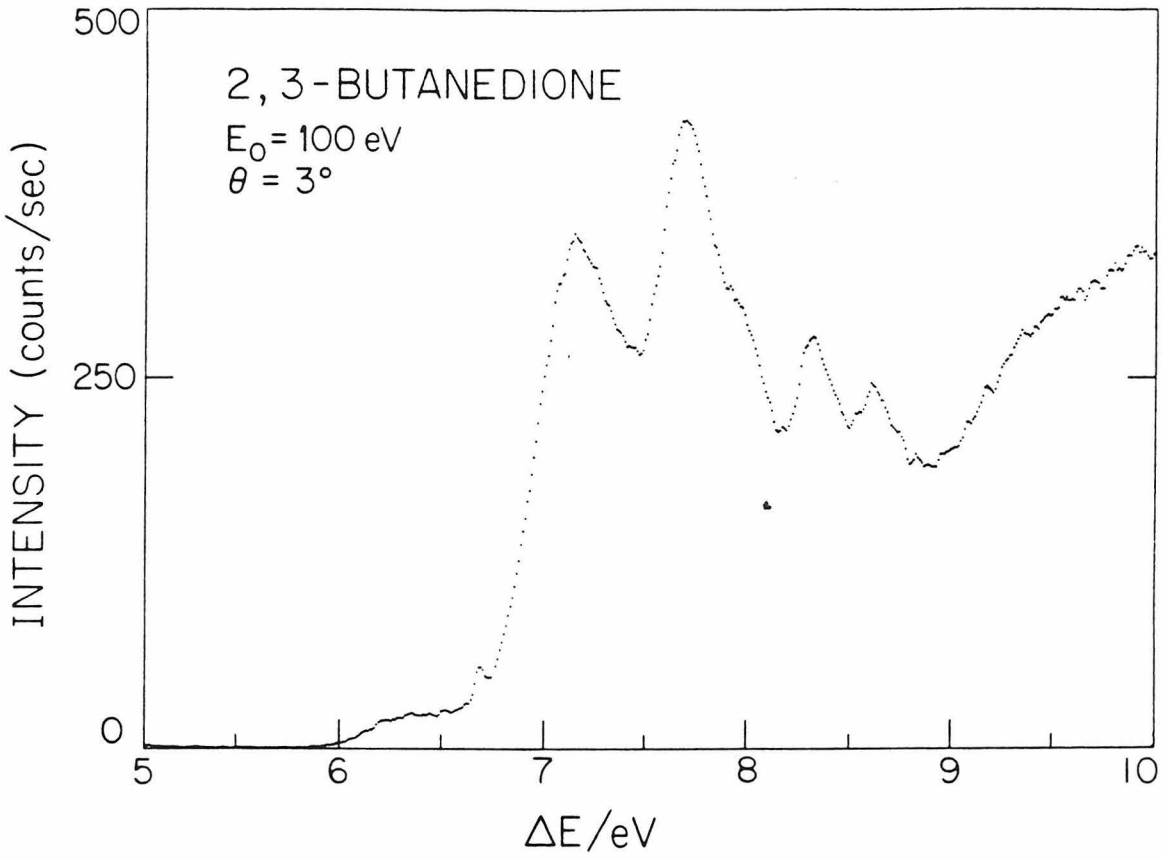
2, 3-BUTANEDIONE
E_0 = 100 eV
θ = 3°
INTENSITY (counts/sec)
500
250
0
5
6
7
8
9
10
ΔE/eV

FIGURE 4.

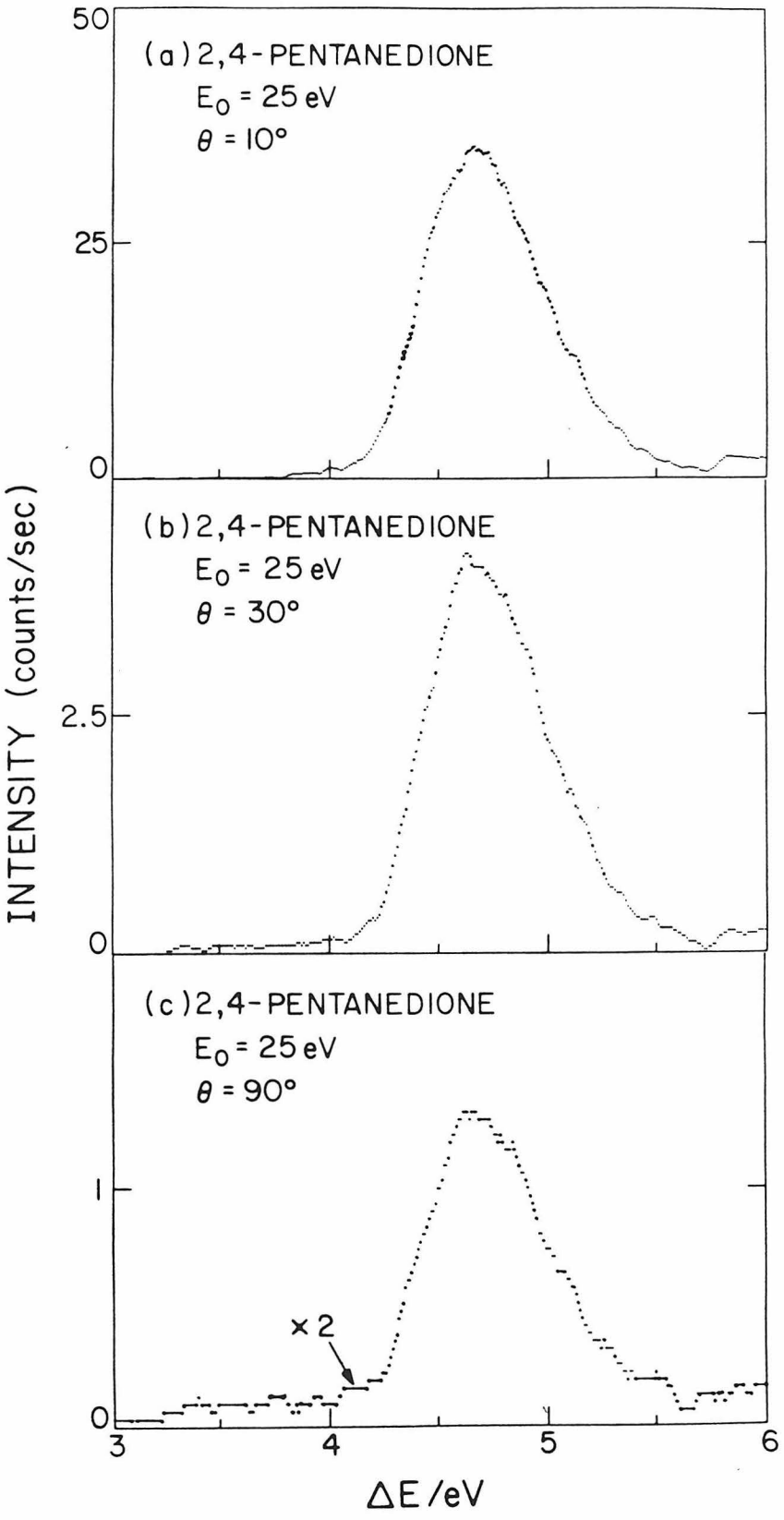
(a) 2,4-PENTANEDIONE
E_0 = 25 eV
θ = 10°
(b) 2,4-PENTANEDIONE
E_0 = 25 eV
θ = 30°
(c) 2,4-PENTANEDIONE
E_0 = 25 eV
θ = 90°
× 2
INTENSITY (counts/sec)
ΔE /eV
50
25
0
2.5
0
1
0
3
4
5
6

FIGURE 5.

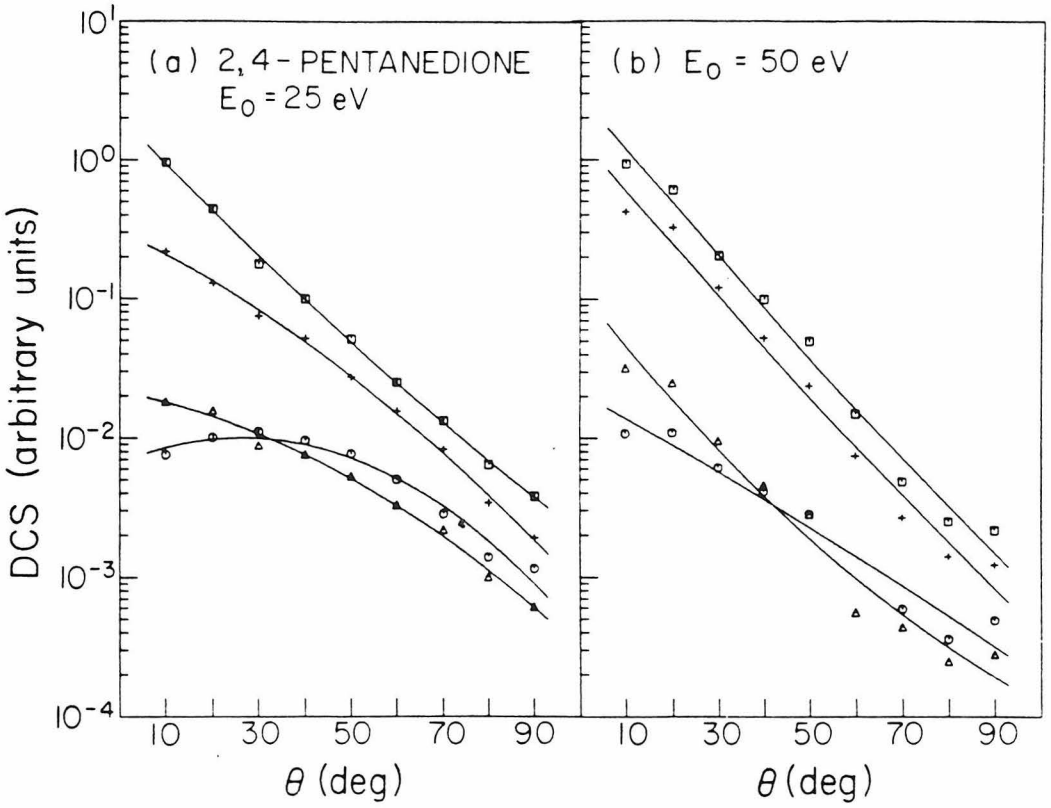
(a) 2,4-PENTANEDIONE
E_0 = 25 eV
(b) E_0 = 50 eV
DCS (arbitrary units)
10^1
10^0
10^{-1}
10^{-2}
10^{-3}
10^{-4}
10
30
50
70
90
θ (deg)

FIGURE 6.

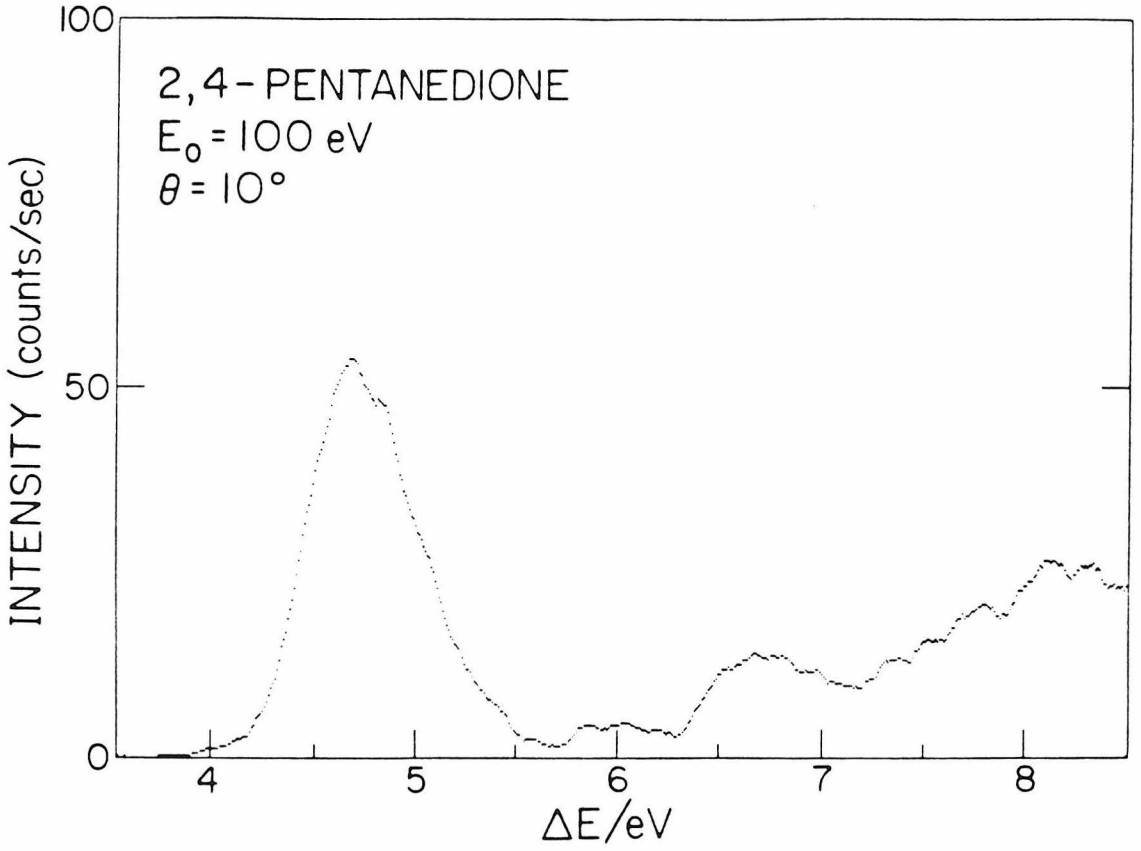
100
50
0
2,4-PENTANEDIONE
E_0 = 100 eV
θ = 10°
INTENSITY (counts/sec)
4
5
6
7
8
ΔE/eV

FIGURE 7.

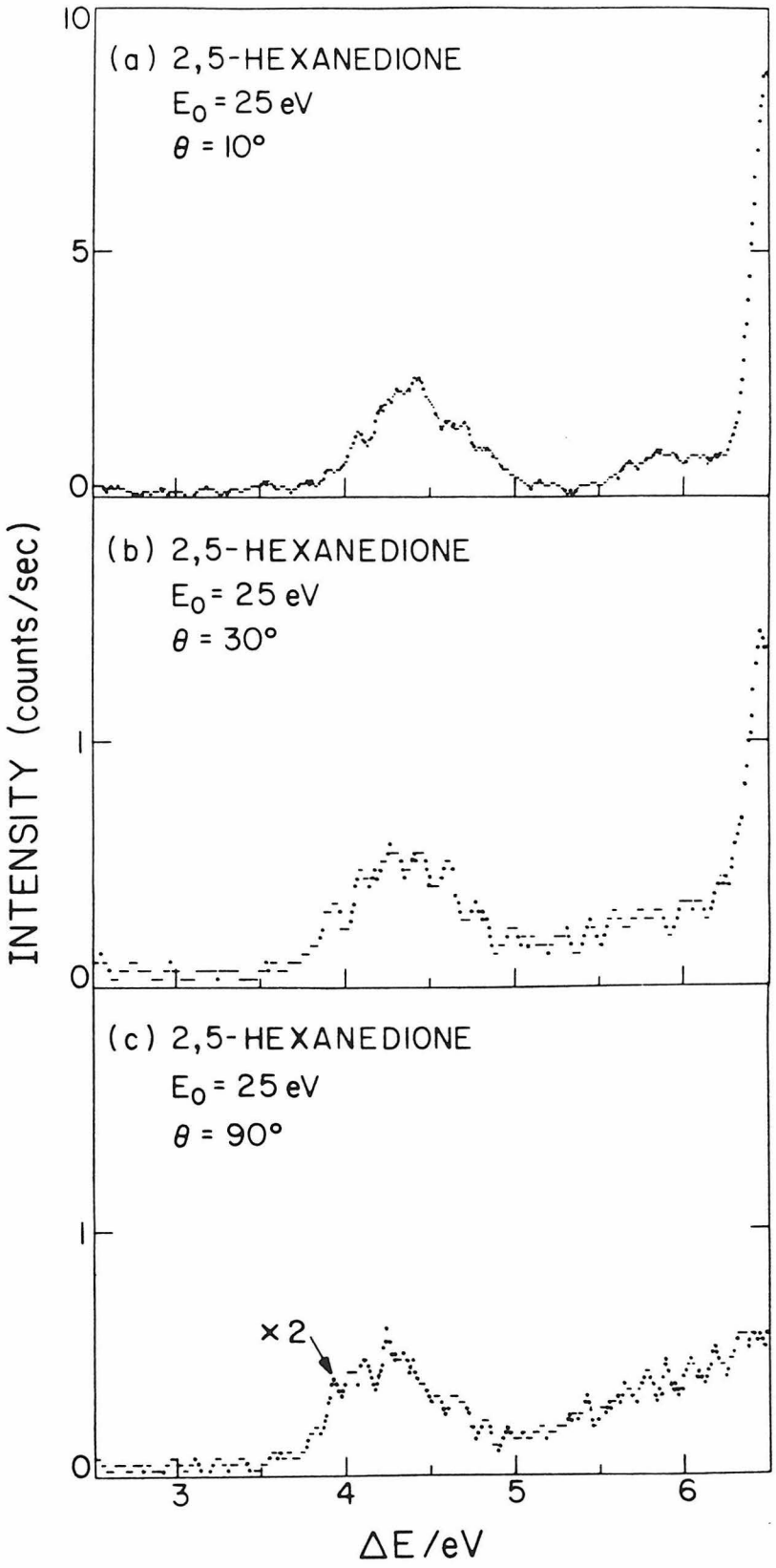
(a) 2,5-HEXANEDIONE
E_0 = 25 eV
θ = 10°
(b) 2,5-HEXANEDIONE
E_0 = 25 eV
θ = 30°
(c) 2,5-HEXANEDIONE
E_0 = 25 eV
θ = 90°
× 2
INTENSITY (counts/sec)
ΔE/eV
10
5
0
1
0
1
0
3
4
5
6

FIGURE 8.

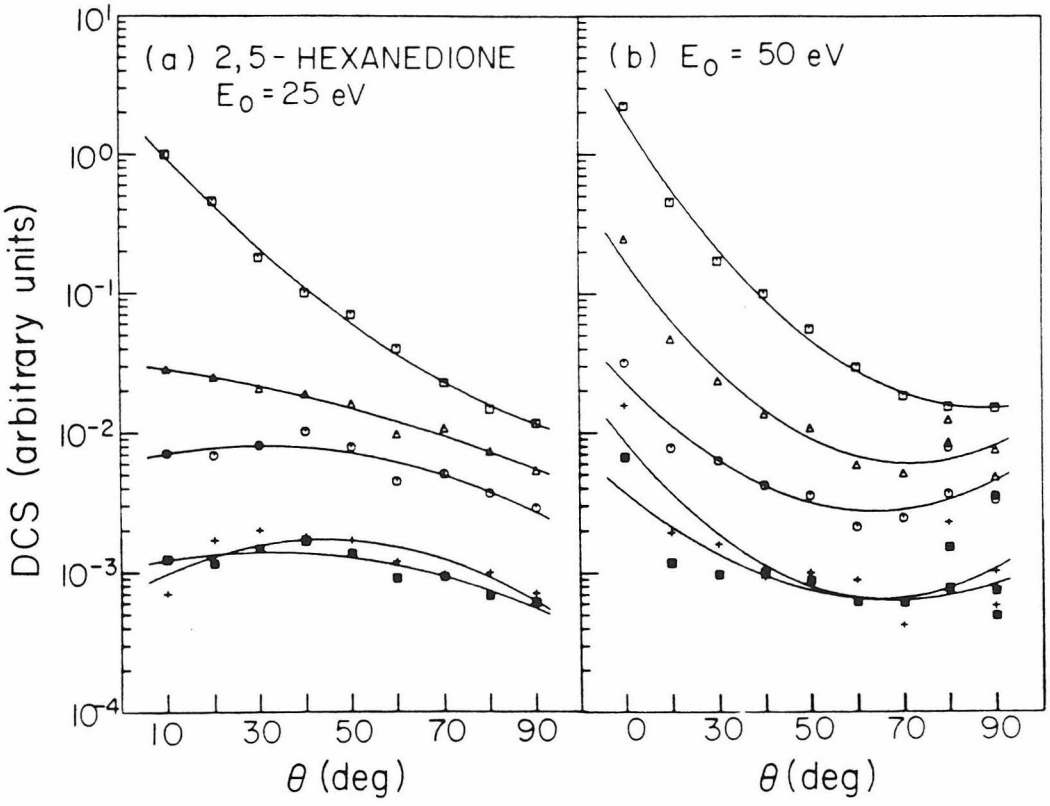
(a) 2,5-HEXANEDIONE
E_0 = 25 eV
(b) E_0 = 50 eV
DCS (arbitrary units)
10^1
10^0
10^{-1}
10^{-2}
10^{-3}
10^{-4}
10
30
50
70
90
0
30
50
70
90
θ (deg)
θ (deg)

FIGURE 9.

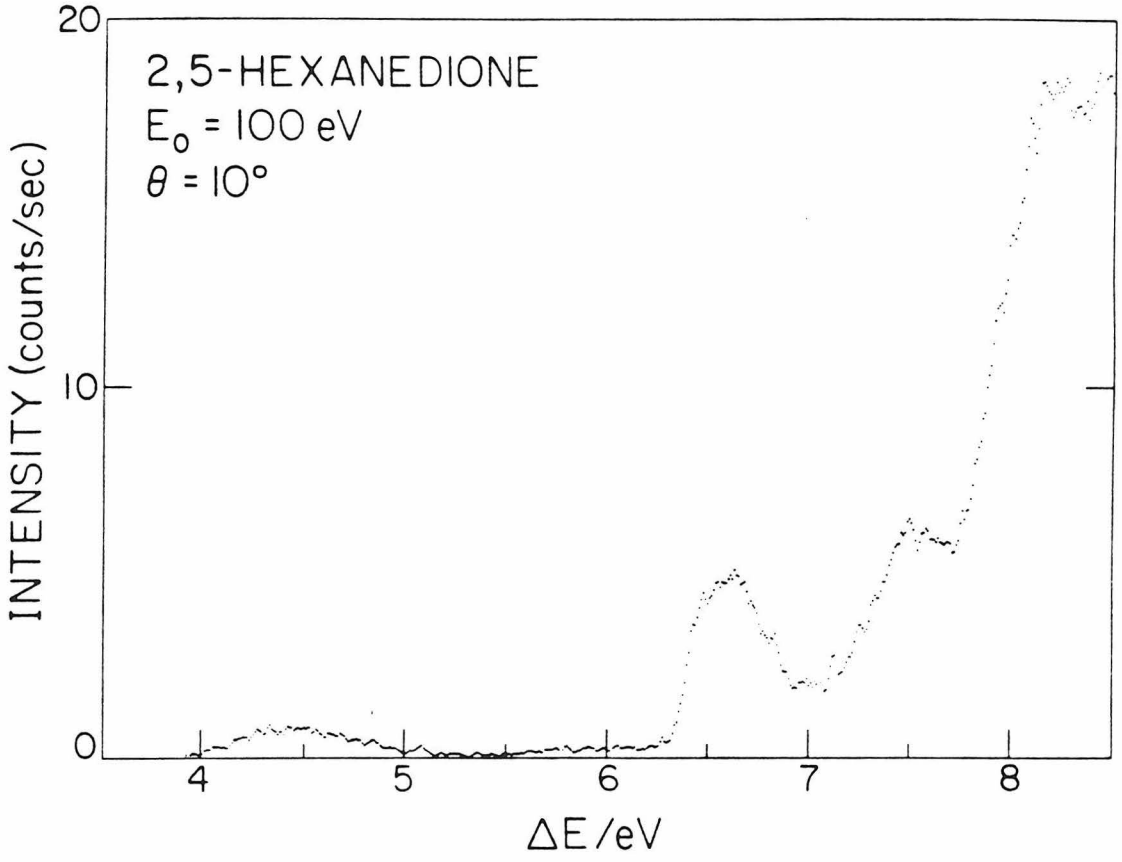
2,5-HEXANEDIONE
E_0 = 100 eV
θ = 10°
INTENSITY (counts/sec)
20
10
0
4
5
6
7
8
ΔE/eV

FIGURE 10.

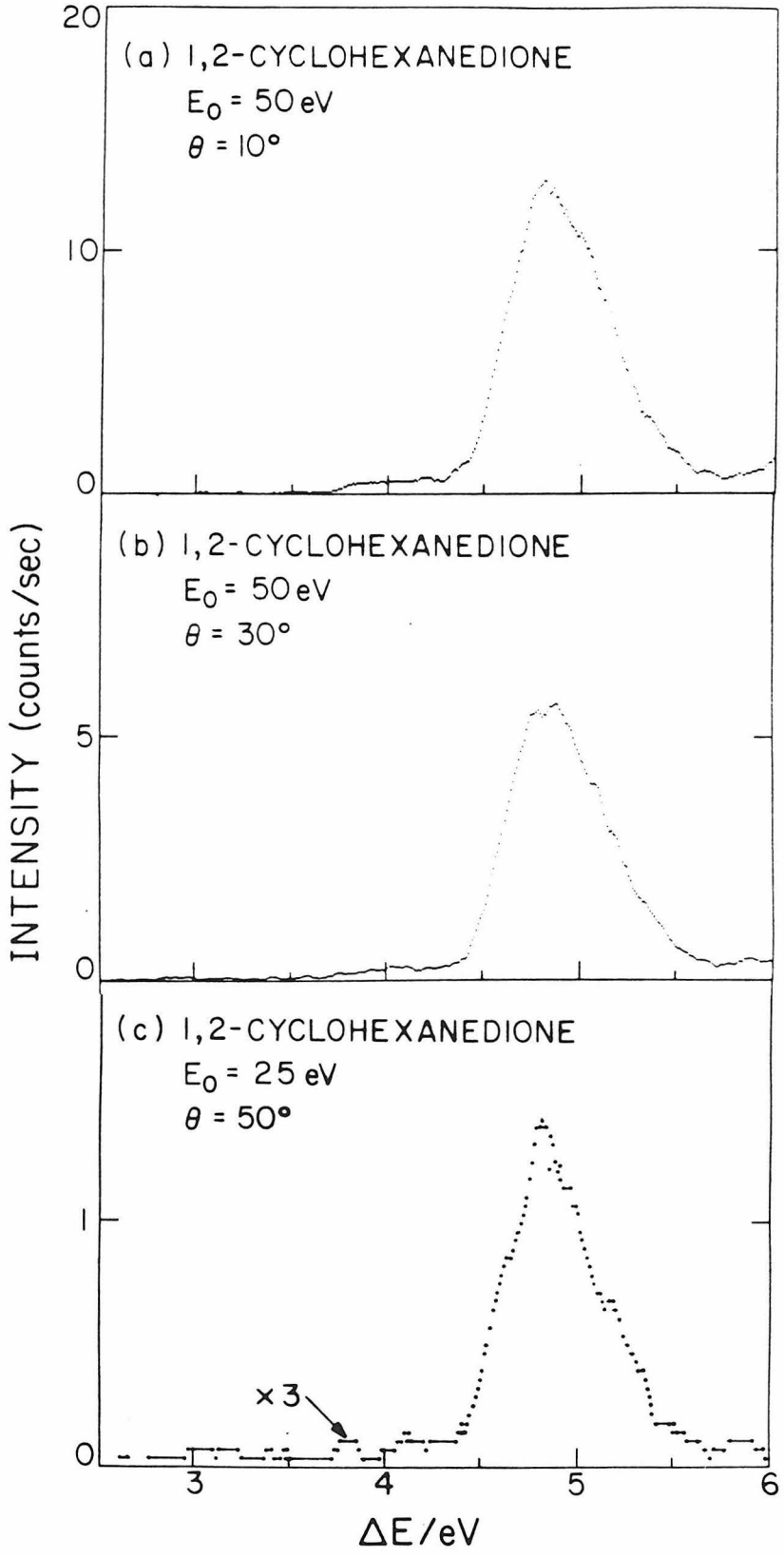
(a) 1,2-CYCLOHEXANEDIONE
E_0 = 50 eV
θ = 10°
(b) 1,2-CYCLOHEXANEDIONE
E_0 = 50 eV
θ = 30°
(c) 1,2-CYCLOHEXANEDIONE
E_0 = 25 eV
θ = 50°
×3
INTENSITY (counts/sec)
ΔE/eV
20
10
0
5
0
1
0
3
4
5
6

FIGURE 11.

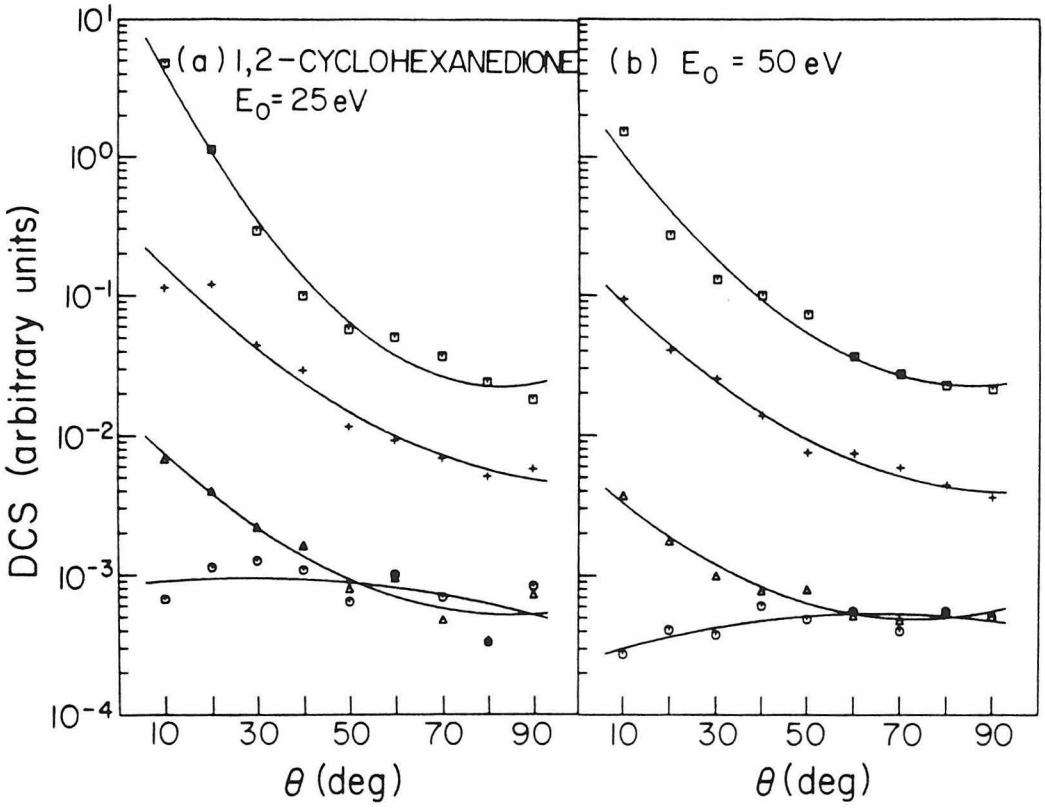
(a) 1,2-CYCLOHEXANEDIONE
E_0 = 25 eV
(b) E_0 = 50 eV
DCS (arbitrary units)
10^1
10^0
10^{-1}
10^{-2}
10^{-3}
10^{-4}
10
30
50
70
90
θ (deg)

FIGURE 12.

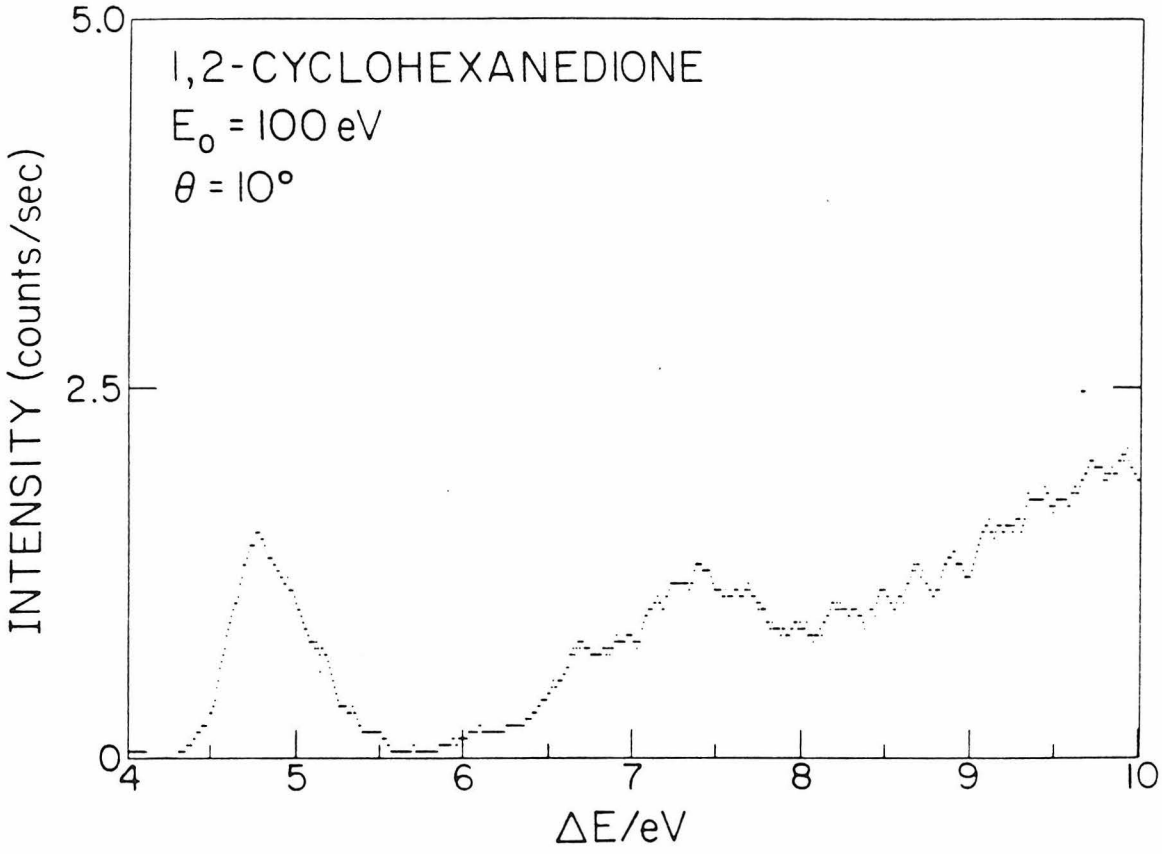
1,2-CYCLOHEXANEDIONE
E_0 = 100 eV
θ = 10°
INTENSITY (counts/sec)
5.0
2.5
0
4
5
6
7
8
9
10
ΔE/eV

FIGURE 13.

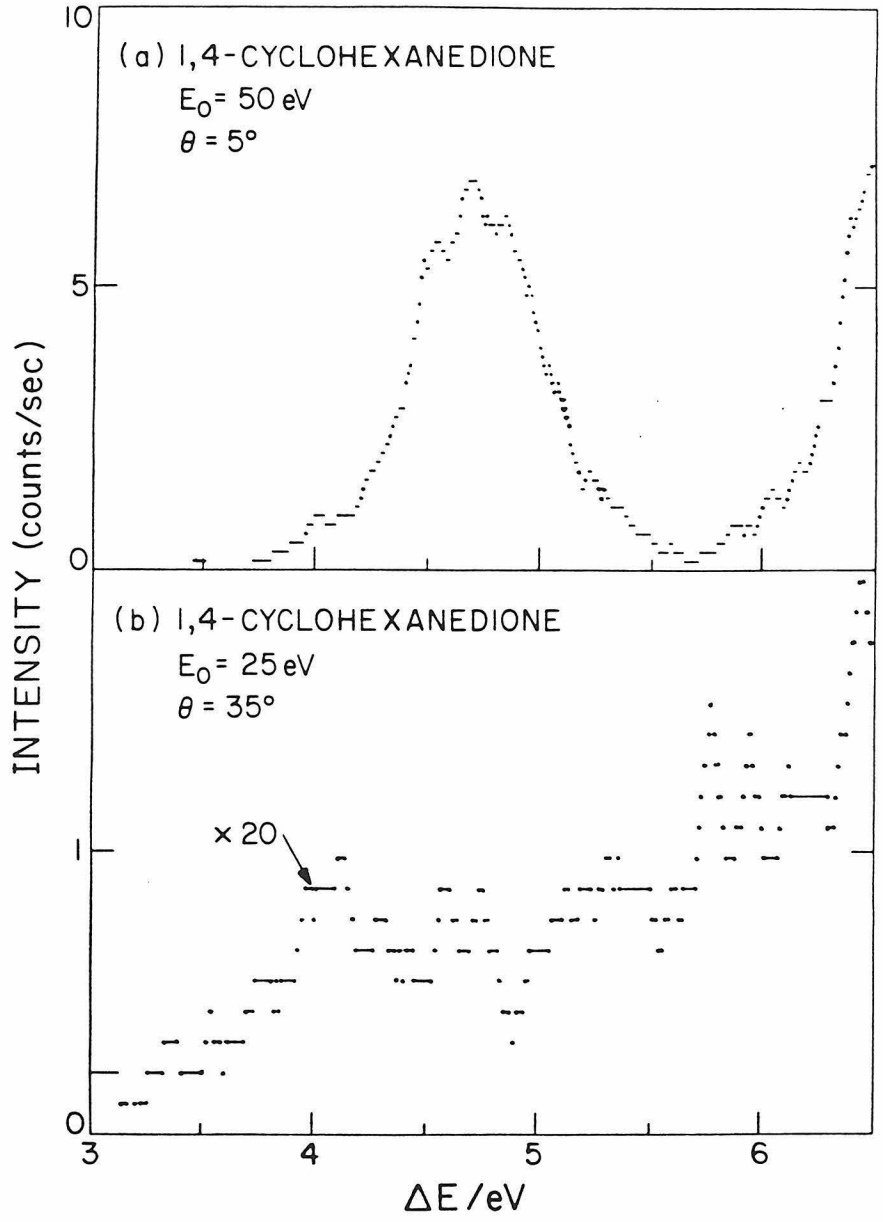
(a) 1,4-CYCLOHEXANEDIONE
E_0 = 50 eV
θ = 5°
(b) 1,4-CYCLOHEXANEDIONE
E_0 = 25 eV
θ = 35°
× 20
INTENSITY (counts/sec)
ΔE /eV
10
5
0
1
0
3
4
5
6

FIGURE 14.

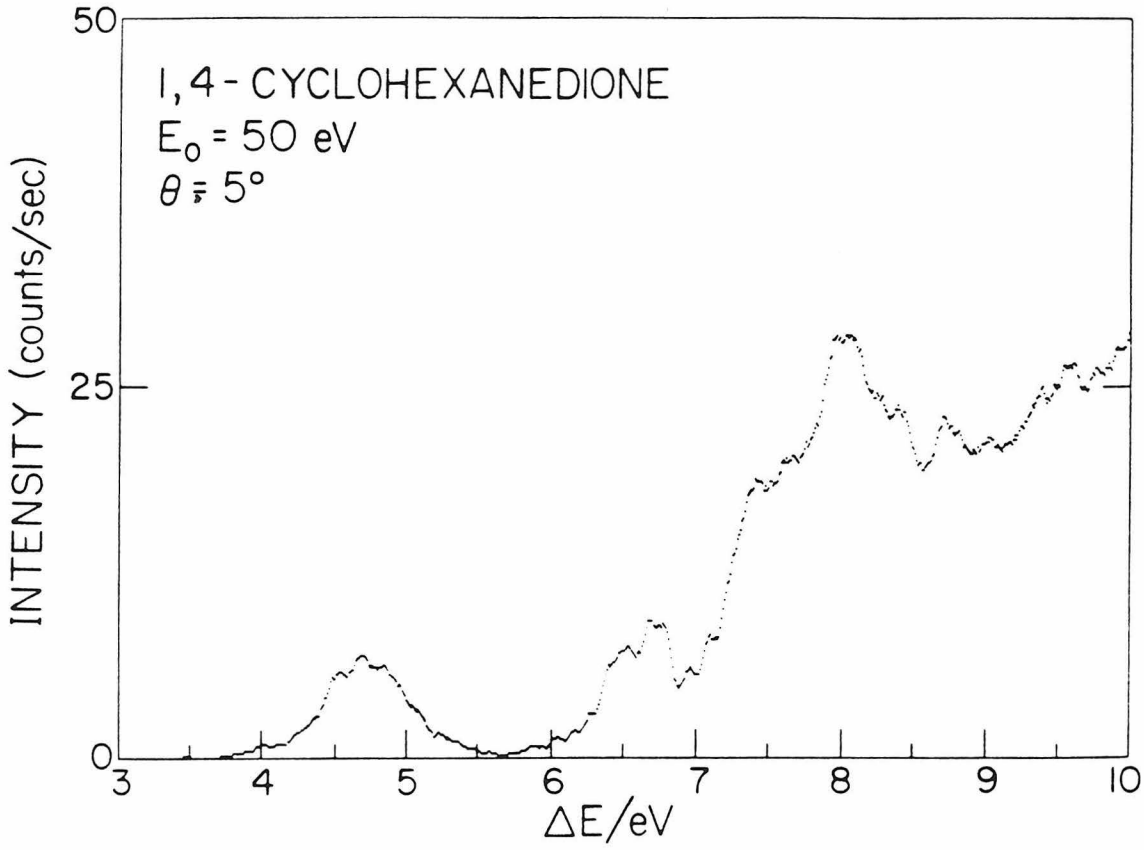
1,4-CYCLOHEXANEDIONE
E_0 = 50 eV
θ = 5°
INTENSITY (counts/sec)
50
25
0
3
4
5
6
7
8
9
10
ΔE/eV

FIGURE 15.

a)

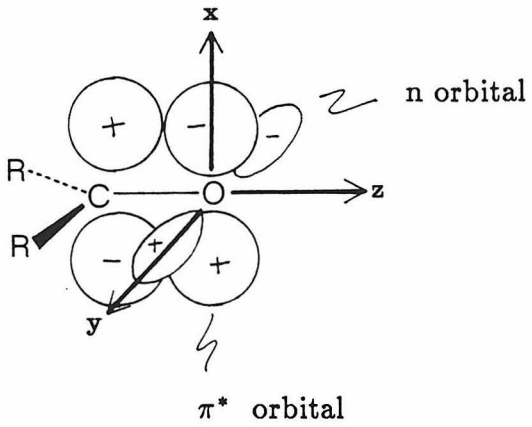

b)

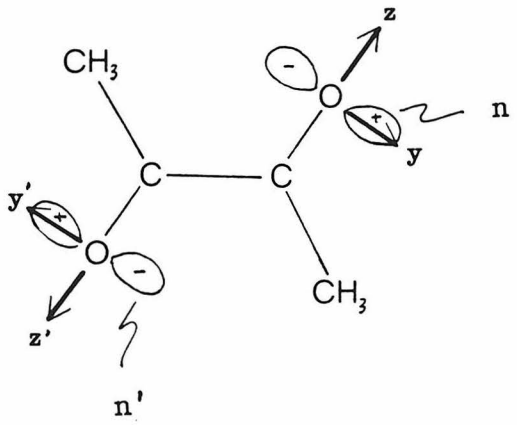

c)

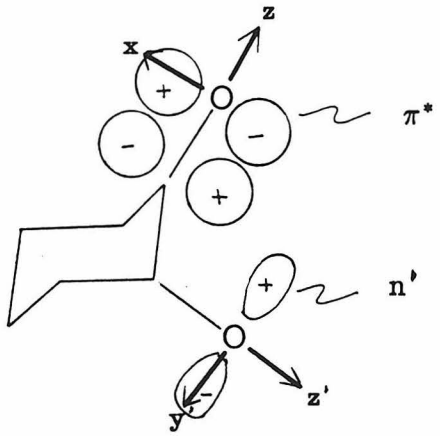

CHAPTER 4

Paper 3: AN ELECTRON-IMPACT SPECTROSCOPY INVESTIGATION OF CH_3 AND SOME OF ITS PYROLYTIC PRECURSORS

An Electron–Impact Spectroscopy Investigation of CH_3 and Some of Its Pyrolytic Precursors[a]

K. N. Walzl[b], C. F. Koerting[c], I. M. Xavier Jr.[d], and A. Kuppermann

Arthur Amos Noyes Laboratory of Chemical Physics,[e]

California Institute of Technology, Pasadena, CA 91125

(received)

Abstract

The electronic spectrum of the methyl radical CH_3 was investigated by the technique of variable-angle electron energy-loss spectroscopy. By means of pyrolytic decomposition three possible sources of this radical were tried (tetramethyl tin, ethyl nitrite, and di-*t*-butyl-peroxide). The spectra of these precursors were obtained. Using di-*t*-butyl-peroxide, relative differential cross sections for the lowest allowed $^2A_1' \leftarrow A_2''$ 3s Rydberg transition in CH_3 (5.73 eV) were determined at incident energies of 50 eV and 25 eV. The differential cross sections for this band are indicative of a spin-allowed transition in a closed shell system and, as expected, in the vicinity of this band no transition of a spin-forbidden nature is detected.

---

[a] This work was supported in part by the U. S. Department of Energy, Contract No. DE-AM03-76F00767, Project Agreement No. DE-AT03-76ER72004.

[b] Work performed in partial fulfillment of the requirements for the Ph.D. degree in Chemistry at the California Institute of Technology.

[c] Present address: E. I. Dupont de Nemours and Co., Inc., Wilmington, DE 19898.

[d] On leave from Departamento de Quimica Fundamental; Universidade Federal de Pernambuco; 50000, Recife, Pernambuco; Brazil.

[e] Contribution No.

1. INTRODUCTION

Free radicals play a major role in upper atmospheric chemistry, interstellar chemistry, and combustion chemistry. Many have low-lying electronic states energetically accessible under combustion conditions. In order to fully understand these processes it is necessary to understand the nature of the electronic states involved.

The methyl radical is one of the most important of the polyatomic free radicals and, being one of the simplest hydrocarbons, is a useful model system for molecular orbital theory. It has been extensively studied by Herzberg through optical techniques.[4] CH_3 is planar with D_{3h} symmetry and has the ground state electron configuration

$$(1a_1)^2(2a_1)^2(2e')^4(2a_2'')^1.$$

The ground state is of $^2A_2''$ symmetry, the unpaired electron lying in a p_z orbital of a_2'' symmetry. The lowest observed transition is the $^2A_1' \leftarrow ^2A_2''$ 3s Rydberg excitation at 5.73 eV. The forbidden excitation to the lowest $^2E'$ valence state has not been observed; however, calculations by Lengsfield *et al.*[5] and McDiarmid[6] place it about 1.5 eV above the lowest 3s Rydberg state. The transitions to the 3p Rydberg states are also dipole symmetry-forbidden in D_{3h} symmetry but Hudgens *et al.*[7] have found them to be at 7.42 eV by a resonantly-enhanced multiphoton ionization technique. The excitation energy of the 3d state is 8.27 eV[4] and the first ionization potential (IP) is at 9.85 eV.[4b]

A useful technique for probing the nature of electronic transitions is the method of variable-angle electron energy-loss spectroscopy. When an electron scatters from and excites an atom or molecule two mechanisms of electronic excitation are possible. The first is the long-range Coulomb excitation and is caused by the electric field produced when an electron passes a target. The

differential cross section (DCS) for a transition excited in this manner exhibits a maximum at the scattering angle $\theta = 0°$ (no change in direction) and decreases by approximately two orders of magnitude as θ increases from 0° to 90° .[1,2] The second mechanism of electronic excitation involves the physical exchange of the incident electron with a target electron. The incident electron may exchange with a target electron of either the same or opposite spin; the former exchange process may or may not result in target excitation while the latter results in excitation to a spin-forbidden state. Transitions excited primarily by this mechanism possess a nearly uniform DCS as a function of scattering angle due to the loss of directional information carried by the incident electron.[1,2]

With the above considerations in mind a variable-angle electron energy-loss spectroscopy study was undertaken of the polyatomic free radical CH_3. It was hoped that this investigation would yield information about possible low-lying, spin-forbidden transitions. Previous electron spectroscopy of free radicals had been limited to stable species that were triatomic or smaller; for example, Rianda *et al.*[3] have determined the electron spectroscopy and differential cross sections for doublet–doublet allowed and doublet–quartet forbidden transitions in NO_2. The present paper reports the first electron impact spectroscopy investigation of a transient polyatomic free radical.

2. EXPERIMENTAL

The spectrometer used in the present experiments has been described previously.[8] Briefly, electrons are emitted from a tungsten filament and focused into a hemispherical monochromator. The monoenergetic electrons are then focused into the scattering region and, after interaction with the target molecules, enter a hemispherical analyzer prior to detection.

In order to generate the methyl radicals for the study, an *in situ* pyrolysis

technique was employed.[8b] A quartz tube of 0.060 inch ID with an outer layer of stainless steel sheathed heater wire (Figure 1) produces an effusive jet of molecules. Pyrolysis temperatures of up to 800° C, as measured by a thermocouple placed on the tube's outer surface, were used in these experiments.

Three sources of methyl radicals were investigated. The first was tetramethyl tin (Aldrich, 99%), known to be a reliable source of methyl radicals.[9] Taylor and Milazzo[19] found a 30% conversion of tetramethyl tin at ~600° C, with 20% of the organic products existing as CH_3. Using our inlet, temperatures of ~ 800° C were required to achieve appreciable decomposition. Unfortunately after five hours of continuous operation the quartz capillary became obstructed with metallic tin.

A second source of methyl radicals that was tried was ethyl nitrite. It is known that ethyl nitrite thermally decomposes by the reaction[10]

$$CH_3\text{–}CH_2\text{–}ONO \rightarrow CH_3\cdot + H_2CO + NO \ .$$

The gaseous ethyl nitrite was synthesized by mixing ethanol (U. S. Industrial Chemicals Co., anhydrous) and isoamyl nitrite (Aldrich, 97%) in a 2:1 ratio by volume; an ester alcoholysis takes place producing isoamyl alcohol and continuously bubbling ethyl nitrite.[11] A pyrolysis temperature of 450° C was used for the decomposition.

The third source of methyl radicals was di-*t*-butyl-peroxide (Columbia Organic Chemicals Co., Inc.). It has been shown[12,13] that the decomposition of di-*t*-butyl-peroxide (TBP) proceeds according to the following scheme:

$$TBP \rightarrow 2\ t\text{-butyl-}O\cdot$$

$$2\ t\text{-butyl-}O\cdot \rightarrow 2\ CH_3\cdot + 2\ (CH_3)_2CO \ .$$

Since this was the precursor that was used for nearly all of the investigation, an optimization of the temperature needed for methyl production was carried out. The ratio of the methyl peak intensity at 5.73 eV to the acetone peak intensity

at 6.36 eV versus temperature was examined at an incident electron energy E_0 = 50 eV and scattering angle $\theta = 10°$ (Figure 2). The ratio was found to possess a maximum at 300 ±50° C and this temperature was used in all subsequent studies. The number density of methyl radicals in the jet at this temperature was estimated to be 10^{13} molecules/cm^3 on the basis of the intensity of the 5.73 eV band.

3. RESULTS AND DISCUSSION

In Figure 3 are shown two electron impact spectra taken at E_0 = 100 eV and $\theta = 0°$ between 4.5 and 9.5 eV energy-loss. Figure 3a is the spectrum of tetramethyl tin obtained using the pyrolysis source at room temperature. It consists of two broad features with an onset at 5.7 eV and maxima at 6.71, 8.24, and 8.57 eV. Only two previous spectra for this compound have been reported. The first describes merely a continuum with an onset at 5.6 eV rising up to 6.2 eV.[20] The second shows a maximum at 6.7 eV and ends at 7.1 eV.[22] Ours is the first reported UV spectrum of this compound extending to the first IP, located at about 9.7 eV.[21] Intense 3s Rydberg transitions are known to occur in molecules with T_d symmetry if the originating orbital is of t_2 type.[23] In this case the 6.71 eV and 8.24 eV features can be fit to the first two members of a Rydberg series with a quantum defect of 0.84 and an IP = 9.62 eV. Figure 3b shows the same spectral region of the compound with the source heated to 800° C. Immediately apparent are the sharp transitions located at 5.70, 8.30, and 8.98 eV. The 5.70 eV transition is assigned to the methyl A_2'' 3s Rydberg excitation. The 8.30 eV and 8.98 eV transitions are assigned to the 3d and 4d Rydberg excitations, respectively. Also of interest is the shoulder extending from 4.90 to 5.75 eV not present in the room temperature spectrum. It is possible that this shoulder is due to incompletely dissociated tetramethyl tin.

As stated previously, operation of the source with tetramethyl tin was limited

to about five hours. In addition, the lowest allowed methyl transition strongly overlaps with the lowest band of the compound, making DCS measurements more difficult. A second precursor that was investigated was ethyl nitrite. It was expected that there could be much overlap of the methyl bands with the spectral features arising from the additional products NO and formaldehyde, and this was indeed found to be the case. Figure 4a shows the spectrum of ethyl nitrite without heating. It consists of several broad structureless features. Previous studies[14,15] have only examined the lowest band in the region between 3.10 and 4.09 eV,[13,14] not shown in Figure 4a. Peaks are observed at 5.69, 6.70, 7.76, 8.24, 8.94, 9.44, and 9.76 eV. In analogy with results for methyl nitrite[24] the transition at 5.69 eV is assigned as $\pi \rightarrow \pi^*$ from an OCH_2CH_3 localized orbital to a NO localized orbital. The remaining bands are probably attributable to Rydberg transitions. Figure 4b shows the spectrum of the pyrolyzed ethyl nitrite; the spectrum is highly congested. No feature can be definitively attributed to a known methyl radical feature; every peak in the spectrum can be assigned to either NO[16] or formaldehyde.[17,18] One interesting observation is that the intensities of two $\gamma(A\ ^2\Sigma^+ \leftarrow X\ ^2\Pi)$ features at 5.92 eV and 6.27 eV are much larger with respect to the nearby $\beta(B\ ^2\Pi \leftarrow X\ ^2\Pi)$ peaks (at 5.47, 5.75, 6.04, and 6.33 eV) than previously reported.[25,26] In fact, under conditions of similar incident electron energy and scattering angle, the height of the transition at 6.27 eV is only about 10% of the height of the 6.34 eV transition.[25,26]

The precursor molecule that was finally used to generate methyl radicals was TBP. Figure 5a shows a spectrum of TBP between 4.25 eV and 7.75 eV energy-loss at $E_0 = 50$ eV and $\theta = 10°$ at room temperature. It consists of a rising continuum with very little structure visible (the sharp feature at 6.67 eV is due to a Hg contamination). In Figure 5b is shown TBP at a pyrolysis temperature of 400° C (results obtained prior to temperature optimization). The spectrum is

drastically different and, as expected, most of the features are due to the pyrolysis product acetone with the exceptions being the sharp peak at 5.74 eV and the broad feature between 5.8 and 6.3 eV. The peak at 5.74 eV is again attributed to the methyl 3s Rydberg transition.

To help confirm the nature of the methyl transition an angular study was conducted. Figure 6a again shows the spectrum of TBP at $E_0 = 50$ eV and $\theta = 10°$ between 5.6 eV and 6.4 eV energy-loss and at the optimum temperature of 300° C. In contrast, the spectrum of TBP under the same conditions except at $\theta = 60°$ is shown in Figure 6b. It is apparent that no drastic changes occur, although the ratio of the methyl 3s Rydberg transition to the acetone A_1 3s (S–S) transition at 6.36 eV goes from approximately 1:2 to 1:3. Increasing the angle further to 90° produces a change in this ratio back to about 1:2; however, due to the increase in the relative intensity of the intervening region of the spectrum the methyl peak is obscured. Most of the increase in the relative intensity between 5.8 and 6.3 eV is due to the presence of the $\pi \rightarrow \pi^*$ (S–T) band of acetone. As previously discussed, the intensity of such spin-forbidden bands are constant with angle while the intensity of fully-allowed bands decreases with angle, thus the relative increase in the acetone $\pi \rightarrow \pi^*$ (S–T) band.

The DCS curves plotted in Figure 7 illustrate the integrated intensity changes for these bands. The elastic peak and the acetone n→3s peak exhibit an intensity decrease of about two orders of magnitude as should fully-allowed bands. The methyl A_2'' 3s Rydberg band seems to be exhibiting this behavior also, but the curve begins to become more constant starting at $\theta = 60°$. This is the angle where the spin-forbidden $\pi \rightarrow \pi^*$ band of acetone begins manifesting itself more strongly and, if this effect is subtracted out using the known angular behavior of this acetone band[18] with the acetone 3s Rydberg transition used as a scaling feature, the DCS curve behaves more like a fully-allowed band. At $E_0 = 50$ eV

there seems to be little contribution from a spin-forbidden transition in methyl in the region of the A_2'' 3s Rydberg band.

For CH_3 one would probably expect no low-lying, spin-forbidden bands to be in evidence. All transitions from the highest occupied a_2'' orbital are spin-allowed because the electron is unpaired. Likewise, only a spin-allowed version of the predicted lowest valence transition is possible. This constrasts with allowed Rydberg transitions converging to the second IP which would have spin-forbidden counterparts. A calculation by Millie and Berthier[27] places the second IP approximately 5 eV higher than the first IP. Thus a spin-allowed excitation from the 2e′ orbital to the 3s orbital would lie at about 10.5 eV and the spin-forbidden excitation at about 9.5 eV, allowing a singlet-triplet splitting of about 1 eV (as Brongersma and Oosterhoff[28] found for the 3s Rydberg transition from a corresponding orbital in methane).

Another angular study was performed with the incident energy lowered to $E_0 = 25$ eV (Figure 8). In this case the DCS behavior is not as marked; however, the general trend suggesting that there is no spin-forbidden contribution to the methyl spectrum in the vicinity of the A_2'' 3s Rydberg band is confirmed.

4. SUMMARY

The spectra of three pyrolytic sources of methyl radicals (tetramethyl tin, ethyl nitrite, di-*t*-butyl-peroxide) were investigated by variable-angle electron energy-loss spectroscopy, both at room temperature and elevated temperatures. Of the three precursors, di-*t*-butyl-peroxide was found to be the most useful for radical generation. The spectrum of the decomposition co-product acetone has only moderate overlap with that of methyl and also is fairly well understood so that its influence can be removed. Regarding the 3s Rydberg excitation in CH_3, it has been found to possess a DCS in accord with its fully-allowed nature.

5. ACKNOWLEDGMENT

One of the authors (IMX) acknowledges a graduate fellowship from CAPES and UFPE (Brazil).

References

1. A. Kuppermann, J. K. Rice, and S. Trajmar, *J. Phys. Chem.* **72**, 3894 (1968).
2. S. Trajmar, J. K. Rice, and A. Kuppermann, *Adv. Chem. Phys.* **18**, 15 (1970).
3. R. Rianda, R. P. Frueholz, and A. Kuppermann, *J. Chem. Phys.* **79**, 5914 (1983).
4. (a) G. Herzberg, *Proc. R. Soc. London Ser.* **A 262**, 291 (1961); (b) G. Herzberg, *Electronic Spectra of Polyatomic Molecules* vol. 3, (Van Nostrand, Princeton, 1966), pp. 347, 513–15.
5. B. H. Lengsfield III, P. E. Siegbahn, and B. Liu, *J. Chem. Phys.* **81**, 710 (1984).
6. R. McDiarmid, *Theor. Chim. Acta* **20**, 282 (1971).
7. J. W. Hudgens, T. G. DiGiuseppe, and M. C. Lin, *J. Chem. Phys.* **79**, 571 (1983).
8. (a) C. F. Koerting, K. N. Walzl, and A. Kuppermann, *Chem. Phys. Lett.* **109**, 140 (1984); (b) C. F. Koerting, Ph.D. Thesis, California Institute of Technology, Pasadena CA (1985).
9. I. S. Zaslonko and V. N. Smirnov, *Kinet. i Katal.* **20**, 575 (1979).
10. F. A. Houle and J. L. Beauchamp, *J. Amer. Chem. Soc.* **101**, 4067 (1979).
11. G. Caldwell and J. Bartmess, *Org. Mass Spect.* **17**, 456 (1982).
12. (a) J. Raley, R. F. Rust, and W. E. Vaughan, *J. Amer. Chem. Soc.* **70**, 88 (1948).
13. L. Batt and S. W. Benson, *J. Chem. Phys.* **36**, 895 (1962).
14. H. W. Thompson and C. W. Purkis, *Trans. Farad. Soc.* **32**, 674 (1936).
15. J. W. Goodeve, *Trans. Farad. Soc.* **30**, 504 (1934).

16. R. P. Frueholz, R. Rianda, and A. Kuppermann, *J. Chem. Phys.* **68**, 775 (1978).

17. S. Taylor, D. Wilden, and J. Comer, *Chem. Phys.* **70**, 291 (1982).

18. K. N. Walzl, C. F. Koerting, and A. Kuppermann, to be submitted.

19. J. E. Taylor and T. S. Milazzo, *J. Phys. Chem.* **82**, 847 (1978).

20. H. W. Thompson and J. W. Linnett, *Proc. R. Soc. London Ser. A* **156**, 108 (1936).

21. S. Evans, J. C. Green, P. J. Joachim, A. F. Orchard, D. W. Turner, and J. P. Maier, *J. Chem. Soc. Farad. Trans. 2* **68**, 905 (1972).

22. P. P. Shorygin, V. A. Petukhov, O. M. Nefedov, S. P. Kolesnikov, and V. I. Shiryaev, *Theoret. Exp. Chem.* **2**, 146 (1966).

23. M. Robin, *Higher Excited States of Polyatomic Molecules* vol. 1, (Academic Press, New York (1974)), pp. 137–38.

24. M. Tanaka, *Bull. Chem. Soc. Japan* **39**, 766 (1966).

25. E. N. Lassettre, A. Skerbele, M. A. Dillon, and K. J. Ross, *J. Chem. Phys.* **48**, 5066 (1968).

26. R. Rianda, Ph. D. Thesis, California Institute of Technology, Pasadena CA (1981).

27. P. Millie and G. Berthier, *Int. Jour. Quant. Chem.* **2S**, 67 (1968).

28. H. H. Brongersma and L. J. Oosterhoff, *Chem. Phys. Lett.* **3**, 437 (1969).

Figure Captions

Figure 1. Schematic diagram showing the free radical beam source. GI: gas inlet, H: heater, QT: quartz tube, SL: swagelock fitting, TS: tantalum shield.

Figure 2. Graph of the ratio of integrated intensity for the methyl 3s Rydberg transition at 5.73 eV to the acetone 3s Rydberg transition at 6.36 eV as a function of temperature. E_0 = 50 eV and $\theta = 10°$.

Figure 3. Energy-loss spectrum of tetramethyl tin with a) pyrolysis source off, b) pyrolysis source on, T = 800° C. For both spectra E_0 = 100 eV and $\theta = 0°$. Incident electron current = 5 nAmp and estimated sample pressure = 1 mtorr.

Figure 4. Energy-loss spectrum of ethyl nitrite with a) pyrolysis source off, b) pyrolysis source on, T = 450° C. For both spectra E_0 = 50 eV and $\theta = 10°$. Incident electron current = 10 nAmp and estimated sample pressure = 1 mtorr.

Figure 5. Energy-loss spectrum of TBP with a) pyrolysis source off, b) pyrolysis on, T = 400° C. For both spectra E_0 = 50 eV and $\theta = 10°$. Conditions same as Figure 4.

Figure 6. Energy-loss spectrum of TBP at a pyrolysis temperature of 300° C and E_0 = 50 eV: a) $\theta = 10°$, b) $\theta = 60°$, c) $\theta = 90°$. Conditions same as Figure 4. Vertical lines indicate magnitude of error in spectral intensity.

Figure 7. DCS plot of pyrolyzed TBP at E_0 = 50 eV. Elastic scattering (EP) × 0.1: + , acetone 3s Rydberg × 100: ○ , methyl 3s Rydberg × 100: □ , methyl 3s Rydberg (corrected by subtracting contribution of acetone spin-forbidden band) × 100: △ . Arbitrary units are the same for all curves, which are multiplied by scaling factor before plotting.

Figure 8. DCS plot of pyrolyzed TBP at E_0 = 25 eV. EP × 0.1: + , acetone 3s Rydberg × 100: ○ , methyl 3s Rydberg × 1000: □ , corrected methyl 3s Rydberg × 1000: △ .

FIGURE 1.

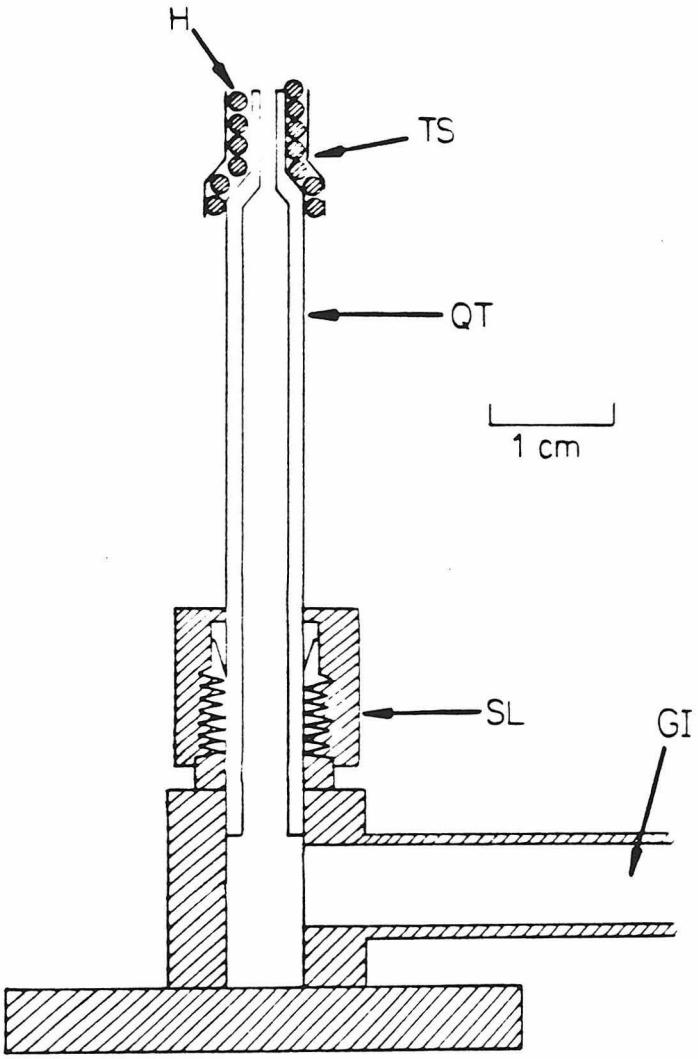

FIGURE 2.

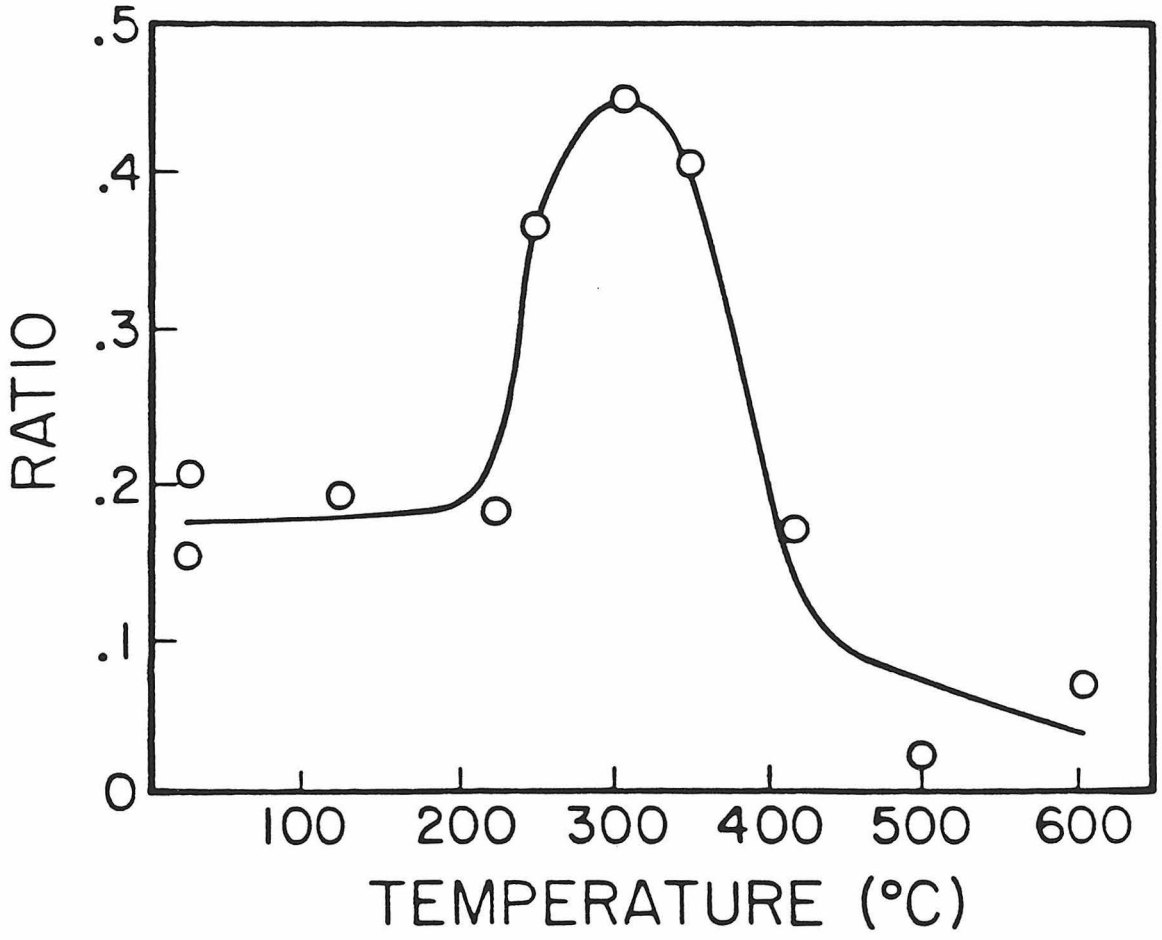

FIGURE 3.

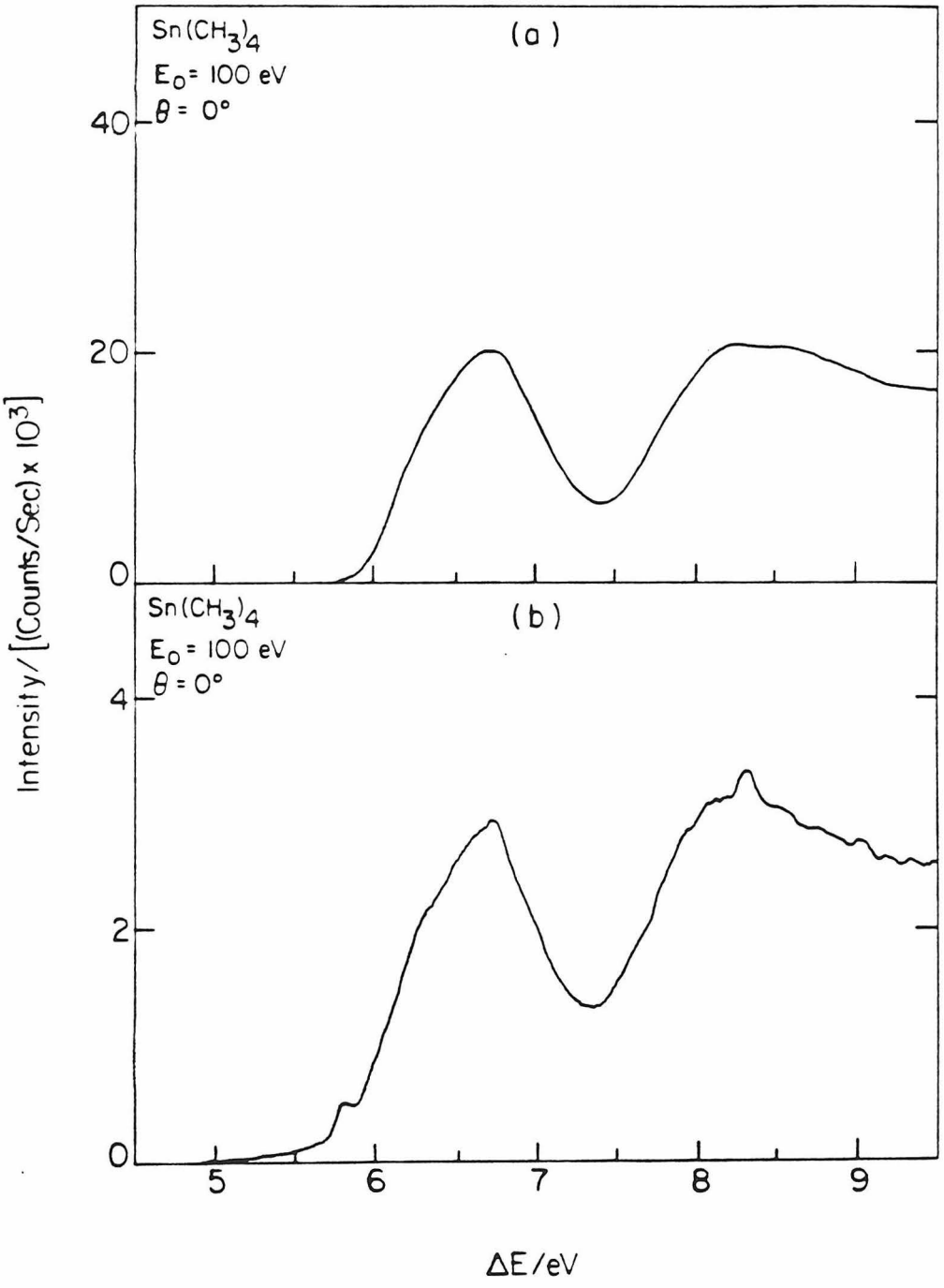
Sn(CH3)4
E0 = 100 eV
θ = 0°
(a)
40
20
0
Sn(CH3)4
E0 = 100 eV
θ = 0°
(b)
4
2
0
Intensity/[(Counts/Sec) x 10³]
5
6
7
8
9
ΔE/eV

FIGURE 4.

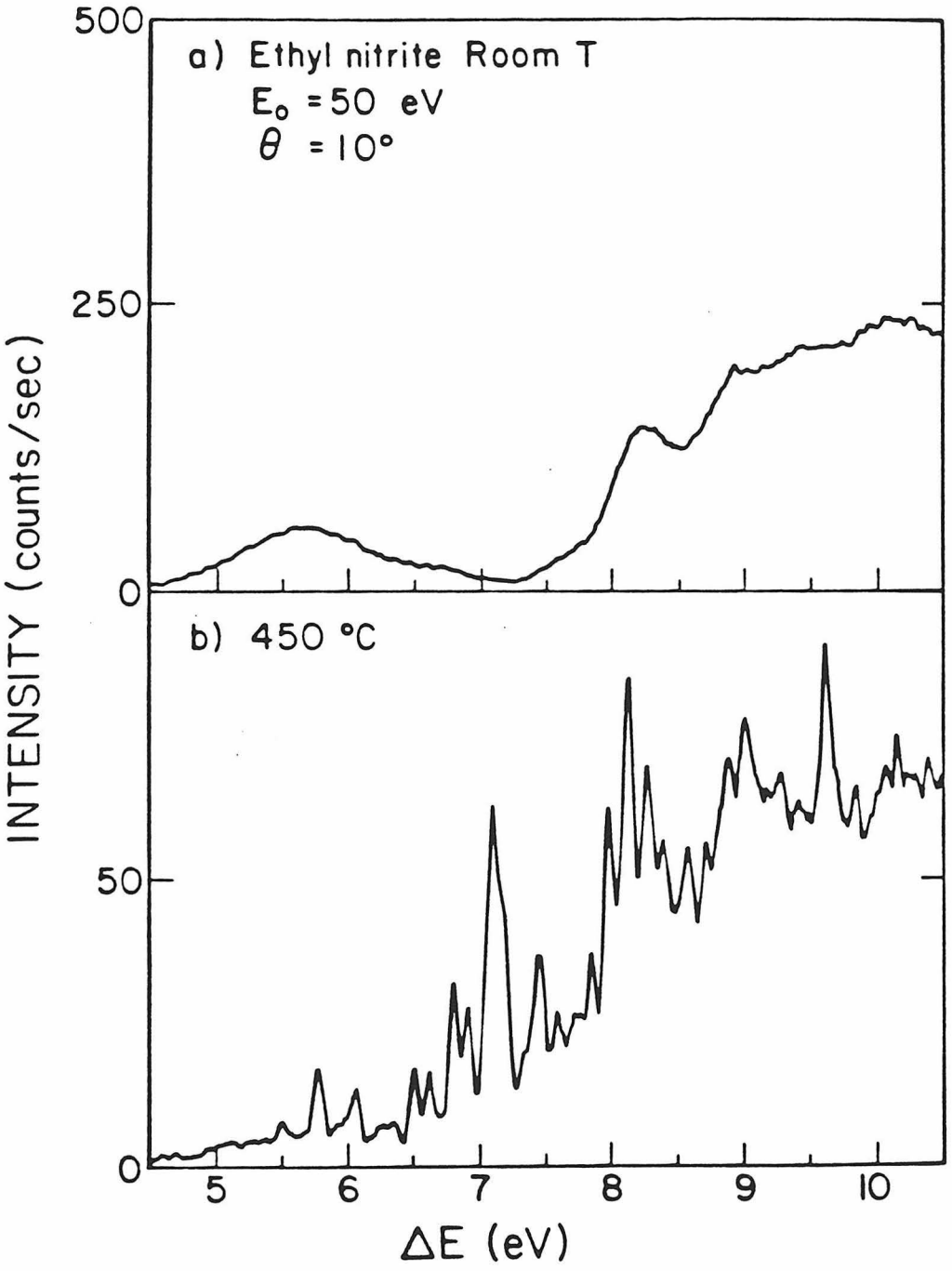
500
250
0
a) Ethyl nitrite Room T
E_o = 50 eV
θ = 10°
b) 450 °C
50
0
INTENSITY (counts/sec)
5
6
7
8
9
10
ΔE (eV)

FIGURE 5.

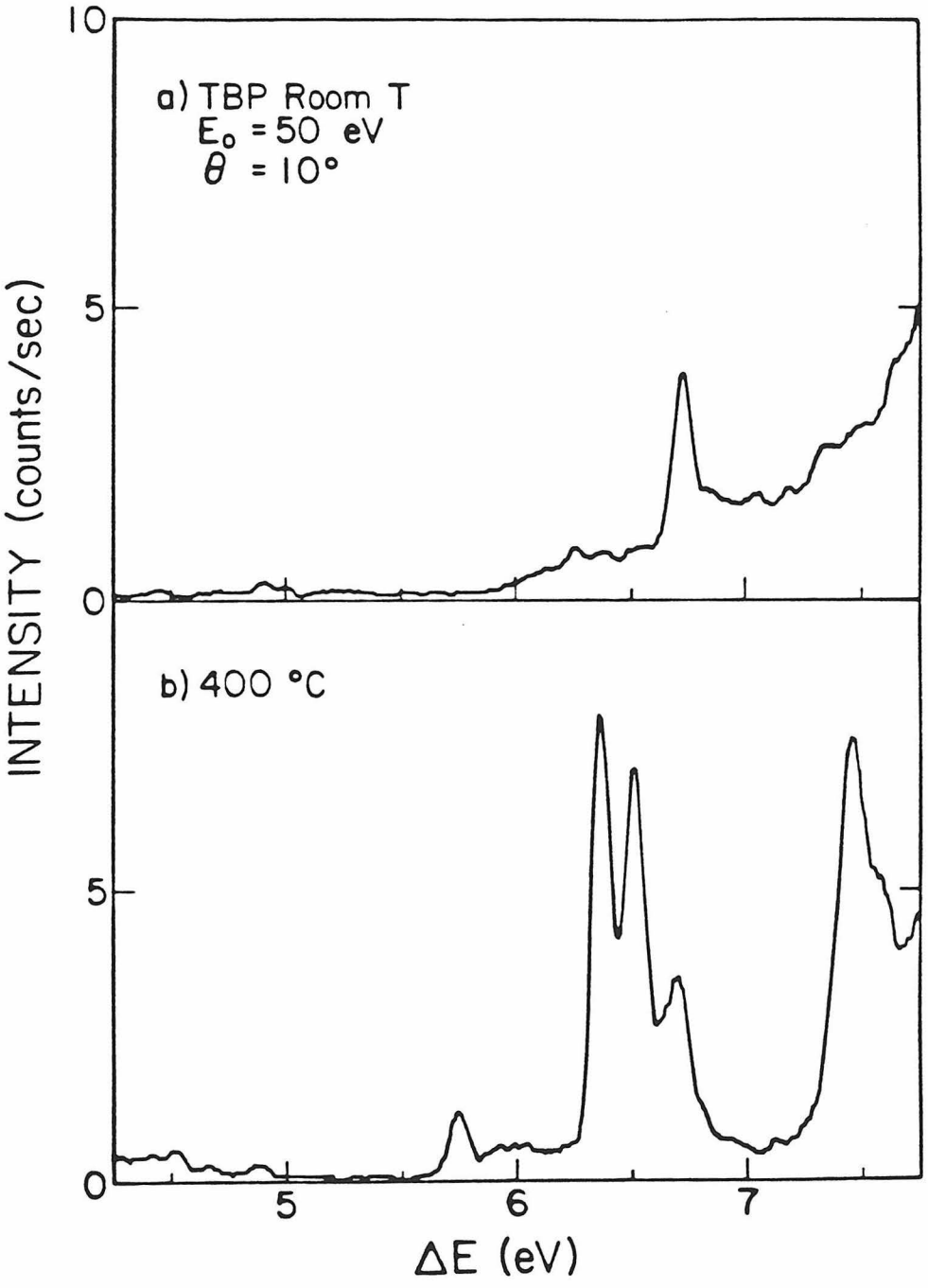
10
a) TBP Room T
E_o = 50 eV
θ = 10°
5
0
INTENSITY (counts/sec)
b) 400 °C
5
0
5
6
7
ΔE (eV)

FIGURE 6.

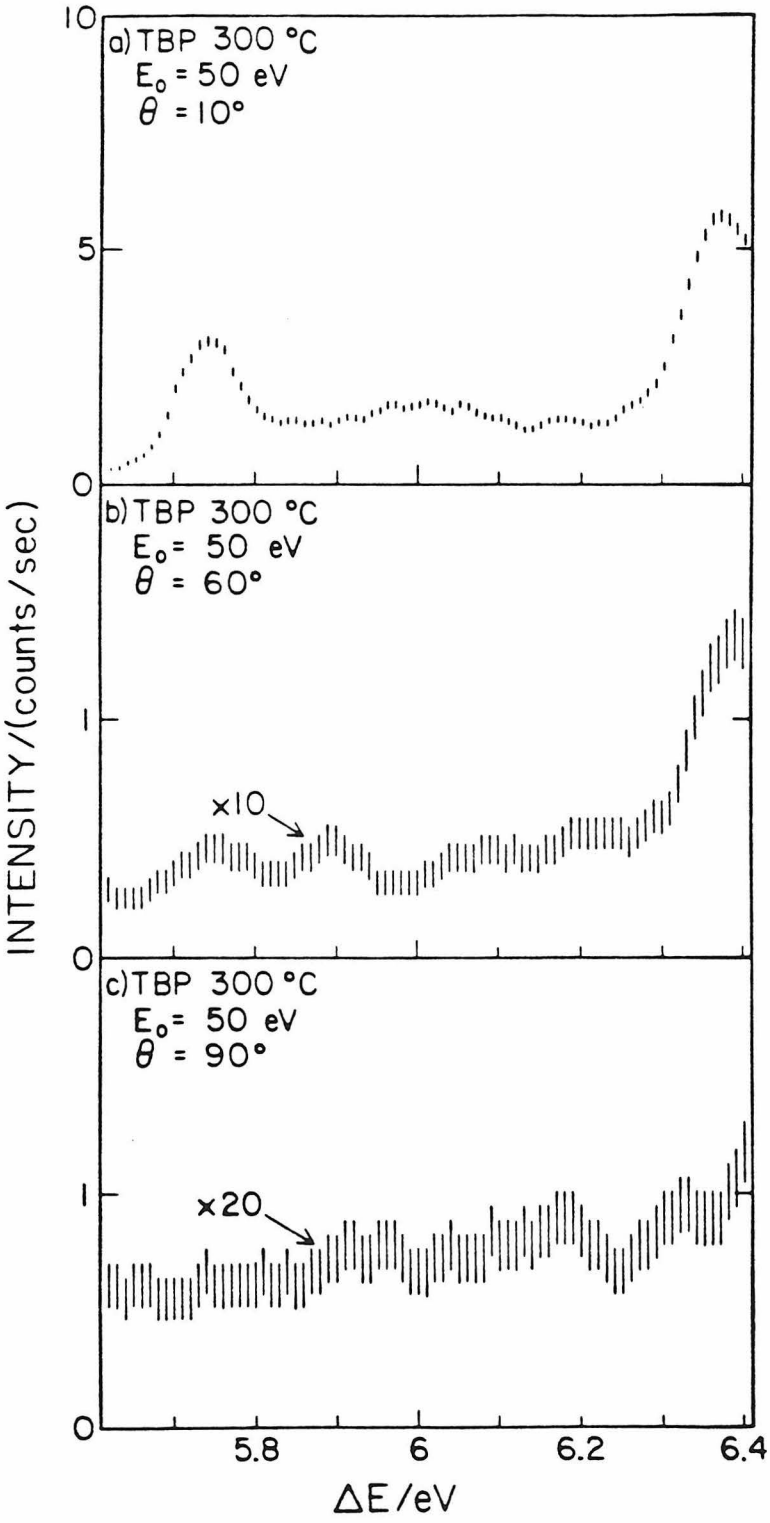
a) TBP 300 °C
E₀ = 50 eV
θ = 10°
b) TBP 300 °C
E₀ = 50 eV
θ = 60°
×10
c) TBP 300 °C
E₀ = 50 eV
θ = 90°
×20
10
5
0
1
0
1
0
5.8
6
6.2
6.4
INTENSITY/(counts/sec)
ΔE/eV

FIGURE 7.

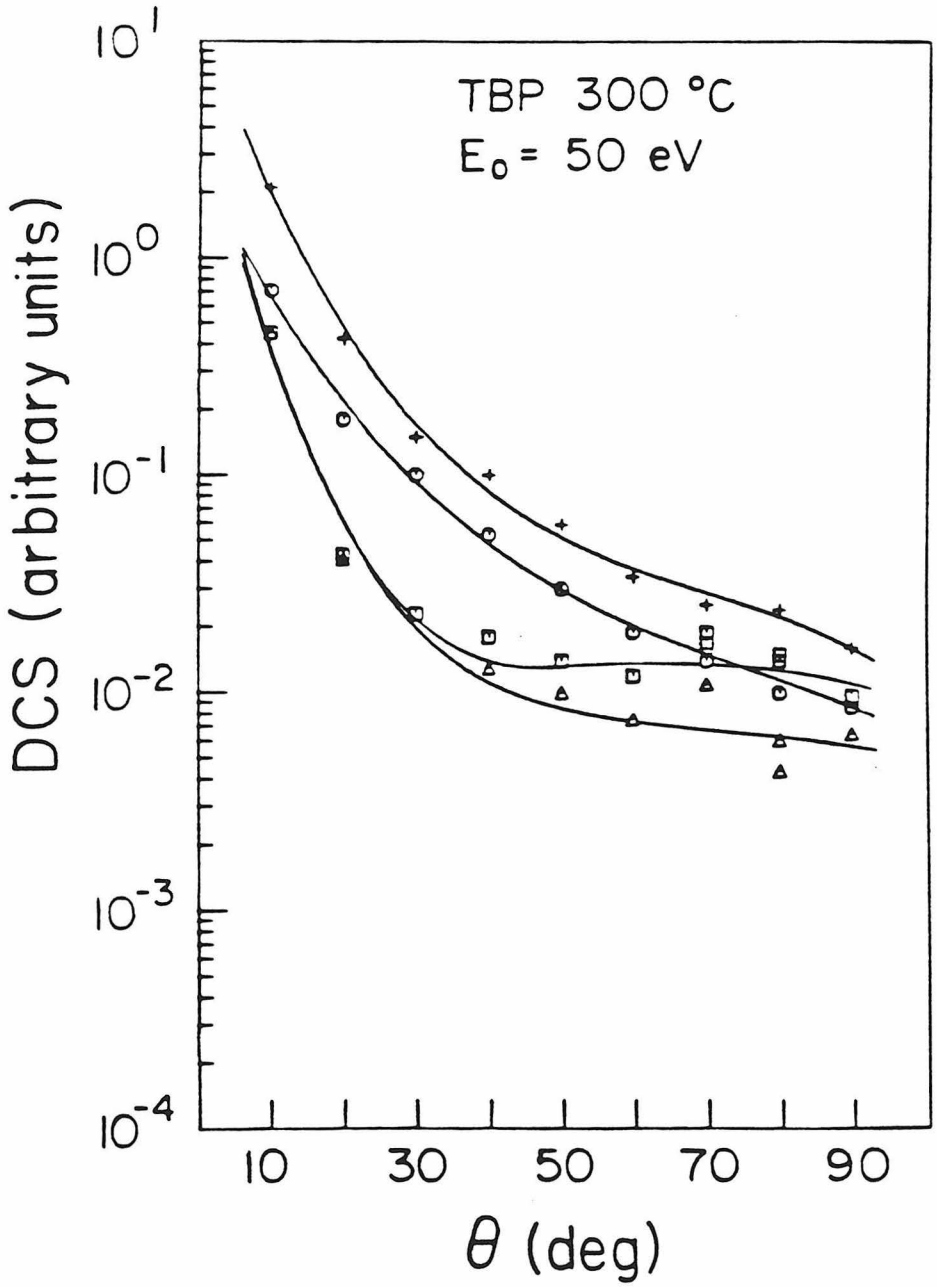
TBP 300 °C
E_0 = 50 eV
DCS (arbitrary units)
10^{1}
10^{0}
10^{-1}
10^{-2}
10^{-3}
10^{-4}
10
30
50
70
90
θ (deg)

FIGURE 8.

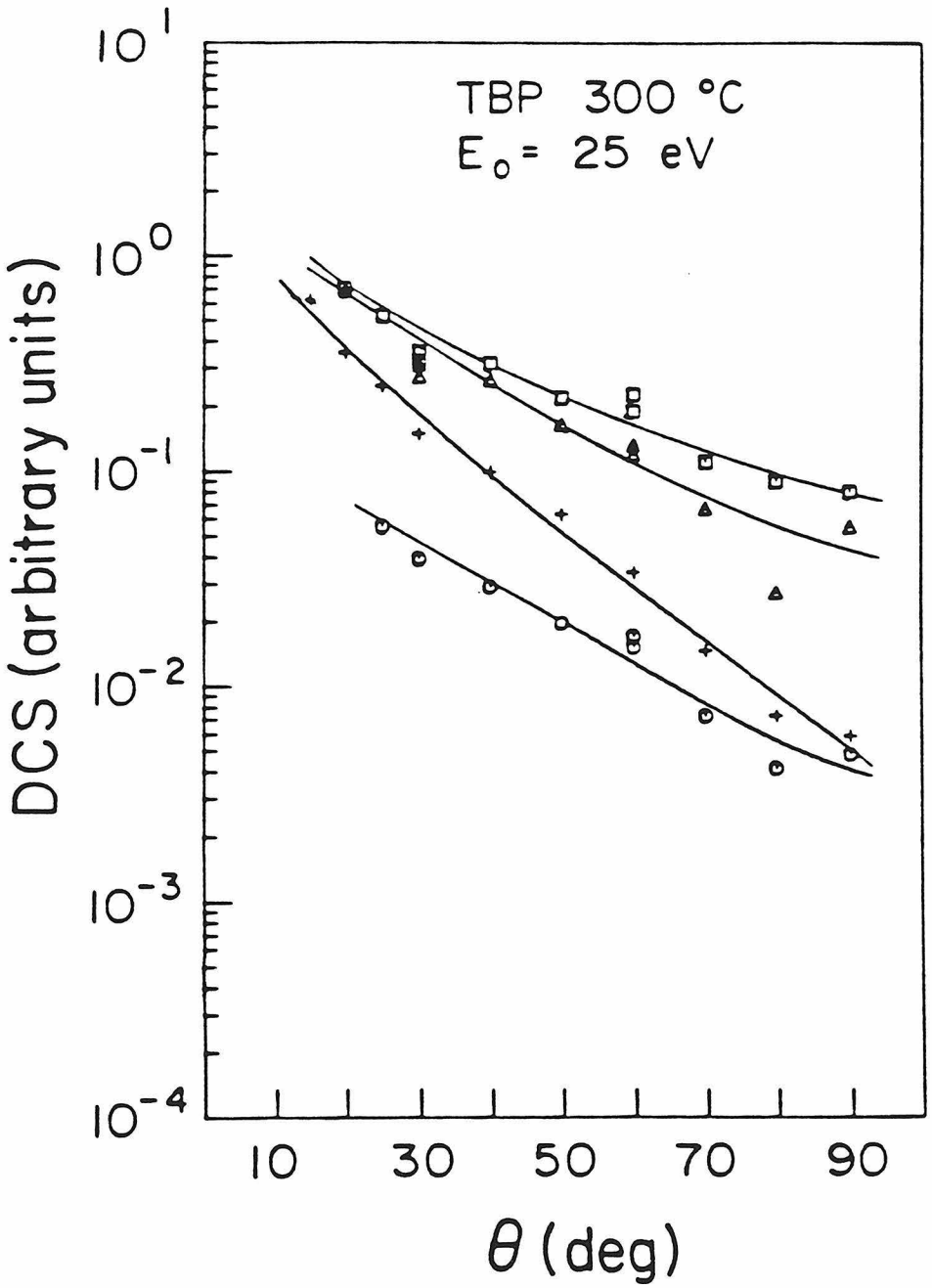
TBP 300 °C
E_o = 25 eV
DCS (arbitrary units)
10^1
10^0
10^{-1}
10^{-2}
10^{-3}
10^{-4}
10
30
50
70
90
θ (deg)

APPENDIX 1. PRELIMINARY ELECTRON-IMPACT INVESTIGATIONS

PYRIDAZINE

The study of the intramolecular interaction between oxygen and/or nitrogen "lone-pair" orbitals is important and interesting. In particular, the azabenzenes have been the subject of extensive experimental[1-6] and theoretical[7] studies. Azabenzenes are compounds isoelectronic with benzene but with nitrogen atoms replacing carbon atoms in the ring. These nitrogen atoms introduce perturbations in the benzene energy levels. New transitions arise from excitation of the now-present lone-pair orbitals; the principal difference between benzene and azabenzene photophysics is due to the introduction of a low-lying n$\rightarrow \pi^*$ excitation in the azabenzenes. A preliminary investigation of pyridazine by variable-angle electron energy-loss spectroscopy was undertaken in order to locate the low-lying singlet-triplet states in this molecule. Pyridazine is the benzene analog with two adjacent nitrogen atoms in the ring; the resulting molecular symmetry is C_{2v}.

Åsbrink *et al.*[3] have previously investigated the pyridazine spectrum by electron-impact spectroscopy under optical conditions (E_0= 150 eV, θ= 0°) and found that $\pi \rightarrow \pi^*$ transitions dominate. Figure 1 shows the pyridazine spectrum between 2.0 eV and 9.5 eV, just above the lowest ionization potential (9.31 eV vertical[2]). Under relatively optical conditions (Figure 1a), one sees four features. The first, with an onset at 3.29 eV and maximum at 3.65 eV, is due to the lowest n$\rightarrow \pi^*$, $^1B_1$ transition.[1,3] The other three features are due to various $\pi \rightarrow \pi^*$ excitations:[1,3] the $^1A_1$ transition with an onset at 4.70 eV and maximum at 5.02 eV, the $^1B_2$ transition with maximum at 6.46 eV, and a combination of $^1B_2$ and $^1A_1$ transitions with a maximum at 7.31 eV. Decreasing

the incident electron energy and increasing the scattering angle (Figure 1b, 1c) causes the manifestation of two bands attributable to spin-forbidden transitions. The lowest, with an onset at 2.75 eV and maximum at 3.08 eV, is due to the n→ π^*, $^3B_1$ excitation and has been seen previously in phosphorescence[1] and threshold-electron excitation spectroscopy.[4] The other, with a maximum at 4.16 eV and overlapping with the n→ π^*, $^1B_1$ band, has not been identified in previous experiments. A reasonable assignment is the $\pi \rightarrow \pi^*$, $^3A_1$ spin-forbidden counterpart of the lowest $\pi \rightarrow \pi^*$ band. Calculations by Leclercq *et al.*[7] place this transition at about 4.9 eV.

CYCLOHEXANONE

Figure 2 shows spectra of cyclohexanone in the low energy-loss region from 3.0 eV to 6.5 eV. Under relatively optical conditions (Figure 2a) one sees a band with an onset at 3.65 eV and a maximum at 4.15 eV which is due to the spin-allowed n→ π^* transition.[8] The onset of the n→3s Rydberg transition is also observed at about 6 eV. A decrease in incident energy and increase in scattering angle (Figure 2b, 2c) reveals the presence of two spin-forbidden bands. The lower, with an onset at 3.44 eV and a maximum at 3.91 eV, is due to the spin-forbidden n→ π^* transition. The other has a maximum at 5.81 eV and is assigned as the spin-forbidden $\pi \rightarrow \pi^*$ transition. The assignment of the valence excitations is supported by the behavior of the respective DCS curves (Figure 3), a spin-forbidden contribution being evidenced by a relatively constant DCS with θ.

The higher energy-loss region between 6.0 eV and 11.0 eV is shown in Figure 4. The many transitions observed in this region are Rydberg in nature[9] and converge to the first ionization potential (IP = 9.15 eV[10]). The complete listing of these transitions (with assignments) is given in Table 1.

References

1. K. K. Innes, J. P. Byrne, and I. G. Ross, *J. Mol. Spec.* **22**, 125 (1967).
2. R. Gleiter, E. Heilbronner, and V. Hornung, *Helv. Chim. Acta* **55**, 255 (1972).
3. L. Åsbrink, C. Fridh, B. Ö. Jonsson, and E. Lindholm, *Int. J. Mass Spec. and Ion Phys.* **8**, 229 (1972).
4. M. N. Pisanias, L. G. Christophorou, J. G. Carter, and D. L. McCorkle, *J. Chem. Phys.* **58**, 2110 (1973).
5. I. Renner and G. J. Schultz, *J. Chem. Phys.* **62**, 1747 (1975).
6. A. Bolovinos, P. Tsekeris, J. Philis, E. Pantos, and G. Andritsopoulos, *J. Mol. Spec.* **103**, 240 (1984).
7. J. Leclercq, P. Yvan, and J. M. Leclercq, *Chem. Phys.* **22**, 233 (1977).
8. A. Udvarhazi and M. A. El-Sayed, *J. Chem. Phys.* **42**, 3355 (1965).
9. M. B. Robin, *Higher Excited States of Polyatomic Molecules* vol. 2 (Academic Press, New York (1975)), p. 80.
10. G. C. Causley and B. R. Russell, *J. Chem. Phys.* **72**, 2623 (1980).

Table 1. Cyclohexanone Rydberg transitions, IP=9.15 eV.

(a) $n_o \rightarrow ns$:

E	n	δ^a	Calc^b
6.30	3	0.81	6.31
6.42	3 $(+1\nu)^c$		
6.57	3 $(+2\nu)$		
6.69	3 $(+3\nu)$		
7.80	4	0.82	7.81
8.40	5	0.73	8.38
8.72	6		8.64
8.87	7		8.79

(b) $n_o \rightarrow np$:

E	n	δ	Calc^d
6.95	3	0.51	6.97
7.06	3 $(+1\nu)^e$		
7.22	3 $(+2\nu)$		
8.05	4	0.48	8.04

(c) $n_o \rightarrow nd$:

E	n	δ	Calc^f
7.55	3	0.08	7.52
7.64	3 $(+1\nu)^g$		
8.24	4	0.13	8.25
8.57	5		8.58

a) Using formula $E = IP - R/(n - \delta)^2$.
b) Calculated with δ =0.81.
c) ν =0.13 eV.
d) Calculated with δ =0.50.
e) ν =0.12 eV.
f) Calculated with δ =0.11.
g) ν =0.09 eV.

Figure Captions

Figure 1. Pyridazine energy-loss spectra at: a) E_0= 50 eV and θ= 20°, b) E_0= 25 eV and θ= 20°, and c) E_0= 25 eV and θ= 50°.

Figure 2. Cyclohexanone energy-loss spectra at: a) E_0= 50 eV and θ= 10°, b) E_0= 30 eV and θ= 30°, and c) E_0= 30 eV and θ= 80°.

Figure 3. Cyclohexanone valence band DCS curves (integrated over the range given): a) E_0= 30 eV, □= elastic peak (EP)×0.1, ○ = n→ π^*(S–S) (3.7 eV to 5.0 eV), △ = n→ π^*(S–T) (3.4 eV to 4.8 eV), = $\pi \rightarrow \pi^*$(S–T)×10 (4.9 eV to 6.1 eV); b) E_0= 50 eV, □= EP×0.1, ○ = n→ π^*(S–S)×10, △= n→ π^*(S–T)×10, + = $\pi \rightarrow \pi^*$(S–T)×100 .

Figure 4. Cyclohexanone energy-loss spectrum between 6.0 eV and 11.0 eV at E_0= 100 eV and θ= 6°.

FIGURE 1.

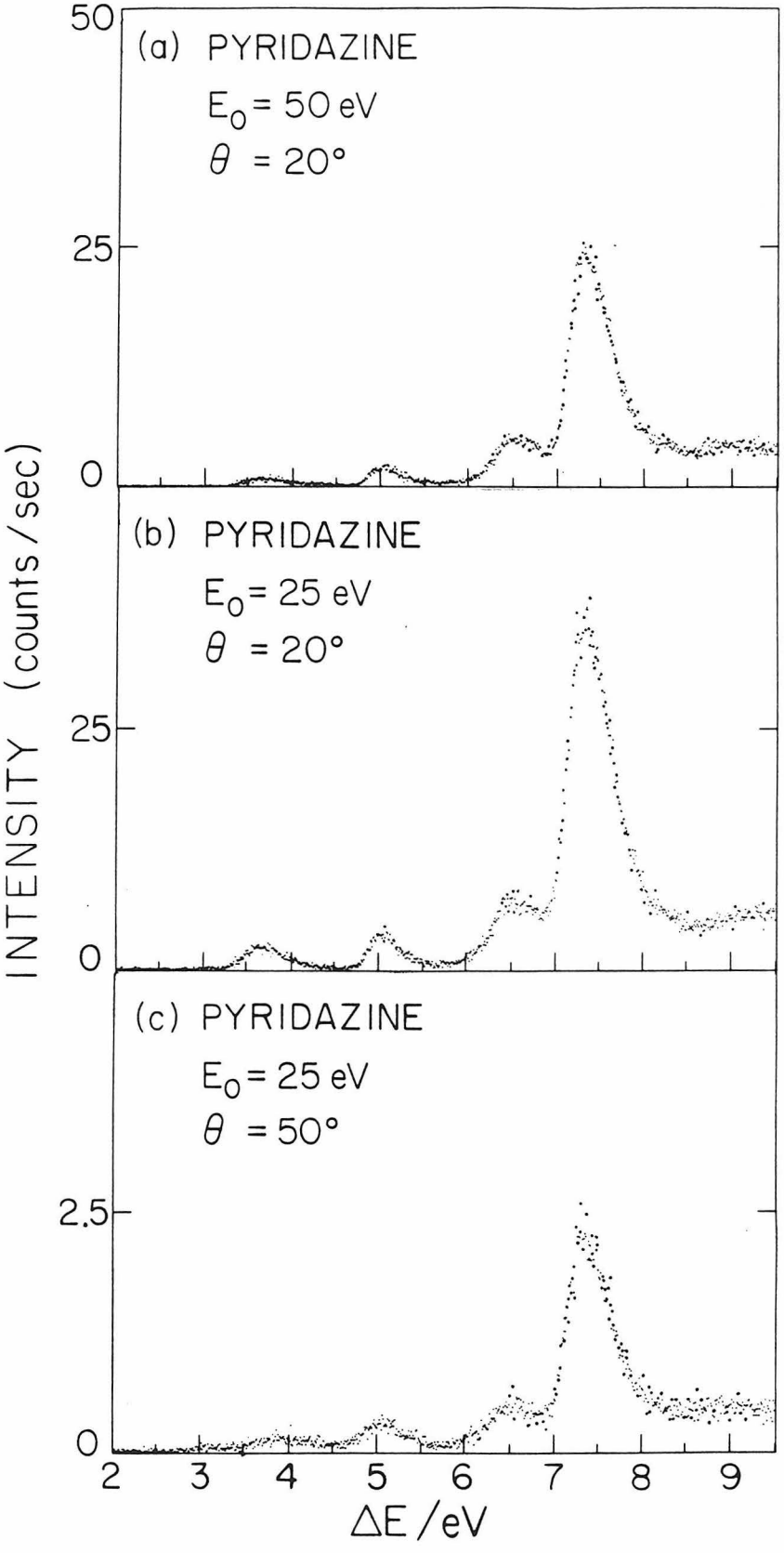
(a) PYRIDAZINE
E_0 = 50 eV
θ = 20°
(b) PYRIDAZINE
E_0 = 25 eV
θ = 20°
(c) PYRIDAZINE
E_0 = 25 eV
θ = 50°
INTENSITY (counts / sec)
50
25
0
25
0
2.5
0
2
3
4
5
6
7
8
9
ΔE / eV

FIGURE 2.

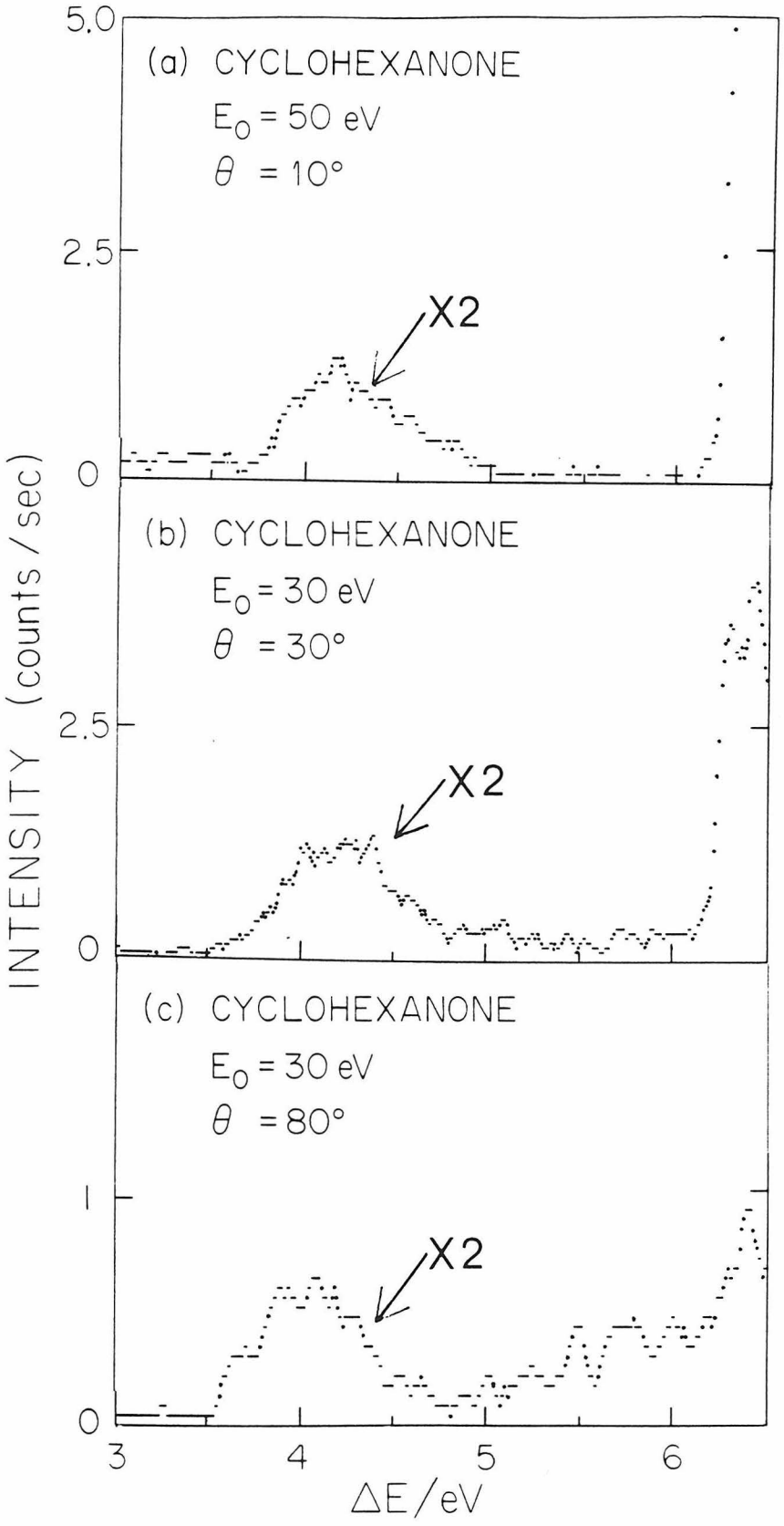
(a) CYCLOHEXANONE
E_0 = 50 eV
θ = 10°
X2
(b) CYCLOHEXANONE
E_0 = 30 eV
θ = 30°
X2
(c) CYCLOHEXANONE
E_0 = 30 eV
θ = 80°
X2
INTENSITY (counts / sec)
5.0
2.5
0
2.5
0
1
0
3
4
5
6
ΔE/eV

FIGURE 3.

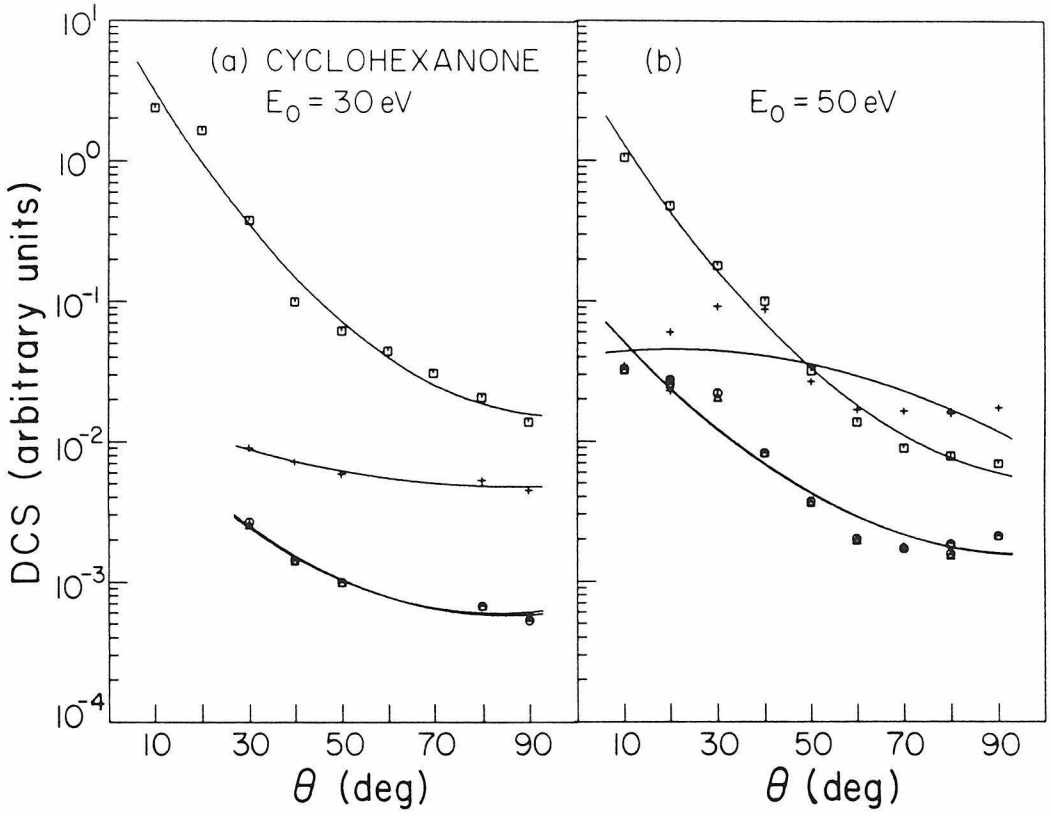
(a) CYCLOHEXANONE
E_0 = 30 eV
(b)
E_0 = 50 eV
DCS (arbitrary units)
10^1
10^0
10^{-1}
10^{-2}
10^{-3}
10^{-4}
10
30
50
70
90
θ (deg)

FIGURE 4.

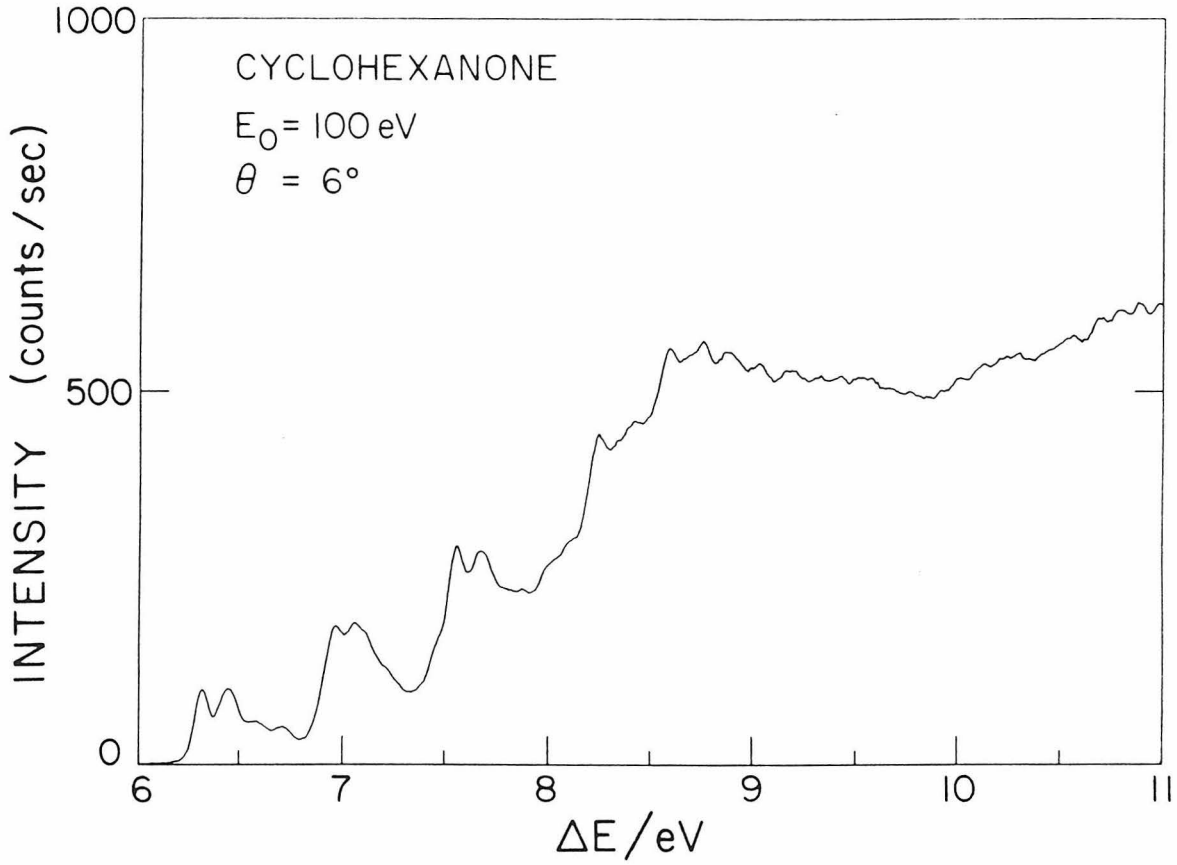
1000
500
0
CYCLOHEXANONE
E_0 = 100 eV
θ = 6°
INTENSITY (counts / sec)
6
7
8
9
10
11
ΔE / eV

APPENDIX 2. APPLICATION OF EIS TO THE ASSIGNMENT OF POLYATOMIC AUTOIONIZING RYDBERG TRANSITIONS

Read and Whiterod[1] have obtained expressions for the behavior of the inelastic differential cross section in the Born approximation as a function of both scattering angle θ and incident electron energy E_0 and have found that the behavior is markedly dependent on the symmetry species of the excited state. Dillon and Spence[2,3] have begun to apply these ideas to autoionizing states of atoms and diatomic molecules (in particular Ne, Ar, and O_2) with good results. It is this author's conjecture (found to be valid, see Chapter 2) that extension to the analyses of autoionizing Rydberg transitions in polyatomic molecules is both reasonable and feasible. Such Rydberg transitions manifest themselves as sharp structure superimposed on a continuum background and, if the background does not vary rapidly with the θ and E_0 ranges studied, the angular and energy dependence information necessary for assignment should be obtainable.

In the Born approximation, an expression for the DCS can be written and, by various mathematical manipulations,[1] it can be shown that

$$\left(\frac{d\sigma}{d\omega}\right) \propto \int |M_0(\Omega)|^2 P d\Omega = 4\pi \sum_l M(l), \tag{1.1}$$

where:

$$M_0(\Omega) = M(Q_s = 0, \Omega) = \sum_i \int \Phi_{el_{n'}} e^{iq\cdot r_i'} \Phi_{el_n} d^3\mathbf{r}. \tag{1.2}$$

Q_s represents the vibrational normal coordinates and $M_0(\Omega)$ is a sum of integrals over initial and final electronic states, slowly varying with a maximum at $Q_s = 0$. P is a rotational averaging term

$$P(\Omega) = \sum_{JMK} p(JMK) \left|\Phi_{rot}(JMK|\Omega)\right|^2, \tag{1.3}$$

where p is the fraction of molecules in the rotational states {JMK}. The M_0's in terms of spherical harmonics are

$$M_0(\Omega) = \sum_{l=0}^{+\infty} \sum_{m=-l}^{+l} 4\pi i^l Y_{lm}^* M(l,m), \tag{2.1}$$

and applying the orthonormality condition gives

$$\frac{d\sigma}{d\Omega} \propto 4\pi \sum_l M(l), \tag{2.2}$$

where

$$M(l) = \sum_{m=-l}^{+l} |M(l,m)|^2, \tag{2.3}$$

and

$$M(l,m) = \sum_i \int \Phi_{el_{n'}} j_l(qr_i') Y_{lm} \Phi_{el_n} d^3\mathbf{r}. \tag{2.4}$$

For small values of qa (valid in the Born approximation), a being a length of molecular dimensions

$$j_l \sim (qa)^l / 1 \cdot 3 \cdot 5 \cdot (2l+1). \tag{2.5}$$

Now, some of the M(l) are zero by symmetry and thus the DCS in (2.2) will be dominated by the first (or first two) non-zero term in the series. The M(l) come from terms M(l,m) which involve integrals over $\Phi_{el_{n'}}$, j_l, Y_{lm}, and Φ_{el_n}; the quantity M(l) is non-zero only if the product of symmetry representations $\Gamma_{n'}^* \times \Gamma_l \times \Gamma_n \times \Gamma_{bessel}$ contains Γ_1, the totally symmetric representation. Γ_{bessel} always equals Γ_1 and in addition Γ_n (the ground state) usually is totally symmetric, so for the product to contain Γ_1 it is usually required that Γ_l contains $\Gamma_{n'}$. Table 1 gives the minimum value of l for which Γ_l contains $\Gamma_{n'=i}$.[1]

Simplification of prior expressions gives for the DCS in the forward direction

$$\frac{d\sigma(0)}{d\omega} \propto q^{2l_0-4} \text{or} \propto E^{2-l_0}. \tag{2.6}$$

More useful is the expression for the DCS as a function of θ

$$\frac{d\sigma(\theta)}{d\omega} \propto q^{2l_0-4}, \tag{3.1}$$

where: $\mathbf{q}=\mathbf{k}_0-\mathbf{k}_f$, $\hbar\mathbf{k} = \mathbf{p} = \mathbf{mv}$. Thus

$$q = |\mathbf{q}| = \hbar m\big((\nu_0 - \nu_f\cos\theta)^2 + (-\nu_f\sin\theta)^2\big)^{\frac{1}{2}}. \tag{3.2}$$

For small θ ($\leq 10°$) expression (3.2) can be rewritten as

$$q = \hbar m\big((\nu_0 - \nu_f)^2 + \nu_f^2\theta^2\big)^{\frac{1}{2}} = \hbar m^{\frac{s}{2}}\sqrt{2}\big((\sqrt{E_0} - \sqrt{E_f})^2 + E_f\theta^2\big)^{\frac{1}{2}}$$

$$q = \hbar m^{\frac{s}{2}}\big(\Delta E_{\frac{1}{2}} + E_f\theta^2\big)^{\frac{1}{2}}, \tag{3.3}$$

where: $\Delta E_{\frac{1}{2}} = (\sqrt{E_0} - \sqrt{E_f})^2$. Thus

$$\frac{d\sigma(\theta)}{d\omega} \propto (\Delta E_{\frac{1}{2}} + E_f\theta^2)^{l_0-2}. \tag{3.4}$$

For practical purposes (i.e., extracting l_0 from spectral data) it is easier to rewrite (3.4) as

$$\frac{d\sigma(\theta)}{d\omega} = C(\Delta E_{\frac{1}{2}} + E_f\theta^2)^{l_0-2} = C'(1 + \frac{E_f}{\Delta E_{\frac{1}{2}}}\theta^2)^{l_0-2}, \tag{3.5}$$

where: C and C′ are proportionality constants. Then

$$\ln\frac{d\sigma(\theta)}{d\omega} = \ln C' + (l_0 - 2)\ln(1 + \frac{E_f}{\Delta E_{\frac{1}{2}}}\theta^2),$$

$$\ln DCS = (\ln DCS)_0 + (l_0 - 2)\ln(1 + \frac{E_f}{\Delta E_{\frac{1}{2}}}\theta^2). \tag{3.6}$$

A plot of $\ln(DCS)$ versus $\ln(1 + \frac{E_f}{\Delta E_{\frac{1}{2}}}\theta^2)$ will give a slope of (l_0-2) and intercept of $\ln(\mathrm{DCS})_0$.

Let us take as an example the Rydberg series in tetrachloroethylene, C_2Cl_4. C_2Cl_4 is a 36 electron system belonging to the point group D_{2h} with an outer molecular orbital configuration

$$\ldots(1b_{1g})^2(3b_{2u})^2(1a_u)^2(3b_{3g})^2\ (2b_{3u})^2 = A_g.$$

The Rydberg orbitals transform according to the symmetries s = a_g, $p_\pi = b_{3n}(x)$ and $b_{2n}(y)$, $p_\sigma = b_{1n}$, and d = a_g. If attention is limited to transitions converging to the first two ionization potentials, 9.5 eV and 11.4 eV[4] (the lowest is not autoionizing but done for comparison), the symmetry species Γ_i (and thus l_0) can be determined (using Table 1) for excitation to various Rydberg orbitals.

The results given in Table 2 show that for Rydberg transitions to the first ionization potential one is able to distinguish transitions to s and d type from p type. For Rydberg transitions to the second ionization potential one can again distinguish s and d type from p type, now with the added possibility of distinguishing p_π from p_σ types. One idea to keep in mind is that the *local symmetry* of the chromophore may be more important than the overall molecular symmetry in determining these rules.

References

1. F. Read, and G. Whiterod, *Proc. Phys. Soc.* **82**, 434 (1963).

2. M. Dillon, and D. Spence, *J. Chem. Phys.* **74**, 2654 (1981).

3. M. Dillon, and D. Spence, *J. Chem. Phys.* **74**, 6070 (1981).

4. W. VonNiessen, L. Åsbrink, and C. Bieri, *J. Electron Spectroscopy* **26**, 173 (1982).

Table 1. Minimum values of l for which Γ_l contains Γ_i .

Group	Γ_i	l_0
C_i	A_g	2
C_{3h}	A'	2
	E''	2
C_4	B	2
C_{4h}	A_g	2
	B_g	2
	B_u	3
	E_g	2
S_4	A	2
C_6	B	3
	E_1	2
C_{6h}	A_g	2
	B_g	4
	B_u	3
	E_{1g}	2
	E_{1u}	3
	E_{2g}	2
D_2	A	2
C_{2v}	A_2	2
C_{2h}	A_g	2
	B_g	2
D_{2h}	A_g	2
	A_u	3
	B_{1g}	2
	B_{2g}	2
	B_{3g}	2
D_3	A_1	2
D_{3d}	A_{1g}	2
	A_{1u}	3
	A_{2g}	4
	E_g	2
C_{3v}	A_2	3

Group	Γ_i	l_0
D_4	A_1	2
	B_1	2
	B_2	2
D_{4h}	A_{1g}	2
	A_{1u}	5
	A_{2g}	4
	B_{1g}	2
	B_{1u}	3
	B_{2g}	2
	B_{2u}	3
	E_g	2
C_{4v}	A_2	4
	B_1	2
	B_2	2
D_{2d}	A_1	2
	A_2	3
	B_1	2
D_6	A_1	2
	B_1	3
	B_2	3
	E_2	2
D_{6h}	A_{1g}	2
	A_{1u}	7
	A_{2g}	6
	B_{1g}	4
	B_{1u}	3
	B_{2g}	4
	B_{2u}	3
	E_{1g}	2
	E_{2g}	2
	E_{2u}	3
C_{6v}	A_2	6
	B_1	3
	B_2	3
	E_2	2

Group	Γ_i	l_0
D_{3h}	A_1'	2
	A_2'	3
	A_1''	4
	E''	2
T	A	3
	E	2
T_h	A_g	4
	A_u	3
	E_g	2
	E_u	5
	T_g	2
O	A_1	4
	A_2	3
	E	2
	T_2	2
O_h	A_{1g}	4
	A_{1u}	9
	A_{2g}	6
	A_{2u}	3
	E_g	2
	E_u	5
	T_{1g}	4
	T_{2g}	2
	T_{2u}	3
T_d	A_1	3
	A_2	6
	E	2
	T_1	3

Table 2. Results for various $\Gamma_i = \Gamma_{Ryd} \times \Gamma_{ion}$

IP	State	Rydberg Orbital and Symmetry		Γ_i	l_0
9.5 ev	$2b_{3u}$	s	a_g	b_{3u}	1
		p_σ	b_{1u}	b_{2g}	2
		p_π	b_{2u}	b_{1g}	2
			b_{3u}	a_g	
		d	a_g	b_{3u}	1
11.4 eV	$3b_{3g}$	s	a_g	b_{3g}	2
		p_σ	b_{1u}	b_{2u}	1
		p_π	b_{2u}	b_{1u}	1
			b_{3u}	a_u	3
		d	a_g	b_{3g}	2

APPENDIX 3. ELECTRON OPTICS DESCRIPTION AND ANALYSES

The electron optics initially used were designed by Flicker[1] and the subsequent system was designed by Dr. D. Edmonson (as described by Rianda[2]). One design objective was to extend the effective impact energy range of prior instruments, especially to lower energies. The present calculated impact energy range is 10 eV to 250 eV. Another objective was to increase the angular range of the instrument, resulting in attainable scattering angles for the Flicker design of -20° to +140°. The angular range of the Edmonson design is only -15° to +100°. The scattering angle is changed via a stainless steel gear wheel on which the electron gun, monochromator, and entrance optics are mounted. Because the path of the electron beam through the spectrometer is 20° with respect to the horizontal, the actual scattering angle is not a linear function of rotation angle but is given by

$$\theta = \cos^{-1}(0.883\cos\theta' + 0.117),$$

where θ' is the rotation angle and θ is the scattering angle. A last design objective was to improve the attainable resolution of the instrument; the present attainable value is about 25 meV.

Figure 1 shows a block diagram of the present spectrometer optics (the Edmonson design[2]). The first stage of the optics is the electron gun (GUN). Electrons are extracted through a 0.050 inch aperture in the Pierce element[3] (forcing rectilinear electron flow) from a heated tungsten filament and accelerated through a 0.035 inch aperture in the anode. Two pairs of cylindrical plate deflectors in the anode allow beam angle trimming to maximize electron current. The anode, condensor, and lens M3 form a condensing lens system (voltage ratio

2:8:1), focusing the anode image onto the entrance window of the fixed ratio decelerator. The decelerator consists of lens elements M3 and HM1, with a deceleration ratio of 12:1, and sets the image size, pencil angle, and beam energy for entry into the hemispherical monochromator. Molybdenum apertures in M3 set the beam angle. The beam is then imaged onto the focal plane of the hemispherical monochromator with magnification 1.5 and pencil angle 0.07 radians. M3 contains another set of cylindrical plate deflectors.

The monochromator (and likewise the energy-loss analyzer) consists of two concentric hemispherical sections with a mean electron path radius of 2.25 inches and a gap between the inner and outer sections of $\frac{9}{16}$ inch. The large path radius was chosen to yield a relatively high energy resolution of about 20 to 25 meV. Electrons passing through the monochromator are accelerated by the 1:12 accelerator (ACC) formed by HM2 and M4. The field lens follows, operable for electrons in the energy range 10 to 200 eV. In the M6 field lens element are a third set of trimmers. The last lens is a weak focusing lens (ENT).

After passing through the scattering region electrons enter an adder lens, having the collisional-loss energy added back with no change in beam focal properties due to the weakness of the lens. The einzel lens next forms the beam image for the 35:1 decelerator which subsequently forms a 0.045 inch image at the analyzer focal plane (EXT). Electrons passing through the hemispherical analyzer (identical to the monochromator) are detected by a Spiraltron electron multiplier (DET).

To aid in tuning the instrument a faraday cup was designed and placed near the scattering region, accessible at an angle of about 60°. Measurements have shown currents of greater than 10 namp at the scattering center to be typical.

The spectrometer is capable of operating in three modes. The first is the more

common energy-loss mode in which the impact energy is fixed and the analyzer sweeps to determine energy-loss. The second is the impact energy mode, used for studying the excitation function of various scattering processes and for detecting resonances. A scan consists of linearly varying the impact energy at constant energy-loss. The third mode, called the residual energy mode, involves sweeping both impact energy and energy-loss so as to keep the difference constant.

An analysis of the operating characteristics of the current electron optical system (revisions by Edmonson[2]) and a comparison with the previous system (designed by Flicker[1]) was performed. The reason for the analysis was two-fold. First, in the initial start-up phase of the experiment (where much difficulty arose in spectrometer tuning) it was expected that any design flaws would be revealed in the analysis. Also, experience gained in the analysis could be applied to the design of another lens system if the need arose.

To perform the analysis, a group of computer programs written by Kuyatt[4] which calculate operating parameters for large lens systems was employed. Substantially used were the two programs entitled LENS and IMAGE. LENS calculates the Gaussian electron rays into and out of each lens in a system given the sizes, positions, and voltages of the elements. IMAGE adjusts a given variable voltage so as to produce an image at a desired position. Many values describing the quality of the system are calculated, but the ones deemed most important for the analysis and comparison (given an image properly located) were: (1) beam angle (BA), (2) pencil angle (PA), and (3) filling factor (FF). The beam and pencil angles indicate the beam divergence. A bundle of rays producing the image forms a pencil and the pencil angle measures the divergence of the bundle. The angle between centers of pencils is the beam angle. The filling factor is the width of the beam relative to the width of the lens.

The results are given in Table 1. It is immediately seen that neither lens

system is better overall than the other. The Flicker gun stage is better, with smaller beam angles, pencil angles, and filling factors. The accelerator/decelerator stages are comparable but the Flicker entrance stage is again better in all three comparison areas. In contrast, the Edmonson exit and detector optics are better, having in general lower beam and pencil angles and smaller filling factors. The conclusion reached is that even though the monochromator-side optics of the prior design seem to be better, the difference is slight. Both systems have reasonably similar operating characteristics that for the most part are good (most beam and pencil angles $< 2°$, most filling factors < 0.50).

References

1. W. M. Flicker, Ph.D. Thesis, California Institute of Technology, Pasadena CA (1976).
2. R. Rianda, Ph.D. Thesis, California Institute of Technology, Pasadena CA (1981).
3. J. R. Pierce, *J. Appl. Phys.* **11**, 548 (1940).
4. C. Kuyatt, *Notes on Electron Optics* (1976), unpublished.

Table 1. Calculated Lens Characteristics

	Flicker[a]				Edmonson[b]			
	Voltages	BA[c]	PA[c]	FF	Voltages	BA	PA	FF
GUN	54	0.066	0.127		40	0.066	0.127	
	240	0.017	0.006	1.26	186	0.020	0.001	1.26
	23	0.089	0.123	0.53	24	0.099	0.129	0.70
ACC	22	0.027	0.035		24	0.032	0.032	
	2.2	0.004	0.064	0.50	2	0.008	0.064	0.45
ENT	23	0.027	0.035		24	0.032	0.032	
	76	0.009	0.022	0.18	204	0.031	0.008	0.33
	54	0.008	0.023	0.34	60	0.012	0.011	0.66
	10	0.028	0.022	0.47				
EXT	10	0.016	0.033		20	0.006	0.014	
	5.0	0.012	0.036	0.27	115	0.025	0.000	0.27
	100	0.046	0.018	0.37	80	0.028	0.000	0.13
	45	0.056	0.024	0.05	20	0.019	0.005	0.17
	11.4	0.029	0.018	0.45	80	0.006	0.005	0.20
	45	0.022	0.003	0.58	3	0.074	0.026	0.18
	7.3	0.061	0.024	0.20				
DET	2.8	0.108	0.027		3.9	0.077	0.027	
	39	0.069	0.008	0.70	80	0.033	0.004	0.36

a) Reference 1.

b) Reference 2.

c) Radians.

FIGURE 1.

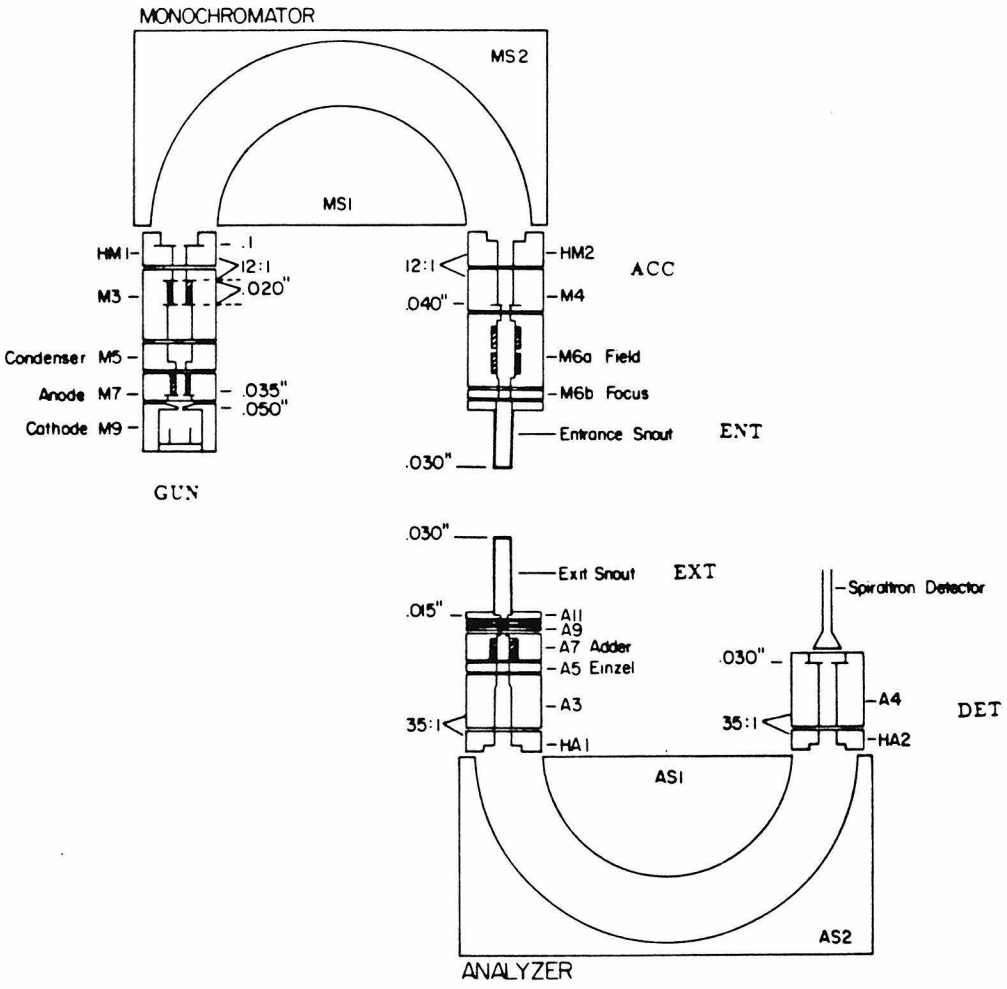
MONOCHROMATOR
MS2
MS1
HM1
.1
12:1
.020"
M3
Condenser M5
Anode M7
.035"
.050"
Cathode M9
GUN
12:1
HM2
ACC
.040"
M4
M6a Field
M6b Focus
Entrance Snout
ENT
.030"
.030"
Exit Snout
EXT
.015"
A11
A9
A7 Adder
A5 Einzel
A3
35:1
HA1
ASI
Spiraltron Detector
.030"
A4
35:1
HA2
DET
AS2
ANALYZER

APPENDIX 4. DESCRIPTION OF EIS III DATA ANALYSIS PROGRAMS

The following instructions describe the programs currently available for data manipulation on the Chemistry Department VAX. All programs will be found in the directory designated USER:[KNW.SPEC].

1. Data Transfer

(a) Mount the diskette in the drive, and then type MOUNT/FOR DYA0: (or DYA1:, DYB0:, DYB1:).

(b) Type RUN PUB:FLOPPY. The program will prompt with a question asking for the drive number in which the diskette is mounted (0, 1, 2, or 3). The program will also ask if the diskette is in FDOS format. The EIS III system does indeed use the FDOS system so respond with Y(es).

(c) The prompt FLOPPY⟩ will appear. Typing D displays the diskette directory; typing T initiates file transfer.

(d) If T is typed the computer will request the FDOS filename (upper-case letters) and, after reading the file, an output filename ('filename'.DAT). When the transfer is completed the FLOPPY⟩ prompt will reappear.

(e) The transfer process may be repeated as many times as necessary. Typing CTRL Z exits the program.

2. Data Decoding

(a) To decode the transferred files into English (from hexadecimal) type RUN EIS3.

(b) The program will request an input file ('filename'.DAT). When completed, the word DONE appears. The output file is named 'filename'.DEC.

(c) The decoded file is now in a form (referred to subsequently as "standard format") that can be printed, edited, or manipulated. It is recommended that each file be examined for bad or incorrect entries before data analysis begins.

3. Preliminary Spectrum Smoothing

(a) The first step in analyzing the spectral results is removing noise-spikes from and smoothing the spectra. The program used for this is a simplified version of ANDATA1 (*vide infra*) called ANDATA. The method of noise-spike removal and smoothing is discussed in detail by Flicker.[1] Briefly, a data channel with a spuriously high value is replaced with a value which is a mean of neighboring values. The smoothing is accomplished via a 5 to 19 point quadratic-cubic routine described by Savitsky and Golay.[2]

(b) To run ANDATA, assign the spectrum to be analyzed (in standard format) to FOR002 and assign the analysis parameter file ('filename'.PAR) to FOR003. The parameter file is constructed as follows:

Line 1 = Type of smoothing for each 256 channel spectrum region = S1, S2, ... S16. 5 = 5-channel smooth, 7 = 7-channel, 9 = 9-channel, 0 = 11-channel, 2 = 13-channel, 4 = 15-channel, 6 = 17-channel, 8 = 19-channel.

Line 2 = Stepsize (in meV).

Line 3 = Background (in counts/second).

Line 4 = 1

Line 5 = 0

Line 6 – Line 9 = Noise-spike removal comparators. If the ratio of adjacent points is greater than the comparator value a noise-spike is assumed. Line 6 = EP, Line 7 = channels with < 10 counts, Line 8 = channels with 10< n <250 counts, Line 9 = channels with >250 counts.

Line 10 = EP flag. 0 = EP, 1 = no EP.

Line 11 = Plot flag. 0 = Plot both raw and smoothed spectra, 1 = plot smoothed spectrum only.

Lines 1 and 11, used in ANDATA1, are not needed in ANDATA but must be included. Finally, assign 'filename'.INT to V9INT and 'filename'.PLT to VEROUT.

(c) Run ANDATA. An intermediate file is created that consists of five small plots of various strengths of smoothing (raw, 7-, 11-, 15-, and 19-channels). These crude spectral plots can be compared and used to decide which strength of smooth will be used in each 256 channel region. To plot on the Versatec plotter type VPLOT 'filename'.INT.

4. Final Spectrum Smoothing and Analysis

(a) The final spectrum smoothing and analysis is accomplished by ANDATA1. After deciding the amount of smoothing required and the background to be subtracted (if any) these values should be entered in the parameter file used for the ANDATA run. In addition to the previous assignments it is necessary to assign 'filename'.SMO to FOR004, 'filename'.OUT to FOR$TYPE, and 'filename'.PLT to FOR001.

(b) After running ANDATA1, 'filename'.SMO will contain the spectrum without noise-spikes and smoothed (in the standard format). 'Filename'.OUT will contain a copy of the raw and modified data plus information concerning peak positions and areas. 'Filename'.PLT contains a crude plot of the spectrum with all the changes described in 'filename'.OUT and can be plotted on the Zeta plotter.

5. Final Spectrum Plotting

(a) When the spectrum has been "cleaned up" to the desired level it should be plotted in a finished form for study and for the record book. This is accomplished with the program called SPECPLT.

(b) Assign the file to be plotted ('filename'.SMO) to FOR002. Assign 'filename'.SPC to FOR001 and 'filename'.FAC to FOR005. 'Filename'.FAC is a file containing any integer expansion factors (maximum of two, one per line). If only one factor is desired the other should be entered as zero. Similarly if no expansion is desired the file should contain two zeros.

(c) Run SPECPLT. 'Filename'.SPC contains the spectrum plot which can be plotted on the Zeta plotter.

(d) If the spectrum does not possess an elastic peak (used to set the energy scale) the program SPECPLTJ must be used instead of SPECPLT.

6. Band Area Calculation

(a) Two band area calculation programs can be used. BANDAREA1 calculates the areas for a set of input spectral regions. BANDAREA2 calculates these areas but also calculates the DCS values using input elastic peak DCS information.

(b) To calculate band areas but not DCS values assign the file to be analyzed ('filename'.SMO) to FOR004 and the file which contains the spectral regions to be examined ('filename'.BND) to FOR003. The first line of this file gives the (integer) number of bands to be examined, the second is the channel size (in meV), the third is a list of the onset voltages for the bands to be examined, and the fourth contains the end voltages for the bands to be examined. Assign 'filename'.BOT to FOR$TYPE.

(c) Run BANDAREA1. 'Filename'.BOT contains the calculated band areas

for each of the bands specified in 'filename'.BND.

(d) To calculate both band areas and differential cross sections again assign 'filename'.BND to FOR003 and assign the set of spectra files to be analyzed ('filename1'.SMO, 'filename2'.SMO, ... 'filenameN'.SMO) to FOR004, FOR005, ... FOR00(N+3). Also assign 'filename'.DAT to FOR002; this file contains information concerning the elastic DCS:

Line 1 = Molecule name.

Line 2 = Incident electron energy of the data.

Line 3 = Band number (nc), angle number (na) (I2I2).

Line 4 = 0.0,0.0,... 0.0 (same number as nc).

Line 5–line (4+na) = angle, DCS value.

(e) Run BANDAREA2, then run DCSCALC. The files named FOR00(N+4) to FOR00(2N+3) will contain both the calculated band areas and differential cross sections.

7. DCS Plotting

(a) Using the differential cross section values calculated by DCSCALC one can construct a data file (X'filename'.DAT) from them to be plotted. The format of this file is:

Line 1 = Molecule name.

Line 2 = Energy.

Line 3 = Nc, na (I2I2).

Line 4 = Curve multipliers (factor1, factor2, ... factor(nc)).

Line 5 – line (4+na) = angle, DCS1, DCS2, ... DCS(nc).

Assign this file to FOR002.

(b) Run DCSPLOT. A file named QMS002.QMS will be created which can be plotted on the Laser printer. The data points will be fit to a third-order polynomial

and this smooth curve will be drawn. If a second-order polynomial fit is preferred then DCSPLOTQ can be run.

8. Publication-Format Plotting

(a) To plot a specific region of a spectrum in a journal-compatible form one uses the program PAPLOT (or the variation DOTPLOT). Assign the spectrum file ('filename'.SMO) to FOR002. Assign 'filename'.PRP to FOR003; this file contains parameters for the plotting. The first line contains a scale expansion factor (zero if not needed), the second line gives the starting voltage desired, and the third line gives the ending voltage.

(b) Run PAPLOT. The file QMS002.QMS will be created; plot this file on the Laser printer.

References

1. W. M. Flicker, Ph.D. Thesis, California Institute of Technology, Pasadena CA (1976).

2. A. Savitsky and M. J. Golay, *Analyt. Chem.* **36**, 1627 (1964).

APPENDIX 5. SMALL CARBONYL RYDBERG TRANSITIONS

Table 1. Formaldehyde Rydberg transitions, IP=10.88 eV.

(a) $n_o \rightarrow ns$, $^1B_2$:

E	n	δ	Calc[a]	Lit[b,c]
7.10	3	1.10	7.07	7.10,7.08
7.35	3 $(+1\nu)$[d]			7.37
7.60	3 $(+2\nu)$			7.62
9.24	4	1.12	9.25	9.26
9.98	5	1.11	9.98	10.02
10.31	6	1.11	10.31	10.33
10.52	7		10.49	10.51
10.59	8		10.59	10.61
10.68	9		10.66	

(b) $n_o \rightarrow np$:

E	n	δ	Calc[e]	Lit[c,d,f]
7.98	$3(b_2)$	0.83	7.99	7.98,7.97
8.13	$3(a_1)$	0.77	8.14	8.14,8.14
8.26	$3(a_1)$ $(+1\nu)$[g]			
8.40	$3(b_1)$	0.66		8.37
8.57	$3(b_1)$ $(+1\nu)$[h]			8.57
8.73	$3(b_1)$ $(+2\nu)$			
9.62	4	0.71	9.58	9.65,9.63
10.14	5	0.73	10.12	10.14,10.13
10.37	6	0.82	10.38	10.39
10.52	7	0.87	10.53	10.53
10.59	8		10.62	10.63
10.68	9		10.68	10.69

(c) $n_o \rightarrow nd$:

E	n	δ	Calc[i]	Lit[c,d]
8.88	$3(a_1)$	0.40	8.87	8.88,8.88
9.02	$3(a_1)$ $(+1\nu)^j$			9.03
9.14	$3(a_1)$ $(+2\nu)$			
9.24	$3(b_1)$	0.12	9.24	9.22
9.37	$3(b_1)$ $(+1\nu)$			
9.84	$4(a_1)$	0.38	9.83	9.84
9.98	$4(b_1)$	0.11	9.98	
10.23	$5(a_1)$	0.42	10.24	10.26

a) Calculated with δ =1.11.
b) Reference 1.
c) Reference 2.
d) ν_1=0.25 eV.
e) Calculated with δ =0.77.
f) Reference 3.
g) ν_2=0.13 eV.
h) ν_3=0.17 eV.
i) Calculated with δ =0.40 and δ =0.12.
j) ν_2=0.13 eV.

Table 2. Formaldehyde Rydberg transitions, IP=14.39 eV.

(a) $\pi(1b_1) \rightarrow ns$:

E	n	δ	Calc[a]
	3		10.74
12.80	4	1.07	12.81
13.50	5	1.09	13.51
13.83	6	1.07	13.83
13.99	7	1.17	14.00

(b) $\pi(1b_1) \rightarrow np$:

E	n	δ	Calc[b]
11.45	3	0.85	
11.60	3 $(+1\nu)$[c]	0.79	
11.75	3 $(+2\nu)$	0.73	11.75
11.90	3 $(+3\nu)$	0.66	
12.05	3 $(+4\nu)$	0.59	
12.20	3 $(+5\nu)$	0.51	
12.33	3 $(+6\nu)$	0.43	
13.12	4	0.73	13.12
13.67	5	0.65	13.64

(c) $\pi(1b_1) \rightarrow nd$:

E	n	δ	Calc[d]
12.40	3	0.39	12.38
13.34	4	0.40	13.34

a) Calculated with δ =1.07.
b) Calculated with δ =0.73.
c) ν_2=0.15 eV.
d) Calculated with δ =0.40.

Table 3. Formaldehyde Rydberg transitions, IP=15.85 eV.

(a) $\sigma(3a_1)\rightarrow$ns:

E	n	δ	Calc[a]	Lit[b]
12.49	3	0.99		12.47
12.64	3 $(+1\nu)$[c]	0.94	12.64	12.64
12.80	3 $(+2\nu)$	0.89		12.81
14.40	4	0.94	14.40	
15.01	5	0.98	15.03	

(b) $\sigma(3a_1)\rightarrow$np:

E	n	δ	Calc[d]	Lit[e]
12.97	3	0.83		12.93
13.12	3 $(+1\nu)$[f]	0.77	13.11	13.11
14.54	4	0.78	14.55	
15.11	5	0.71	15.09	
15.35	6	0.78	15.35	
15.51	7	0.67	15.50	

(c) $\sigma(3a_1)\rightarrow$nd:

E	n	δ	Calc[g]
13.83	3	0.40	13.84
13.99	3$(+1\nu)$[h]	0.30	
14.83	4	0.35	14.80
15.17	5	0.53	15.21
15.41	6	0.44	15.42

a) Calculated with δ =0.94
b) Reference 1.
c) ν_2=0.15 eV.
d) Calculated with δ =0.77.
e) Reference 4.
f) ν_2=0.15 eV.
g) Calculated with δ =0.40.
h) ν_2=0.16 eV.

Table 4. Acetone Rydberg transitions, IP=9.71 eV.

(a) $n_o \rightarrow ns$:

E	n	δ	Calc[a]	Lit[b,c]
6.36	3	0.98	6.20	6.36,6.35
6.51	3 $(+1\nu)^d$	0.94		6.50
6.64	3 $(+2\nu)$	0.89		6.63
6.80	3 $(+3\nu)$			
6.98	3 $(+4\nu)$			
8.09	4	1.10	8.17	8.09,8.08
8.23	4 $(+1\nu)$			8.22
8.44	4 $(+2\nu)$			
8.86	5	1.00	8.85	8.82,8.83
9.01	5 $(+1\nu)$			
9.19	6	0.88	9.16	9.12,9.15
9.34	7	0.94	9.33	9.30,9.31
9.46	8	0.62	9.43	9.42
9.51	9	0.75	9.50	9.47

(b) $n_o \rightarrow nd$:

E	n	δ	Calc[g]	Lit[b,c]
7.75	3d	0.37	7.74	7.71
7.88	3d $(+1\nu)^h$			7.87,7.84
7.95	3d′	0.22	7.92	7.96
8.67	4d	0.38	8.68	8.69,8.68
9.08	5d	0.35	9.08	9.04
9.11	5d′	0.24	9.11	9.12

a) Calculated with $\delta = 1.03$.
b) Reference 5.
c) Reference 6.
d) $\nu_4 = 0.15$ eV.
e) Calculated with $\delta = 0.58$.
f) $\nu_4 = 0.12$ eV.
g) Calculated with $\delta = 0.37$ and $\delta = 0.24$.
h) $\nu_4 = 0.13$ eV.

Table 5. Acetaldehyde Rydberg transitions, IP=10.21 eV.

(a) $n_o \rightarrow ns$:

E	n	δ	Calc[a]	Lit[b,c]
6.81	3	1.00	7.00	6.82,7.10
6.95	3 $(+1\nu)$[d]			6.97
7.15	3 $(+1\nu')$[e]			7.14
7.29	3 $(+1\nu'')$[f]			
8.82	4	0.87	8.76	8.82
8.95	4 $(+1\nu)$			
9.43	5	0.82	9.38	9.43
9.66	6		9.68	9.71
9.86	7		9.84	9.88
9.96	8		9.94	
10.02	9		10.00	

(b) $n_o \rightarrow nd$:

E	n	δ	Calc[g]	Lit[b]
8.40	3d	0.26	8.36	8.43
8.54	3d $(+1\nu)$			8.56
8.69	3d′	0.01	8.69	
9.21	4d	0.31	9.22	9.24
9.36	4d′	0.00	9.36	9.38
9.66	5d		9.60	9.64

a) Calculated with $\delta = 0.94$.
b) Reference 7.
c) Reference 8.
d) $\nu_6 = 0.14$ eV.
e) $\nu' = \nu_{10} + 2\nu_6 = 0.34$ eV.
f) $\nu'' = \nu_{10} + 2\nu_6 = 0.48$ eV.
g) Calculated with $\delta = 0.29$ or 0.01.

References

1. M. J. Weiss, C. E. Kuyatt, and S. Mielczarek, *J. Chem. Phys.* **54**, 4147 (1971).

2. D. C. Moule and A. D. Walsh, *Chem. Rev.* **75**, 67 (1975).

3. S. Taylor, D. Wilden, and J. Comer, *Chem. Phys.* **70**, 291 (1982).

4. M. Praet and J. Delwiche, *Intern. J. Mass Spect. Ion Phys.* **1**, 321 (1968).

5. W. -C. Tam, and C. E. Brion, *J. Electron Spectroscopy* **4**, 139 (1974).

6. R. Huebner, R. J. Celotta, S. R. Mielczarek, and C. E. Kuyatt, *J. Chem. Phys.* **59**, 5434 (1973).

7. W. -C. Tam, and C. E. Brion, *J. Electron Spectroscopy* **3**, 467 (1974).

8. E. H. Van Veen, W. L. Van Dijk, and H. H. Brongersma, *Chem. Phys.* **16**, 337 (1976).